博士論文番号：1081003
(Doctoral student number)

Identification and characterization of a stigmatic autoinhibited Ca^{2+}-ATPase that is required for compatible pollination in the Brassicaceae

（アブラナ科植物の受粉過程で機能する Ca^{2+}輸送体の同定と解析）

Igarashi, Motoko

Nara Institute of Science and Technology
Graduate School of Biological Sciences
Intercellular Communications Laboratory (Prof. Seiji Takayama)

Submitted on 2014/08/05

Contents

List of abbreviations 3

Introduction 4

Figure 8

Chapter 1: Genome-wide transcriptome analysis of papilla cells: search for genes functioning in cross- and self-pollination

1-1 Introduction 9

1-2 Materials and Methods 10

1-3 Results 12

1-4 Discussion 16

Figures 19

Chapter 2: Identification and functional analysis of an autoinhibited Ca^{2+}-ATPase, ACA13, that is required for cross-pollination

2-1 Introduction 27

2-2 Materials and Methods 28

2-3 Results 33

2-4 Discussion 39

Figures 43

Conclusions 60

Acknowledgments 62

References 63

Supplemental tables 76

List of abbreviations

ACA	autoinhibited Ca^{2+}-ATPase
ACT8	actin 8
BiFC	bimolecular fluorescence complementation
$[Ca^{2+}]_{cyt}$	cytoplasmic Ca^{2+} concentration
CAM	calmodulin
C24	*A. thaliana* accession C24
C24 SI	C24 expressing *BrS9-SP11:SCRb* and *ΨSRK:SRKb*
C24 WT	C24 wild type
CFP	cyan-emitting fluorescent protein
Col-0	*A. thaliana* accession Columbia
Cy3-CTP	cyanine-3-cytidine 5'-triphosphate
ECA	endoplasmic reticulum (ER)-type calcium ATPase
EMS	ethyl methanesulfonate
FC	fold-change
FDR	false discovery rate
flg22	flagellin
FLS2	flagellin-sensing 2
FRET	fluorescence resonance energy transfer
GLR	glutamate receptor-like channel
GUS	ß-glucuronidase
K616	a yeast strain lacking *PMC1*, *PMR1* and *CNB1*
LCM	laser capture microdissection
RIN	RNA integrity number
SCR	*S*-locus cysteine-rich protein
SCR_b	SCR of the S_b-haplotype
SI	self-incompatibility
SLR1	*S*-locus related-1
SLR1-BP	SLR1 binding protein
SP11	*S*-locus protein 11
SRK	*S*-receptor kinase
SRK_b	SRK of the S_b-haplotype
XTH	xyloglucan endotransglucosylase/hydrolase
YC3.60	Yellow Cameleon 3.60
YFP	yellow-emitting fluorescent protein

Introduction

In the sexual reproduction of angiosperms, diverse events take place: after a pollen grain is captured on a stigma, it hydrates and germinates to produce a pollen tube, which grows through the stigma and style tissue, and enters an ovule where the two sperm cells are released for fertilization. Interactions between haploid pollen and the diploid pistil occur during this process. If a pollen grain is recognized as compatible, these events proceed to completion, but if it is recognized as incompatible, they are interrupted at some point.

In the Brassicaceae, the dry stigma is covered with papilla cells where a pollen grain makes initial contact with the pistil. In self-incompatible species, if a cross-pollen grain (i.e., a non-self-pollen grain from the same species) adheres to the papilla cell, the pollen coat dissolves from the pollen grain and forms a 'foot' between the pollen grain and the papilla cell surface, like an attachment (Elleman and Dickinson, 1986, 1990). Water is transported from the papilla cell to the pollen grain along the 'foot' for pollen hydration, and the pollen grain germinates a pollen tube which penetrates the papilla cell to grow between the inner and outer cell wall layers (Elleman et al., 1992; Dickinson, 1995). If a self-pollen grain lands on the papilla cell, pollen hydration, pollen germination and pollen tube penetration are all inhibited, so that fertilization does not occur. A dissection of actin cytoskeleton dynamics in papilla cells of *Brassica rapa* showed that actin polymerization was induced after cross-pollination, whereas actin filaments were reorganized and eventually depolymerized after self-pollination, and these events are thought to control differences in vacuole structure in the papilla cell (Iwano et al., 2007).

In the interaction between pollen and the papilla cell of the Brassicaceae, cross-pollen is probably recognized as compatible through unknown factors from the pollen grain which inform the papilla cell that the pollen grain is from the same species. After a cross-pollen grain is accepted by the papilla cell, further unknown factors from the papilla cell are thought to trigger compatibility responses, such as water transport to the pollen grain and actin polymerization in the papilla cell. In the current study, this signal transduction leading to compatible pollination is termed 'compatibility signaling'. Pollen grains from different species are usually not accepted presumably because their compatibility signal is different from that of the papilla cell. Previous studies demonstrated that pollen adhesion to the papilla cell is more stable if the two belong to the same species than if they belong to different

species, which indicates that the binding affinity between pollen and the papilla cell is species-specific (Luu et al., 1998; Zinkl et al., 1999). Furthermore, the pollen coat, a mixture of different lipids on the pollen surface, has been found to contain factors that function in compatibility signaling (Heslop-Harrison et al., 1974; Elleman and Dickinson, 1990). Classical studies demonstrated the 'mentor' pollen effect: pollen grains from different species can hydrate and germinate a pollen tube on the stigma if they are mixed with cross-pollen grains from the same species (Hiscock and Dickinson, 1993; Sarmah and Sarla, 1995). Male sterile mutants displaying defective long-chain lipid synthesis, and consequently lacking a proper pollen coat, do not hydrate on the papilla cell (Preuss et al., 1993; Hülskamp et al., 1995).

Several candidate factors that may function in compatibility signaling have been found. A cell wall glycoprotein, *S*-locus related-1 (SLR1), has high sequence similarity to the extracellular domain of the *S*-domain receptor kinase family, and is secreted from the stigma. SLR1 binds in vitro to two SLR1 binding proteins (SLR1-BP1 and SLR1-BP2) purified from the pollen coat, and is thought to function in pollen adhesion (Luu et al., 1997, 1999; Doughty et al, 1998; Takayama et al., 2000). Disruption of glycine-rich oleosin-domain protein 17 (GRP17) in the pollen coat caused delayed initiation of pollen hydration, indicating that GRP17 triggers water transport from the papilla cell (Mayfield and Preuss, 2000). To date, however, very little is known about factors in compatibility signaling that function in the papilla cell.

Self-pollen of self-incompatible species such as *B. rapa* and *Arabidopsis lyrata* is recognized as incompatible through the self-incompatibility (SI) system. This is controlled by a single polymorphic *S*-locus in which at least one female determinant gene and one male determinant gene are present as a pair called the *S*-haplotype (Takayama and Isogai, 2005). An interaction occurs between the female determinant *S*-receptor kinase (SRK), which is expressed in the papilla cell, and the male determinant *S*-locus protein 11 (SP11, also named SCR for *S*-locus cysteine-rich protein), which is located in the pollen coat. If the *S*-haplotypes of SRK and SP11 are identical, the intracellular kinase domain of SRK is autophosphorylated, and an SI signaling cascade is triggered in the papilla cell (Takayama et al., 2001).

Downstream of the SRK-SP11 interaction, candidate effector molecules have been identified. *M*-locus protein kinase (MLPK) is a membrane-anchored cytoplasmic serine/threonine protein kinase. An MLPK mutant (*mm*) showed a self-compatible phenotype, and overexpression of *MLPK* in this mutant restored SI (Murase et al., 2004). A bimolecular

fluorescence complementation (BiFC) assay suggested interactions between MLPK isoforms and SRK (Kakita et al., 2007). Armadillo repeat-containing 1 (ARC1) reportedly interacts with SRK in a yeast two-hybrid assay, and may function in the ubiquitin-mediated degradation of compatibility factors such as exocyst subunit EXO70 family protein A1 (EXO70A1) which is thought to have a role in vesicle trafficking (Gu et al., 1998; Samuel et al., 2009). However, conflicting data on the participation of these candidates in SI signaling have also been reported (Kitashiba et al., 2011). Further factors need to be identified to understand the mechanism of the SI response in the papilla cell that is triggered after the SRK-SP11/SCR interaction.

In previous research, self-incompatible species such as *B. rapa* and *B. oleracea* were used as plant materials, which was not practical for genetic and molecular analyses because of their long life cycle and their very low efficiency of generating transgenic plants. *Arabidopsis thaliana* is the model self-compatible Brassicaceae species, having lost SI during evolution, probably by disruption of either *SRK* or *SCR* (Sherman-Broyles et al., 2007; Tsuchimatsu et al., 2010). *A. thaliana* has about 150 papilla cells on a stigma, and after a pollen grain adheres to a papilla cell, it hydrates and germinates within 20 min; pollen tube penetration into the papilla cell occurs within 30 min (Sessions and Zambryski, 1995; Iwano et al., 2004). Nasrallah et al. (2004) reported that *SRK* of the S_b-haplotype (SRK_b) and *SCR* of the S_b-haplotype (SCR_b) from the self-incompatible species *A. lyrata* could be isolated and transferred to *A. thaliana* C24 accession (C24), and this transformed line showed the SI phenotype, suggesting that C24 retains the downstream genes required for the SI response. In my laboratory, one C24 line expressing *A. lyrata* SRK_b and another expressing SCR_b and SRK_b have also been successfully established (Kanatani, 2008; Takehisa, 2009). Pollen grains from C24 WT are used as cross-pollen, and pollen grains expressing SCR_b are used as self-pollen when they are attached to papilla cells expressing SRK_b. With these C24 lines, efficient studies are possible because the plants are simple to handle, and genomic information and broad application tools are available.

Using these lines, I searched for factors that function in the papilla cell during cross- and self-pollination. In Chapter 1, I describe microarray analysis of papilla cells, which was performed to identify genes that are preferentially expressed (i) in papilla cells compared to their underlying cells, and (ii) after cross- or self-pollination. From expression patterns in the microarray data, I hypothesized that cytoplasmic Ca^{2+} concentration ($[Ca^{2+}]_{cyt}$) increases in the papilla cell after self-pollination. In Chapter 2, I describe a search for Ca^{2+} transporter(s)

and characterization of a Ca^{2+} pump, which I performed to identify a factor(s) that regulates the different Ca^{2+} dynamics during cross- and self-pollination. I identified *autoinhibited Ca^{2+}-ATPase 13* (*ACA13*), whose expression was high in the papilla cell before pollination and became higher after cross- and self-pollination, as a candidate, and screened mutant lines from a C24 TILLING collection for functional analysis. I determined that ACA13 accumulates only after cross-pollination on the papilla cell membrane at the pollen tube penetration site, where it functions to export Ca^{2+} to cross-pollen for supporting pollen germination and pollen tube growth.

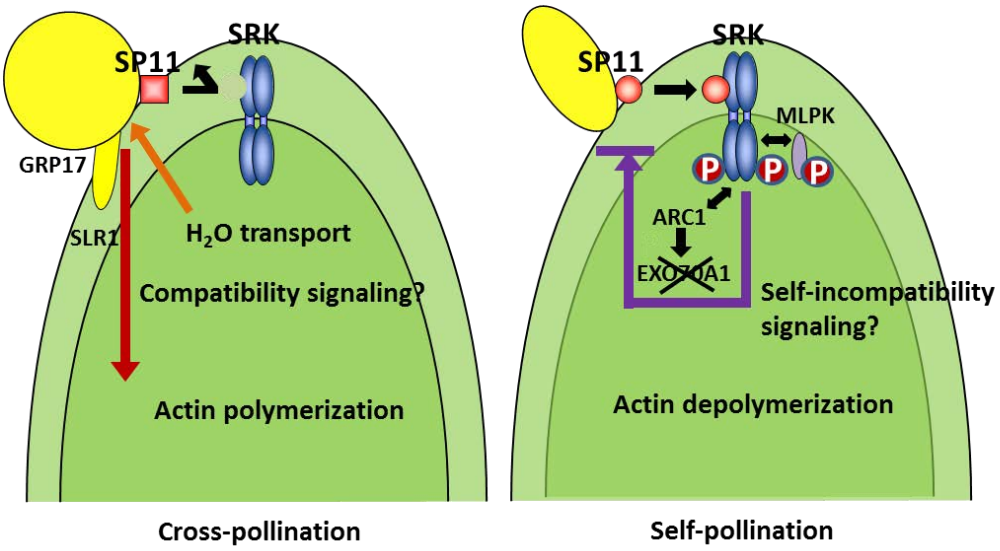

Figure 1. Model for compatibility signaling and SI signaling in the Brassicaceae.
In cross-pollination, water is thought to be transported from the papilla cell (green) to the pollen grain (yellow), and actin bundle formation increases. SRK and SP11/SCR do not interact. SLR1 and GRP17 are candidates for regulatory factors in pollen adhesion and pollen hydration. In self-pollination, SP11/SCR binds to SRK, which is then autophosphorylated. Actin bundles disassemble. MLPK and ARC1 are candidates for regulatory factors which function after SRK-SP11/SCR interaction.

Chapter 1

Genome-wide transcriptome analysis of papilla cells: search for genes functioning in cross- and self-pollination

1-1 Introduction

In the Brassicaceae, the papilla cell has crucial roles in pollen-pistil interactions during cross- and self-pollination. On the papilla cell, a cross-pollen grain hydrates and germinates a pollen tube, which penetrates into the papilla cell, whereas a self-pollen grain is rejected. Different cell biological changes in the papilla cell have been reported during these compatibility and SI responses, which must be controlled by unknown factors.

Using *A. thaliana*, transcriptome analyses of stigmas have been performed by microarray and cDNA subtraction, to identify genes involved in the early stage of pollen-pistil interaction (Swanson et al., 2005). A large number of genes that were expressed in stigmas, but not in ovaries or in seedlings, were found; however, the data were based on RNA samples from whole stigmas, which contain papilla cells but also other underlying cells, such as those of the transmitting tract in which the pollen tube subsequently grows to the ovule. Tung et al. (2005) attempted to identify papilla cell-specific genes by microarray analysis using a mutant line whose papilla cells were ablated by expressing diphtheria toxin subunit A (DT-A), which has an inhibitory effect on protein synthesis. Papilla cell-specific genes were determined by calculating differences between expression levels in WT and in the DT-A mutant (Tung et al., 2005). However, some effect from the toxic DT-A treatment on the range of genes detected cannot be excluded with this method. Additionally, transcription analysis in the papilla cell after cross- and self-pollination has not been reported. It remains unclear whether and how the compatibility and SI responses in the papilla cell are regulated by gene expression.

To better understand the molecular landscape of the papilla cell during cross- and self-pollination, I performed transcriptome analyses using microarray combined with laser capture microdissection (LCM), which is an excellent method for investigating gene expression in particular cell types. Ohara (2010) established and initiated experiments with this method for papilla cell samples in my laboratory, and I carried out further experiments

and analyses. First, I identified genes that are expressed preferentially in papilla cells compared to their underlying cells, and then I determined gene expression at 15 min and 30 min after cross- and self-pollination.

1-2 Materials and Methods

All chemicals and reagents used in this work were obtained from the companies Wako and Nacalai Tesque, unless otherwise specified in the text.

Plant materials and growth conditions

A. thaliana plants of C24 wild type (C24 WT), and C24 plants transformed with *Agrobacterium tumefaciens* carrying either *ΨSRK:SRK$_b$* [*SRK$_b$* from *A. lyrata* fused with the promoter *ΨSRK*] (Kanatani, 2008), or *BrS$_9$-SP11:SCR$_b$* [*SCR$_b$* from *A. lyrata* fused with the promoter *SP11* from *B. rapa S$_9$*-haplotype] and *ΨSRK:SRK$_b$* (C24 SI) (Takehisa, 2009), were grown at 23 °C under 14 h light and 10 h dark. The *SRK$_b$* insert in C24 expressing *ΨSRK:SRK$_b$* and the *SCR$_b$* insert in C24 SI were checked by PCR amplification with KAPA Taq (Kapa Biosystems) polymerase and the primer pairs listed in Supplemental Table 1. C24 SI was checked also by pollination test using aniline blue staining.

Sample collection by LCM and RNA extraction

Flower buds in late stage 12 (Smyth et al., 1990) were collected from C24 expressing *SRK$_b$*. They were fixed in 75% ethanol : 25% acetic acid on ice, either without pollination or 15 and 30 min after pollination with pollen from C24 WT (as cross-pollination) or C24 expressing *SCR$_b$* and *SRK$_b$* (as self-pollination). The samples were dehydrated, and then embedded in paraffin wax (Paraplast X-tra, Thermo Fisher Scientific) using an H2850 Microwave Processor (Energy Beam Sciences), as described by Ohara (2010). A Microm HM340E microtome (Thermo Fisher Scientific) was used to cut the buds in 14-μm-thick vertical sections. The sectioned samples were fixed on PEN Membrane Frame Slides (Molecular Devices), and papilla cells and the underlying cells were isolated separately using the ArcturusXT Laser Capture Microdissection System (Molecular Devices). Pollen grains were not collected when they were attached to the papilla cells after pollination. Total RNA was extracted with a PicoPure RNA Isolation Kit (Molecular Devices), and its quality and

quantity were determined using an Agilent 2100 Bioanalyzer (Agilent Technologies). The method used for RNA extraction was based on that of Takahashi et al. (2010).

Microarray experiment

For three biological replicates each from unpollinated, cross-pollinated (after 15 min and 30 min) and self-pollinated (after 15 min and 30 min) samples, a microarray experiment was performed according to the manufacturer's protocol, with minor modifications. One-color spike mix (Agilent Technologies) was mixed with the total RNA, and after cDNA was synthesized at 40 °C for 6 h, cRNA synthesis and subsequent amplification were performed with cyanine-3 (Cy3)-cytidine 5'-triphosphate (CTP) using a Quick Amp Labeling Kit One-Color (Agilent Technologies). The Cy3-labeled cRNA was purified with an RNeasy Mini Kit (QIAGEN) and quantitated using a NanoDrop ND-1000 UV-VIS spectrophotometer (NanoDrop Technologies). Cy3-labeled cRNA (1500 ng) was hybridized on an Arabidopsis (version3) Gene Expression Microarray, comprising 4x44K (Agilent Technologies) microarray slides, which contain 37,683 *A. thaliana* oligonucleotide probes per array. After washing, the slides were scanned with an Agilent G2565BA DNA microarray scanner (Agilent Technologies), and signal intensity was obtained using Feature Extraction 10.5.1.1 (Agilent Technologies).

Statistical analysis

GeneSpring GX12 (Agilent Technologies) was used for microarray data analysis. For inter-array comparison, 75-percentile normalization was carried out across all microarray data, and the normalized data were converted to the $\log_2$ scale. For each comparison between two conditions, the raw data were filtered according to expression and flags which are based on signal intensity, and were used only if the following two criteria were met for all three replicates in both conditions: (i) signal intensity was between 20% and 100% within the data set, and (ii) a 'detected' flag was present. To compare gene expression between two conditions, Student's *t*-test ($P < 0.05$) was performed with a paired method (for 'papilla cells vs underlying cells' and 'cross- vs self-pollination'), and subsequently, a fold-change (FC) analysis was conducted from positive real numbers of normalized expression values for each comparison (FC > 4.0 for 'papilla cells vs underlying cells' and FC > 2.0 for 'cross-pollination vs self-pollination'). TAIR locus ID of TAIR10 (http://www.arabidopsis.org/) was converted from Entrez Gene ID. Statistical evaluation of microarray data from RNA

samples with low RNA integrity number (RIN) was performed with the normalized intensity values (on the $\log_2$ scale).

For functional categorization of genes, Classification SuperViewer Tool with MapMan as the classification source was used with manual adjustment (Provart and Zhu, 2003; Thimm et al., 2004) (http://bbc.botany.utoronto.ca/ntools/cgi-bin/ntools_classification_superviewer.cgi). Gene Ontology analysis was performed using agriGO with default settings, and manually adjusted for hierarchical display for GO terms with false discovery rate (FDR) < 0.01 (Du et al., 2010) (http://bioinfo.cau.edu.cn/agriGO/).

The papilla cell samples collected at 30 min after cross-pollination must have included transcripts derived from the growing pollen tube. For each of 122 genes expressed preferentially at 30 min after cross-pollination, the difference in expression between cross- and self-pollination was calculated, and if the difference value was lower than a 'presumed pollen tube expression value', the gene was subtracted from the 122 genes. The 'presumed pollen tube expression value' was computed as follows: 20 genes expressed specifically and highly in the 'semi in vivo PT' (i.e., pollen tube growing in semi-in vivo conditions) data of Qin et al. (2009) were selected, and for those 20 genes, the detected expression difference between cross- and self-pollination was assumed to be entirely attributable to expression from the growing pollen tube. However, the expression values of Qin et al. (2009) were scaled differently from those of mine, which were generated by different microarrays and different analysis methods. Therefore, to calculate the 'presumed pollen tube expression value', the expression values of Qin et al. (2009) could only be used with a proportional conversion. For those 20 pollen tube-specific genes, the difference in expression between cross- and self-pollination from my data corresponded on average to 0.26% of the expression value from the 'semi in vivo PT' data. Therefore, the 'presumed pollen tube expression value' for each of the 122 genes was estimated to be 0.26% of the expression value in the 'semi in vivo PT'.

1-3 Results

Sample preparation and microarray analysis

First, to identify genes expressed preferentially in the papilla cell compared to its underlying cell (papilla cells vs underlying cells), I collected flower buds at late stage 12 (Smyth et al., 1990) from C24 expressing SRK_b, and checked that they were not pollinated

naturally. I fixed them without pollination, and isolated papilla cells and their underlying cells separately using LCM (Figure 1-1). Next, to determine genes that are expressed in the papilla cell preferentially after cross- or self-pollination (cross- vs self-pollination [15 min]; cross- vs self-pollination [30 min]), I pollinated flower buds at late stage 12 with either C24 WT pollen grains (cross-pollen) or C24 pollen grains expressing SCR_b (self-pollen), and fixed them at either 15 min or 30 min after pollination. For these comparisons after pollination, only papilla cells (but not their underlying cells) were dissected, and any attached pollen grains were excluded.

For each sample, I extracted total RNA from approximately 300-600 sections from approximately 100 flower buds per replicate. Amplified cRNA samples were labeled with Cy3-CTP, and hybridized on an Arabidopsis 4x44K oligonucleotide microarray (Table 1-1). The experiment was repeated for three biological replicates. I normalized the data by applying a 75-percentile normalization, and filtered them using the criteria described in Materials and Methods. Preliminary experiments showed that gene expression in the papilla cell is sensitive to minor variation in plant growth conditions (K. Ohara, personal communication). Therefore, I collected samples only within the following pairs: 'papilla cells vs underlying cells', 'cross- vs self-pollination [15 min]' and 'cross- vs self-pollination [30 min]', and also compared the obtained expression data only within those pairs.

Evaluation of microarray data according to RNA quality

The quality of extracted RNA, which is commonly measured by RIN, can affect the detection of transcriptional differences by microarray analysis (Copois et al., 2007). Among the 18 RNA samples prepared in this study, the RIN scores of two samples for the first replicate collected at 15 min after cross- ('15 min cross 1') or self-pollination ('15 min self 1') were markedly lower (1.9 and 2.0, respectively) than those of the other samples (Table 1-1). Therefore, I first examined whether the quality of microarray data from these two samples was adequate for further statistical analyses with the support of Dr. Gen Tamiya and Dr. Masao Ueki at Tohoku University.

To investigate whether the gene expression pattern of the data sets '15 min cross 1' and '15 min self 1' is different from those of other data sets, scatter plots were drawn for all combinations among three replicates, and Pearson product-moment correlation coefficients and Spearman's rank correlation coefficients were calculated. The scatter plots showed a similar pattern between all combinations, and the correlation coefficients were high (Figure

1-2), which indicates that the expression pattern of '15 min cross 1' and '15 min self 1' data sets is comparable with those of the other data sets. I therefore used all these data for further analyses.

Identification of genes expressed preferentially in the papilla cell

To identify genes expressed preferentially in the papilla cell, I compared gene expression levels in papilla cells and in underlying cells before pollination. Of 37,683 total probes, 14,115 were detected as valid for this comparison. I found that 587 genes were expressed more than 4-fold higher in papilla cells than in underlying cells, and, conversely, that 340 genes were expressed preferentially in underlying cells (Table 1-2).

The 587 genes included 70 of the 115 genes that were reported as papilla cell-specific by Tung et al. (2005), and two homologs of known genes that are thought to be specific for the papilla cell. *SLR1* (*AT3G12000*) is a homolog of *B. rapa SLR1*, which encodes a protein that is thought to bind SLR1-BP1 and SLR1-BP2 from pollen coat, presumably to strengthen pollen adhesion to the papilla cell surface (Luu et al., 1999; Takayama et al., 2000) (highlighted in bold characters in Supplemental Table 2). *AT2G33850* is a homolog of *B. napus Pis63*, which encodes a secretory protein of ca. 32 kDa (Robert et al., 1994). *Pis63* was defined as being expressed specifically in papilla cells by in situ hybridization and promoter-GUS assay; transgenic plants with reduced *Pis63* expression displayed a decreased ability for pollen germination and reduced seed set (Robert et al., 1994, 1999; Kang and Nasrallah, 2001) (highlighted in bold characters in Supplemental Table 2). These results imply that the 587 identified genes are a valid representation of genes expressed in the papilla cell, and should include reasonable candidates that function in interactions between pollen and the papilla cell.

To obtain an overview of the 587 genes, I next sorted them into functional categories using Classification SuperViewer with the MapMan source (Provart and Zhu, 2003; Thimm et al., 2004) (Figure 1-3; Supplemental Table 2). The largest category was 'miscellaneous enzymes' with more than 10% of the 587 genes, followed by 'protein fate', 'RNA fate', 'lipid metabolism', 'signaling', 'transport' and 'secondary metabolism'. This categorization indicates that these 587 genes encompass a broad spectrum of candidates.

I then evaluated the 587 genes by Gene Ontology analysis with FDR < 0.01 using agriGO (Du et al., 2010) to obtain their biological characteristics, which are shown in hierarchical structure in Table 1-3. The GO term 'Lipid metabolic process', including 'fatty

acid biosynthetic process' and 'wax biosynthetic process', was represented most significantly, and indicates active biosynthesis of long-chain and very-long-chain fatty acids in the papilla cell (highlighted in bold characters in Table 1-3). In addition, genes involved in 'phenylpropanoid biosynthetic process' (and, within this category, 'flavonoid biosynthetic process' and 'lignin biosynthetic process'), and genes participating in 'response to stimulus', were also represented significantly in the papilla cell, indicating that genes contributing to strengthening the cell wall and acting in response to various stresses are included in these 587 genes. These characteristics generally reflect the structure of the papilla cell, namely that most parts of the cell face the exterior environment to capture pollen grains.

Identification of genes expressed in the papilla cell preferentially after cross- or self-pollination

If genes are highly expressed in the papilla cell after either cross- or self-pollination, they may be reasonable candidates for genes that function in compatibility or SI signaling. To analyze cross- vs self-specificity in gene expression at an earlier time after pollination, I first compared the expression levels of 14,542 probes that were valid for the two conditions at 15 min after pollination. I found three genes expressed at least 2-fold higher after cross-pollination than after self-pollination, and nine genes expressed preferentially after self-pollination (Table 1-4, 1-5, 1-6).

I then compared the expression levels of 13,199 probes that were valid for microarray data at 30 min after cross- and self-pollination, to determine gene expression in the papilla cell at a later time after pollination. I identified 122 genes that were expressed at least 2-fold higher after cross-pollination than after self-pollination. However, because pollen tubes had penetrated and grown in the papilla cells at this time after cross-pollination, some of these 122 genes must have been expressed within the pollen tube growing in the papilla cell. Based on transcription data for pollen tubes growing in semi-in vivo conditions by Qin et al. (2009), 42 of the 122 genes were probably expressed from pollen tubes, and their removal yielded 80 genes (Table 1-4; Supplemental Table 3). At 30 min after self-pollination, 87 genes were identified as being expressed more than 2-fold higher compared to cross-pollination (Table1-4; Supplemental Table 4).

At 15 min after pollination, cross-pollen on the papilla cell has hydrated and is in the process of germinating, whereas self-pollen remains inert. However, only a few genes were expressed differently between cross- and self-pollination. The three genes expressed

preferentially after cross-pollination encode the following proteins: (i) an unknown protein (AT3G22620) with a structural domain that occurs in several proteins such as plant lipid-transfer proteins, proteinase/alpha-amylase inhibitors and seed storage proteins; (ii) xyloglucan endotransglucosylase/hydrolase 24 (XTH24, AT4G30270), which belongs to a large family of cell wall enzymes; and (iii) an uncharacterized protein (AT2G07714) with 196 amino acids (Table 1-5). Most genes that function in the papilla cell during cross-pollination are probably already expressed before pollination and regulated by post-transcriptional modification; alternatively, they may be expressed after both cross- and self-pollination, and their activity may be controlled by inhibition at some point after self-pollination.

Among the nine genes that were expressed preferentially at 15 min after self-pollination, four have been reported by Kaplan et al. (2006) to be induced after a transient increase of $[Ca^{2+}]_{cyt}$. In that study, a microarray analysis of *A. thaliana* seedlings was performed, using the Ca^{2+} sensor aequorin and the calmodulin antagonist W7, to determine the transcriptome at cytoplasmic Ca^{2+} transients, and early Ca^{2+}-responsive genes were identified including the four: *dicarboxylate carrier 2* (*DIC2*), *salt tolerance zinc finger* (*STZ*), *salt-inducible zinc finger 1* (*SZF1*) and *calmodulin like protein 37* (*CML37*). In addition to *CML37*, *CML29* was also represented among the nine genes. Members of the CML family encode Ca^{2+} sensors that bind Ca^{2+} and interact with target proteins to modulate their activity (McCormack et al., 2005). Furthermore, *STZ*, *SZF1* and *CML37* were also highly expressed at 30 min after self-pollination (indicated with asterisks in Table 1-6). These data suggested the possibility that a transient elevation of $[Ca^{2+}]_{cyt}$ occurs in the papilla cell after the SRK-SCR interaction during self-pollination.

1-4 Discussion

Among the genes that were expressed more than 4-fold higher in papilla cells than in underlying cells, most prominently enriched were genes involved in fatty acid synthesis. The GO term ‘wax biosynthetic process’ contains genes encoding long-chain acyl-CoA synthetases such as LACS1 (AT2G47240) and LACS2 (AT1G49430), which catalyze the activation of fatty acid to Acyl-CoA chain-length-dependently, and a very-long-chain enoyl-CoA reductase (CER10, AT3G55360) that is involved in very-long-chain fatty acid elongation (Schnurr et al., 2004; Lü et al., 2009; Zheng et al., 2005). Disruption of those

genes caused reduced production of cuticular wax and morphological defects in the plants (Schnurr et al., 2004; Lü et al., 2009; Zheng et al., 2005). 'Monocarboxylic acid metabolic process' contains genes encoding 3-ketoacyl-CoA synthases such as KCS1 (AT1G01120) and KCS2 (AT1G04220), also known to function in fatty acid elongation for biosynthesis of cutin and cuticular wax, in which fatty acid is elongated with 22- to 36-carbon chains (Todd et al., 1999; Franke et al., 2009; Bernard and Joubès, 2013). This reflects that the papilla cell is covered with cuticle wax, which generally serves as protection from water loss (Hiscock and Allen, 2008; Bernard and Joubès, 2013).

Although only a few genes were expressed preferentially after cross-pollination, they may be involved in the pollination process. The function of AT3G22620 has not been reported; however, it is up-regulated in *A. thaliana* overexpressing the transcription factor MYB domain protein 41 (MYB41), which binds upon phosphorylation to the promoter of *AT3G22620* (Cominelli et al., 2008; Hoang et al., 2012). *MYB41* is induced by abiotic stresses such as drought, abscisic acid and salt treatments, and plants overexpressing *MYB41* show abnormal cuticle and enhanced salt tolerance. As lipid-transfer proteins are generally known to function in cuticle deposition (Wang et al., 2011; Seo et al., 2011), AT3G22620 may participate in cuticle wax accumulation under the MYB41 transcription factor (Hoang et al., 2012; Cominelli et al., 2007; Lippold et al., 2009). XTHs are known to have a xyloglucan endotransglucosylase activity and a xyloglucan endohydrolase activity, and are thought to have various functions such as cell wall loosening, cell wall strengthening and integration of new xyloglucans into the cell wall (reviewed by Rose et al., 2002; Cosgrove, 2005). *XTH24* has been reported to be expressed in meristem and organ/tissue branch points, and the protein is thought to modify the cell wall under mechanical stress (Medford et al., 1991; Rose et al., 2002). When a pollen tube penetrates into the papilla cell, the cuticle layer needs to be breached, and the papilla cell wall is loosened, probably by physical distortion or enzymic activity (Hiscock and Allen, 2008; Elleman et al., 1992). Although it is unknown whether cuticle on the papilla cell has a specific function during pollination, and how the cell wall is modified during pollen tube growth into the papilla cell, these genes may have a role in pollen tube penetration during cross-pollination.

Interestingly, among the genes preferentially expressed after self-pollination, I identified several that have been reported to be induced after transient $[Ca^{2+}]_{cyt}$ elevation, which suggests that $[Ca^{2+}]_{cyt}$ in the papilla cell rises only after self-pollination. Ca^{2+} is an essential second messenger that operates, for instance, in stress responses to diverse biotic

and abiotic stimuli, in which elevated $[Ca^{2+}]_{cyt}$ is sensed, and this triggers the transmission of downstream signals (Hashimoto et al., 2011). Ca^{2+}-mediated signaling has been reported downstream of plant receptor-ligand interactions, including those between the pattern recognition receptor flagellin-sensing 2 (FLS2) and bacterial flagellin (flg22) (Jeworutzki et al., 2010; Tena et al., 2011). Elevation of $[Ca^{2+}]_{cyt}$ in the SI response is known in *Papaver rhoeas*. An interaction occurs in the stigma between the female determinant *P. rhoeas* stigma *S* (PrsS) and the male determinant *P. rhoeas* pollen *S* (PrpS), and $[Ca^{2+}]_{cyt}$ in the pollen tube increases shortly after a self-pollen grain has germinated on the stigma. Depolymerization of the actin cytoskeleton follows rapidly, and culminates in programmed cell death of the pollen tube (Franklin-Tong et al., 1993, 2002; Poulter et al., 2010; de Graaf et al., 2012). As in *P. rhoeas*, Ca^{2+}-mediated signaling may function to control the SI response in the papilla cell after the SRK-SCR interaction in the Brassicaceae.

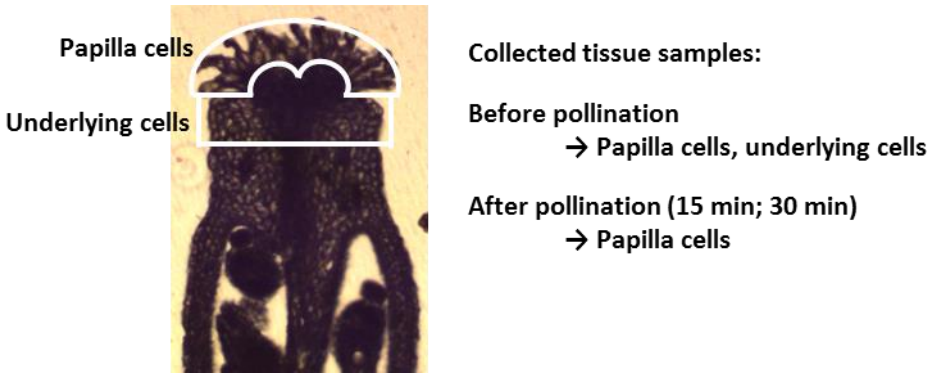

Figure 1-1. Collection of tissue samples.

Papilla cells and underlying cells were collected by laser microdissection from pistils of C24 expressing SRK_b.

Table 1-1. RNA samples for microarray analysis.

Sample	Replicate	Number of sections	Total RNA (ng)	RIN	
Underlying cells before pollination	1	424	62.6	5.0	
	2	432	71.8	4.2	
	3	331	47.7	4.7	
Papilla cells before pollination	1	482	11.8	4.4	
	2	488	15.9	3.6	
	3	570	44.9	5.0	
Papilla cells at 15 min after cross-pollination	1	618	9.3	1.9	*
	2	614	63.7	3.6	
	3	549	32.2	4.9	
Papilla cells at 15 min after self-pollination	1	591	18.5	2.0	*
	2	628	37.6	4.7	
	3	538	47.6	4.9	
Papilla cells at 30 min after cross-pollination	1	483	64.1	4.3	
	2	547	73.1	4.8	
	3	611	106.6	4.8	
Papilla cells at 30 min after self-pollination	1	447	36.0	4.7	
	2	578	96.2	4.5	
	3	574	94.6	4.6	

The number of collected tissue sections, quantity (Total RNA) and quality (RNA Integrity Number [RIN]) of extracted total RNA for microarray analysis are listed for each of three replicates. Asterisks indicate samples with low RIN scores.

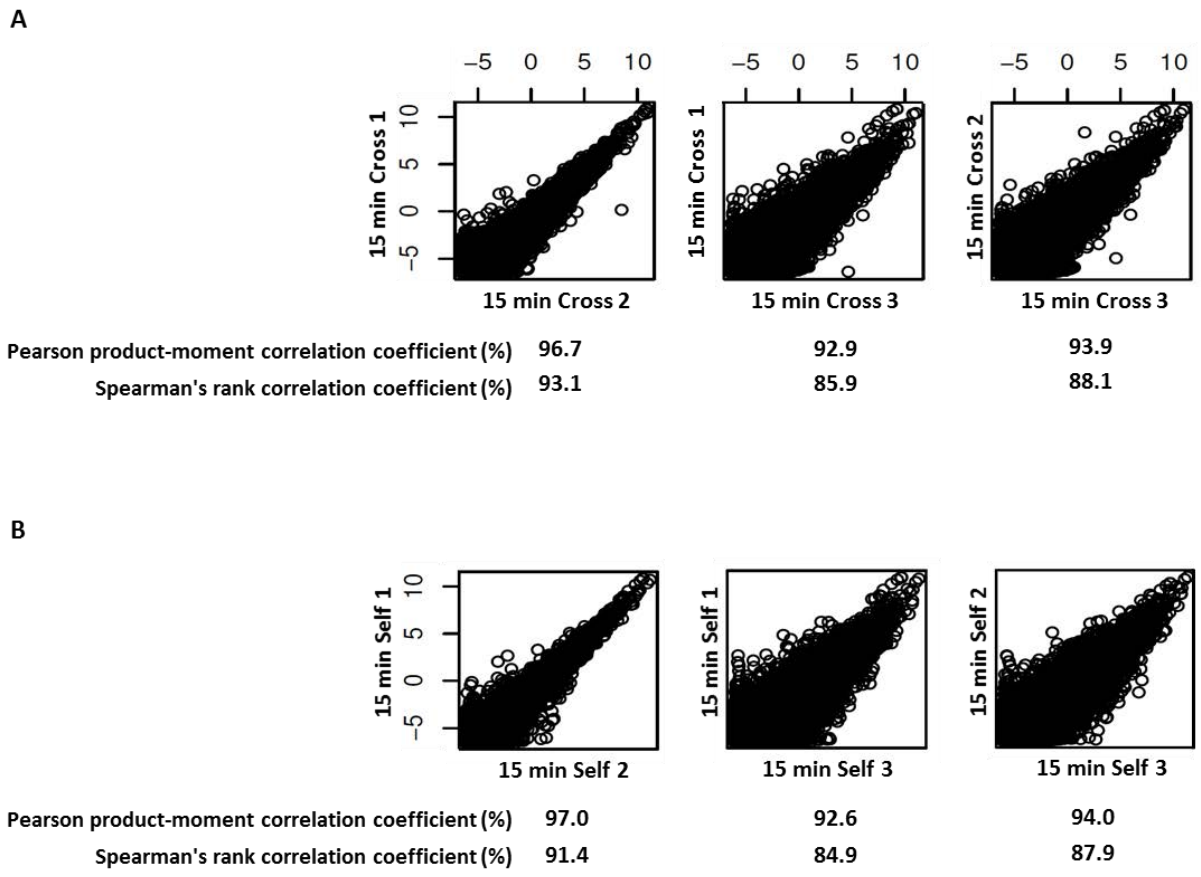

Figure 1-2. Scatter plots of normalized expression data.

(**A**) and (**B**) Scatter plots of normalized expression data (log_2 scale) are shown with Pearson product-moment correlation coefficients and Spearman's rank correlation coefficients in % for '15 min cross' (**A**) and '15 min self' (**B**) data sets.

Table 1-2. Numbers of genes expressed preferentially either in papilla cells or in underlying cells before pollination.

Cell type specificity			Number of genes
Papilla cells / Underlying cells	>	4.0	587
Underlying cells / Papilla cells	>	4.0	340

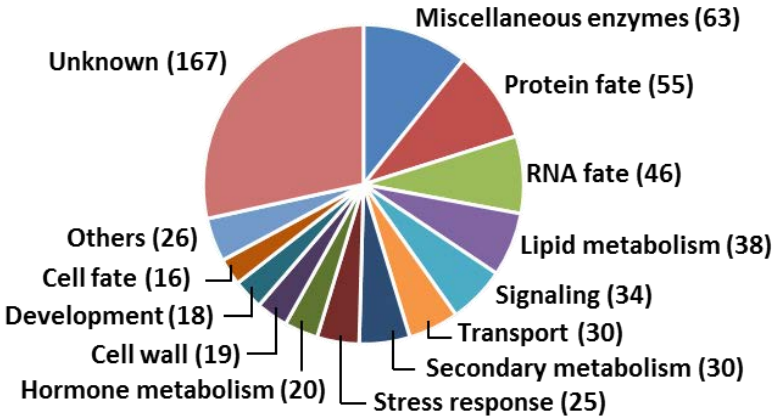

Figure 1-3. Functional categorization of the 587 genes that were preferentially expressed in papilla cells.

The categories are modified from SuperViewer classification with MapMan source (Provart and Zhu, 2003; Thimm et al., 2004). 'Others' includes 13 minor categories, and 'unknown' indicates unassigned genes. Numbers of genes are shown in brackets.

Table 1-3. Gene Ontology analysis of papilla cell-specific genes.

GO accession, GO term	Query	Total	FDR
GO:0008152 metabolic process			
GO:0044238 primary metabolic process			
GO:0006629 lipid metabolic process	54	841	9.1E-15
GO:0044255 cellular lipid metabolic process	32	618	6.5E-07
GO:0006631 fatty acid metabolic process	26	225	1.0E-11
GO:0006633 fatty acid biosynthetic process	21	140	2.5E-11
GO:0010166 wax metabolic process	7	24	1.9E-05
GO:0010025 wax biosynthetic process	7	23	1.7E-05
GO:0000038 very-long-chain fatty acid metabolic process	5	22	1.6E-03
GO:0008202 steroid metabolic process	8	84	2.6E-03
GO:0008610 lipid biosynthetic process	32	439	6.4E-10
GO:0006519 cellular amino acid and derivative metabolic process	25	682	2.7E-03
GO:0006575 cellular amino acid derivative metabolic process	24	315	6.0E-08
GO:0042398 cellular amino acid derivative biosynthetic process	22	233	1.0E-08
GO:0009699 phenylpropanoid biosynthetic process	19	141	1.1E-09
GO:0009813 flavonoid biosynthetic process	11	69	2.8E-06
GO:0009809 lignin biosynthetic process	6	42	2.6E-03
GO:0009698 phenylpropanoid metabolic process	21	175	7.2E-10
GO:0009808 lignin metabolic process	6	47	4.1E-03
GO:0009812 flavonoid metabolic process	11	78	7.1E-06
GO:0019748 secondary metabolic process	30	489	6.0E-08
GO:0044237 cellular metabolic process			
GO:0006725 cellular aromatic compound metabolic process	26	399	2.3E-07
GO:0019438 aromatic compound biosynthetic process	21	237	6.0E-08
GO:0042180 cellular ketone metabolic process	35	882	3.8E-05
GO:0043436 oxoacid metabolic process	34	859	5.2E-05
GO:0019752 carboxylic acid metabolic process	34	859	5.2E-05
GO:0032787 monocarboxylic acid metabolic process	30	408	1.5E-09
GO:0046394 carboxylic acid biosynthetic process	24	417	6.2E-06
GO:0006082 organic acid metabolic process	34	860	5.2E-05
GO:0016053 organic acid biosynthetic process	24	417	6.2E-06
GO:0051179 localization			
GO:0010876 lipid localization	7	24	1.9E-05
GO:0051704 multi-organism process			
GO:0051707 response to other organism	23	599	2.7E-03
GO:0050896 response to stimulus	107	4057	2.2E-06

GO:0009719 response to endogenous stimulus	35	1068	1.3E-03
GO:0009725 response to hormone stimulus	31	982	5.2E-03
GO:0009628 response to abiotic stimulus			
GO:0009314 response to radiation	25	613	6.4E-04
GO:0009416 response to light stimulus	25	596	4.5E-04
GO:0009411 response to UV	9	83	4.5E-04
GO:0009607 response to biotic stimulus	27	638	2.0E-04
GO:0009605 response to external stimulus	20	429	7.2E-04
GO:0009611 response to wounding	14	197	2.1E-04
GO:0006950 response to stress	59	2320	3.8E-03
GO:0006952 defense response	29	766	5.6E-04
GO:0042221 response to chemical stimulus	59	2085	3.0E-04
GO:0010033 response to organic substance	42	1342	6.4E-04
GO:0009987 cellular process			
GO:0009664 plant-type cell wall organization	7	79	8.9E-03
GO:0032502 developmental process			
GO:0048869 cellular developmental process	21	520	2.7E-03

GO accessions and GO terms of biological processes whose false discovery rate (FDR) was < 0.01 are shown. 'Query' indicates the number of genes from the 587 genes expressed preferentially in the papilla cell, and 'Total' indicates the number of genes registered for the GO accessions.

Table 1-4. Number of genes expressed in papilla cells preferentially after either cross- or self-pollination.

Cross - Self specificity			Number of genes	
			15 min	30 min
Cross-pollination / Self-pollination	>	2.0	3	122 (80)
Self-pollination / Cross-pollination	>	2.0	9	87

Of the 122 genes expressed more strongly at 30 min after cross-pollination, 42 genes were judged to have been expressed in pollen tubes that had penetrated the papilla cells.

Table 1-5. Genes expressed in papilla cells preferentially at 15 min after cross-pollination.

TAIR locus	Description	FC
AT3G22620	bifunctional inhibitor/lipid-transfer protein	2.4
AT4G30270	xyloglucan endotransglucosylase/hydrolase protein (XTH24)	2.5
AT2G07714	transcription factor-related protein	2.1

Genes are listed whose fold change (FC) was greater than 2.0.

Table 1-6. Genes expressed in papilla cells preferentially at 15 min after self-pollination.

TAIR locus	Description	FC	
AT4G24570	dicarboxylate carrier (DIC2)	2.1	
AT1G27730	zinc finger protein (STZ/ZAT10)	2.5	*
AT3G55980	salt-inducible zinc finger (SZF1)	3.2	*
AT5G42380	calmodulin-like protein (CML37)	2.1	*
AT5G17480	calmodulin-like protein (CML29)	2.3	
AT1G28480	glutaredoxin (GRX480)	2.4	
AT4G34410	ethylene-responsive transcription factor (ERF109)	2.1	
AT3G07830	polygalacturonase-like protein (PGA3)	2.2	
AT4G29780	unknown protein	2.2	

Genes are listed whose FC was greater than 2.0. Asterisks indicate comparably higher expression also at 30 min after self-pollination.

Chapter 2

Identification and functional analysis of an autoinhibited Ca^{2+}-ATPase, ACA13, that is required for cross-pollination

2-1 Introduction

In the microarray analysis in Chapter 1, several genes that have been reported to be up-regulated after a transient increase of $[Ca^{2+}]_{cyt}$ were expressed more strongly after self-pollination than after cross-pollination. This indicated that an increase of $[Ca^{2+}]_{cyt}$ occurs inside the papilla cell after self-pollination, which was indeed confirmed in a recent study in my laboratory. Iwano et al. performed $[Ca^{2+}]_{cyt}$ monitoring using Yellow Cameleon 3.60 (YC3.60), a Ca^{2+} indicator based on fluorescence resonance energy transfer (FRET) technology using cyan- and yellow-emitting fluorescent proteins (CFP and YFP) (Nagai et al., 2004). Measurement of $[Ca^{2+}]_{cyt}$ in the papilla cell from C24 expressing *SRK$_b$* and *YC3.60* showed that $[Ca^{2+}]_{cyt}$ in papilla cells rose rapidly when a self-pollen grain was applied, but not with a cross-pollen grain (M. Iwano et al., unpublished data) (Figure 2-1A). This elevation of $[Ca^{2+}]_{cyt}$ was also observed when SCR_b protein was added to protoplasts prepared from papilla cells of C24 expressing *SRK$_b$* and *YC3.60* (Ito, 2014). These findings indicated strongly that a Ca^{2+}-mediated signaling pathway acts after the SRK-SCR interaction to regulate the SI response in the papilla cell.

On the other hand, studies over decades have shown the importance of Ca^{2+} during cross-pollination; Ca^{2+} is required for pollen germination, and a tip-focused Ca^{2+} gradient is essential for pollen tube growth (reviewed by Steinhorst and Kudla, 2013). Previously, Ca^{2+} channels such as cyclic nucleotide-gated channel 18 (CNGC18), stretch-activated Ca^{2+} channels (SACs) and glutamate receptor-like channels (GLRs) were found to contribute to Ca^{2+} influx across the plasma membrane of the pollen tube (Dutta and Robinson, 2004; Frietsch et al., 2007; Michard et al., 2011). In my laboratory, a pollination assay using the membrane-impermeable Ca^{2+} indicator Calcium Green applied to the stigma surface was recently established to measure $[Ca^{2+}]$ in the extracellular environment of the papilla cell. An assay using *B. rapa* as well as C24 expressing *SRK$_b$* demonstrated that the intensity of Calcium Green fluorescence at the surface of the papilla cell increased shortly after

cross-pollination, which corresponds to the time of pollen germination, whereas no change was observed when a self-pollen grain was applied (Iwano et al., 2014; M. Iwano, unpublished data) (Figure 2-1B). Interestingly, this distinct behavior of fluorescence intensity on the papilla cell surface also occurred when cross- and self-pollen coat were applied instead whole pollen grains (Iwano et al., 2014). These data suggest strongly that Ca^{2+} is exported from the papilla cell only to a cross-pollen grain, and that this process is regulated by compatibility signaling.

These different Ca^{2+} dynamics of the papilla cell during cross- and self-pollination must be regulated precisely by a Ca^{2+} transporter(s), which is presumably activated by either compatibility or SI signaling. To identify a Ca^{2+} transporter(s) that functions in the papilla cell during cross- and self-pollination, I first searched for highly expressed Ca^{2+} transporter(s) in the microarray data, selected an autoinhibited Ca^{2+}- ATPase, ACA13, as a candidate, and then performed functional analyses during cross- and self-pollination.

2-2 Materials and Methods

All chemicals and reagents used in this work were obtained from the companies Wako and Nakalai Tesque, unless otherwise specified in the text.

Multiple sequence alignment and phylogenetic analysis

Amino acid sequences of the type IIB Ca^{2+}-ATPases ACAs and endoplasmic reticulum (ER)-type calcium ATPase (ECA) 1, obtained from The Arabidopsis Information Resource (TAIR), were aligned using Clustal W 2.1 (Larkin et al., 2007) with the Gonnet matrix (Gonnet et al., 1992) for evaluating evolutionary divergence (http://www.ebi.ac.uk/Tools/msa/clustalw2/). The type IIA Ca^{2+}-ATPase ECA1 was used as an outgroup of ACAs, which belong to the other group, type IIB (Geisler et al., 2000). A phylogenetic tree was generated by the neighbor-joining method (Saitou and Nei, 1987) using MEGA 6 software (Tamura et al., 2013). Evolutionary distances were computed by the Poisson correction method (Zuckerkandl and Pauling, 1965), and are displayed as branch length. A bootstrap test (Felsenstein, 1985) with 2000 replicates was performed, and the bootstrap values were calculated as percentages.

Heat map visualization of gene expression

An expression heat map of ACA family members was created with Excel (Microsoft), based on the normalized expression levels in positive real numbers from microarray data in Chapter 1.

Plant materials and growth conditions

A. thaliana plants with either a C24 background or a Columbia accession (Col-0) background were used in this study. Col-0 WT and Col-0 expressing *ACA13:ß-glucuronidase* (*GUS*) were grown to observe ACA13 expression. ACA13 mutant lines from the C24 TILLING library were backcrossed twice with C24 expressing *ΨSRK:SRK$_b$* and *BrS$_9$-SRK:YC3.60*, and then selfed to obtain homozygous and wild type plants expressing *SRK$_b$* and *YC3.60* (*aca13*/*aca13* and *ACA13*/*ACA13*) in the BC_2F_2 generation (Nagai et al., 2004; Kanatani, 2008; Ito, 2014). C24 WT and C24 expressing *BrS$_9$-SP11:SCR$_b$* and *ΨSRK:SRK$_b$* (Takehisa, 2009) (C24 SI) were grown as pollen donors for cross- and self-pollination. C24 expressing *ΨSRK:SRK$_b$* and *BrS$_9$-SRK:ACA13-Venus*, and Col-0 expressing *BrSLG:ACA13-Venus* were used to analyze ACA13 localization (Kanatani, 2008; Yakabe, 2009). Point mutations were confirmed by sequencing PCR fragments amplified from genomic DNA with EX Taq (TaKaRa) polymerase and the primer pairs listed in Supplemental Table 1. *SRK$_b$*, *SCR$_b$* and *YC3.60* inserts were checked by PCR amplification with KAPA Taq (Kapa Biosystems) polymerase and the primer pairs also listed in Supplemental Table 1. SI was checked by pollination test using aniline blue staining, and *YC3.60* and *ACA13-Venus* insertions were confirmed by fluorescence observation with a confocal microscope (LSM 710, Carl Zeiss) excited with either 440-nm or 514-nm light. All plants were grown at 23°C under 14 h light and 10 h dark in a growth chamber.

Histochemical localization of *GUS* expression

From Col-0 expressing *GUS* fused with 1,940 bp upstream of the *ACA13* start codon including the *ACA13* promoter sequence, 3-week-old plants, flower buds and flowers were collected, and incubated in a 4-chloro-3-indolyl ß-D-glucuronic acid (X-glu) solution (2 mM X-glu and 50 mM phosphate buffer, pH 7.0) at 37°C for 18 h. The samples were washed four times with 70-100% ethanol, and observed with a zoom stereo microscope (SZH10, Olympus).

RT-PCR

Total RNA was extracted from stigmas and other tissues of Col-0 WT with an RNeasy Plant Mini Kit (QIAGEN) according to the manufacturer's protocol. Approximately 50 ng DNase-treated total RNA was used for cDNA synthesis using Oligo(dT)$_{12-18}$ Primer and SuperScript III reverse transcriptase (Invitrogen) according to the manufacturer's protocol. PCR was performed for 35 cycles using KAPA Taq (Kapa Biosystems) polymerase. As an expression control, *actin 8* (*ACT8*, *AT1g49240*) was used. The sequences of the primer pairs are shown in Supplemental Table 1.

TILLING screening

An *A. thaliana* C24 TILLING library containing 3509 ethyl methanesulfonate (EMS)-mutagenized lines was screened for mutants of ACA13 according to the methods described by Lai et al. (2012) with minor modifications. The following three GeneScan primer pairs (Applied Biosystems) labeled with 6-FAM (forward) or VIC (reverse) fluorescent dye were designed to cover the full-length *ACA13* sequence, which is 3054 bp long and has no introns: (i) ACA13-1F Tilling and ACA13-1R Tilling (T_m 53°C) for amplification between 93 bp upstream and 1159 bp downstream of the start codon; (ii) ACA13-2F Tilling and ACA13-2R Tilling (T_m 54 °C) for amplification between 938 bp and 2161 bp downstream of the start codon; and (iii) ACA13-3F Tilling and ACA13-3R Tilling (T_m 52°C) for amplification between 1946 bp and 3170 bp downstream of the start codon. The sequences of the primer pairs are shown in Supplemental Table 1. The fragments were amplified from genomic DNA template by [94°C for 3 min, 8 cycles of (94°C for 30 sec, T_m+4°C - T_m-3°C {diminished by 1°C per cycle} for 30 sec, 72°C for 90 sec), and 22 cycles of (94°C for 30 sec, T_m-2°C for 30 sec, 72°C for 90 sec), 72°C for 7 min]. The PCR fragments were treated with CEL1 SURVEYOR nuclease (Transgenomic), and mutations were detected by fragment analysis with GeneMapper 4.0 (Applied Biosystems).

Aniline blue staining of pollen tubes

Pollen tube growth in the pistil of the mutant lines was examined by aniline blue staining of callose, a major component of the pollen tube cell wall, as described by Kho and Baër (1968) and Kakita (2007) with minor modifications. Flowers in stage 13 (Smyth et al., 1990), from which petals and anthers had been removed one day before, were collected and pollinated with pollen from C24 WT or C24 SI. Two hours after pollination, the pistils were

fixed in 75% ethanol : 25% acetic acid at room temperature (RT) overnight. The fixative solution was replaced with 1 N NaOH and the samples incubated at 60°C for 25 min, after which the NaOH was removed and the pistils were stained with aniline blue solution (2% w/v aniline blue and 2% w/v K_3PO_4) in the dark at RT for two hours. The stained pistils were fixed on a glass slide with 70% glycerol, and pollen tube growth was observed using a UV filter with 365-nm excitation under an Axiophoto2 fluorescence microscope (Carl Zeiss) with Axio Vision Rel.4.7 imaging software (Carl Zeiss).

Pollination assay

Flowers in stage 13 (Smyth et al., 1990), from which petals and anthers had been removed one day before, were collected from *ACA13*/*ACA13* and *aca13*/*aca13* plants, and the pistils were fixed on a cover slip. A piece of 1% agar was placed on the pistils to prevent desiccation. Using a micromanipulator (Narishige), pollen grains from C24 WT were applied individually to the papilla cells, and the timing of pollen germination and pollen tube penetration was monitored with an Axiovert 135 light microscope (Carl Zeiss).

$[Ca^{2+}]_{cyt}$ monitoring (YC3.60 ratiometric imaging)

Flowers in stage 13 (Smyth et al., 1990), from which petals and anthers had been removed one day before, were collected from *ACA13*/*ACA13* and *aca13*/*aca13* plants. These plants were expressing SRK_b and *YC3.60*. The pistils were mounted on a cover slip, and a piece of 1% agar was placed on the pistils to prevent desiccation. For observation of $[Ca^{2+}]_{cyt}$ after self-pollination, a C24 SI pollen grain was applied to a papilla cell using a micromanipulator (Narishige). With a confocal microscope (LSM 710, Carl Zeiss) excited with 440-nm light, using a Plan Apo 20×/0.8 objective lens, emission of cyan (CFP, 481 nm) and yellow (YFP, 530 nm) fluorescence in papilla cells were measured every 1 min, and the YFP/CFP ratio was calculated.

Calcium Green assay

Flowers in stage 13 (Smyth et al., 1990), from which petals and anthers had been removed one day before, were collected from *ACA13*/*ACA13* and *aca13*/*aca13* plants. A drop of 10 μM Calcium Green (Calcium Green 5N, hexapotassium salt, Molecular Probes) solution containing 0.005% Tween 20 was placed on the stigmas, which were then air-dried for 30 min. The pistils were mounted on a cover slip, and a piece of 1% agar was placed on

the pistils to prevent desiccation. A pollen grain from either a C24 WT or a C24 SI plant was applied to a papilla cell using a micromanipulator (Narishige). The sample was observed with an LSM 510 META confocal microscope (Carl Zeiss) excited with 488-nm light using a Plan Apo 20×/0.8 objective lens. Fluorescence images were collected every 1 min at a fluorescence emission of 525 nm.

Live-cell imaging of ACA13 localization

Flowers in stage 13 (Smyth et al., 1990), from which petals and anthers had been removed one day before, were collected from C24 expressing *SRK$_b$* and *ACA13-Venus*, and mounted on a cover slip. Venus fluorescence in papilla cells was observed with a confocal microscope (LSM 710, Carl Zeiss) excited with 514-nm light, using a Plan Apo 20×/0.8 objective lens. Fluorescence emission of 570 nm was captured. For observation of ACA13-Venus before pollination, the pistils were immersed in water to obtain clear images. For observation of ACA13 localization after pollination, a piece of 1% agar was placed on the pistils to prevent desiccation. A C24 WT or C24 SI pollen grain was applied to a papilla cell using a micromanipulator (Narishige), and fluorescence images were collected.

Immune electron microscopy

Stigmas before and after pollination were collected from Col-0 expressing *ACA13-Venus*, and rapidly frozen (KF80, Leica). Subsequently, the samples were treated with an acetone solution containing 0.01% OsO_4 at -80°C for 3 days, and then brought slowly to room temperature and embedded in Spurr's resin. Ultrathin sections were cut and mounted on Formvar-covered nickel grids. Sections were incubated with 3% hydrogen peroxide solution for 30 min and washed with distilled water. After blocking with 0.1% gelatin in PBST (PBS containing 0.05% Tween 20), the sections were incubated with rabbit anti-GFP antibody (Secant Chemicals) and then with 15-nm gold-conjugated goat anti-rabbit IgG (Biocell Research Laboratories). After immunolabeling, the sections were stained with uranyl acetate and lead citrate. As a cytochemical control, specimens were incubated without primary antibody or with non-immune rabbit IgG. Samples were observed with a transmission electron microscope (H-7100, Hitachi).

2-3 Results

Search for a Ca^{2+} transporter that functions in the papilla cell during cross- and self-pollination

Ca^{2+} transporter(s) must be responsible for the different Ca^{2+} dynamics observed in the papilla cell during cross- and self-pollination. To identify Ca^{2+} transporter(s) that export Ca^{2+} from the papilla cell during cross-pollination, and that increase $[Ca^{2+}]_{cyt}$ in the papilla cell after self-pollination, I first searched for candidates using the microarray data described in Chapter 1. Because of the generally low $[Ca^{2+}]_{cyt}$ relative to the high electrochemical potential including $[Ca^{2+}]$ in the extracellular space, Ca^{2+} efflux from the cytoplasm occurs via an energized system (reviewed by Dodd et al., 2010). *A. thaliana* possesses three families of proteins involved in energized Ca^{2+} transport: ACAs, which are similar to the animal calmodulin (CAM)-stimulated Ca^{2+}-ATPases (PMCAs), ECAs, and calcium-proton exchangers (CAXs) (reviewed by Dodd et al., 2010). Of these, I focused on ACAs because of their mode of regulation. As well as the 10 transmembrane-spanning domains, ACAs have an N-terminal auto-inhibited regulatory domain, which contains CAM-binding domains and phosphorylation sites (Geisler et al., 2000) (Figure 2-2). CAM binding to the CAM-binding domains activates ACAs as Ca^{2+} pumps, which transport Ca^{2+} from the cytosol to intracellular Ca^{2+} stores such as the vacuole or ER, or to extracellular space (Bonza and De Michelis, 2010). An x-ray protein structure analysis combined with Ca^{2+} pump activity tests showed that ACA8 possesses two CAM-binding domains, and displays Ca^{2+} pump activity that is regulated by a two-step mechanism (Tidow et al., 2012) (Figure 2-3). Phosphorylation of serine residues, on the other hand, inhibits the activity of ACAs (Hwang et al., 2000, Giacometti et al., 2012) (Figure 2-3). Hwang et al. (2000) and Giacometti et al. (2012) have determined regulatory phosphorylation sites using the yeast strain K616 expressing *ACA2* or *ACA8* mutants in which serine residues were mutated to aspartate to mimic phosphorylation. These phosphorylation sites are apparently not conserved between ACA2 and ACA8 (Figure 2-3). From these structural features, I hypothesized that ACA(s) at the plasma membrane of the papilla cell are activated by CAM binding in cross-pollination, which must be controlled by compatibility signaling, to export Ca^{2+} to the cross-pollen grain. Further, I speculated that ACA(s) are inactivated in self-pollination by phosphorylation of serine residues at the N terminus, which must be triggered by an SI phosphorylation signaling cascade, to inhibit Ca^{2+}

export to the pollen grain, and that this inhibition causes $[Ca^{2+}]_{cyt}$ elevation in the papilla cell (Figure 2-4).

A. thaliana possesses 10 ACAs, as shown in the phylogenetic tree in Figure 2-5. To select candidate transporter(s), I investigated expression of the 10 *ACA*s from the microarray analysis described in Chapter 1. Expression of *ACA13* was remarkably high in papilla cells before pollination compared to that of the other *ACA* members, and it was further induced after both cross- and self-pollination (Figure 2-6). In addition, expression of *ACA1* and *ACA11* showed a similar pattern to that of *ACA13*, although their expression levels were lower. In a microarray analysis using stigmas of self-compatible Col-0, *ACA1* and *ACA13* were induced after pollination and treatment with pollen coat from WT pollen (Moriyama, 2007). However, ACA1 is reportedly localized to plastids or the ER, and ACA11 to the vacuole, making them unlikely to be strong candidates for my hypothesis (Huang et al., 1993; Dunkley et al., 2006; Lee et al., 2007). Although the localization and function of ACA13 are unknown, the microarray analyses clearly implied that ACA13 is involved in the pollination process. I therefore focused on ACA13.

Complementation test of ACA13 function as a Ca^{2+} pump

For investigation of ACA13 function, it was crucial to examine whether ACA13 displays Ca^{2+} pump activity. A complementation test using the yeast strain K616 was performed in collaboration with Dr. Hideki Nakayama and Dr. Pulla Kaothien-Nakayama at Nagasaki University. The mutant strain K616 lacks both of its own Ca^{2+}-transporting P-type ATPases, PMC1 and PMR1, which transport Ca^{2+} with high affinity from the cytoplasm to the vacuole and the Golgi complex, respectively (Cunningham and Fink, 1994; Geisler et al., 2000). K616 also lacks calcineurin subunit B-type 1 (CNB1), which inhibits another Ca^{2+} efflux transporter, vacuolar H^+/Ca^{2+} antiporter 1 (VCX1), with low affinity (Cunningham and Fink, 1994; Geisler et al., 2000) (Figure 2-7A). These Ca^{2+} transporters are thought to regulate $[Ca^{2+}]_{cyt}$ homeostasis in yeast; K616 can grow on high-Ca^{2+} medium because of VCX1, but it fails to grow on Ca^{2+}-depleted medium unless an exogenous high-affinity Ca^{2+} pump such as ACA is introduced (Geisler et al., 2000) (Figure 2-7B). To test whether Ca^{2+} pump activity in K616 is complemented by exogenous ACA13, *ACA13* was expressed under the *GAL1* promoter, which up-regulates expression of *ACA13* in the presence of galactose, but not on medium containing glucose (Flick and Johnston, 1990; Geisler et al., 2000). ACA9 was used as a positive control because its function as a Ca^{2+} pump has already been

confirmed by complementation tests using K616 (Schiøtt et al., 2004). By expressing Δ*N-ACA13*, which lacks the 65 N-terminal amino acid residues including the predicted auto-inhibited regulatory domain (see Figure 2-3) and thus yields constitutively active ACA13, K616 grew on Ca^{2+}-depleted medium, whereas K616 expressing full-length *ACA13* or harboring empty vector failed to do so (Figure 2-7B). From this result, the function and activation of ACA13 as a Ca^{2+} pump were confirmed, as it has been for ACA8 and ACA9, whose activation is probably controlled by CAM-binding. In further experiments, ACA13-Venus was also confirmed to function as a Ca^{2+} pump (Iwano et al., 2014).

Expression of *ACA13*

In the microarray analysis, *ACA13* was shown to be expressed highly in the papilla cell, and to be further up-regulated after pollination. To examine the tissue distribution of ACA13 protein in *A. thaliana*, I performed a *GUS* reporter gene assay using Col-0. *GUS* expression under the control of the *ACA13* promoter was mainly observed in the stigma and anther, but also in young leaves and in the root tip region (Figure 2-8A and B). *GUS* expression in the stigma was low at stage 12, but rose at the early stage of flower stage 13, shortly before the stigmas were pollinated naturally and the elevated expression persisted until after pollination (Figure 2-8A). To confirm these results, the expression pattern of *ACA13* mRNA was evaluated by RT-PCR, using *ACA13*-specific primers. Although expression of *ACA13* was also observed in pollen, ovary and leaves, expression in the stigma was higher than that in these organs (Figure 2-8C). Furthermore, in situ hybridization performed by Moriyama (2007) showed that *ACA13* is expressed in papilla cells before pollination, and that the expression increased after pollination not only in the papilla cells but also in the transmitting tract where pollen tubes subsequently grow (Figure 2-8D). These data suggest that ACA13 is a Ca^{2+} transporter expressed highly in the stigma before and during cross-pollination.

Screening and establishment of ACA13 mutant lines from a TILLING collection

To obtain mutant lines of ACA13 for phenotype observation, I screened a C24 TILLING library which was recently established in my laboratory and contains 3,509 EMS-mutagenized lines in the M_2 generation (Lai et al., 2012). Because the full-length genomic sequence of *ACA13* is 3054 bp, point mutations were screened in three overlapping sections of about 1200 bp each. I identified three nonsense mutants whose amino acids at

positions 56 (arginine, R), 315 (tryptophan, W) and 836 (glutamine, Q) had changed to stop codons; 33 missense mutants which had an amino acid change; and 20 sense mutants without an amino acid change (Figure 2-9). I used the three nonsense mutant lines (R56X, W315X and Q836X) for further investigations.

If ACA13 functions in the reproduction process, homozygous plants of these mutant lines may show some defect in their fertility. While homozygous plants in the M_3 populations of the W315X and Q836X lines grew normally and were fertile, homozygous mutant plants in the M_2 population of the R56X line showed reduced growth and were sterile (Figure 2-10). To investigate closely the participation of ACA13 in the pollination process, I obtained heterozygous plants of the R56X line in the M_2 population, which grew normally and were fertile, and backcrossed one of them (plant No. 3) with C24 expressing *SRK$_b$* and *YC3.60* to allow phenotype observation and $[Ca^{2+}]_{cyt}$ monitoring during self-pollination. In the BC_1F_2 generation, R56X mutant plants segregated into homozygous, heterozygous and wild type. The dwarf and sterile phenotype was visible again; however, one of 18 homozygous plants showed normal growth and fertility, and also one of 14 wild type plants displayed the dwarf and sterile phenotype. These results indicate that a point mutation in another gene that is linked closely to *ACA13* on the genome caused the dwarf and sterile phenotype in the R56X mutant line. I backcrossed the only homozygous plant showing normal growth (plant No. 24) with C24 expressing *SRK$_b$* and *YC3.60* for the second time, and obtained a segregating population in the BC_2F_2 generation after selfing. For the W315X and Q836X lines, I also backcrossed the mutant plants twice with C24 expressing *SRK$_b$* and *YC3.60* and generated *ACA13*/*ACA13* and *aca13*/*aca13* plants in the BC_2F_2 generation (Figure 2-10).

Phenotype of ACA13 nonsense mutant lines

Using *ACA13*/*ACA13* and *aca13*/*aca13* plants, I examined their phenotypes closely. Although plant growth did not differ between *ACA13*/*ACA13* and *aca13*/*aca13* plants, silique length was significantly ($P < 0.01$ for the R56X and Q836X lines, and $P < 0.05$ for the W315X line) reduced in *aca13*/*aca13* plants compared to *ACA13*/*ACA13* plants (Figure 2-11A and B). In addition, *aca13*/*aca13* plants of all three mutant lines showed a significantly ($P < 0.01$) lower number of seeds per silique than *ACA13*/*ACA13* plants (Figure 2-11C). These results are consistent with that using a Col-0 T-DNA line having a disrupted *ACA13*, which showed diminished seed set (Iwano et al., 2014).

To investigate the cause of reduced fertility, I next performed aniline blue staining of growing pollen tubes at two hours after manual cross-pollination using C24 WT pollen. However, in both *ACA13*/*ACA13* and *aca13*/*aca13* pistils, pollen tube growth was visually indistinguishable (Figure 2-12). Additionally, after self-pollination using C24 SI pollen, no pollen tube growth was observed in either *ACA13*/*ACA13* or *aca13*/*aca13* pistils, demonstrating that SI is intact in these mutant lines (Figure 2-12).

Because ACA13 was being expressed at a high level in the papilla cell prior to pollination, it is likely that the reduced seed set of *aca13*/*aca13* plants was caused by some disfunction of the papilla cell at an early time after cross-pollination. To analyze the behavior of the ACA13 mutant papilla cell during pollen germination and pollen tube penetration, I performed a pollination assay with the W315X line. Pollen grains from C24 WT were applied to papilla cells from *ACA13*/*ACA13* and *aca13*/*aca13* plants, and germinated pollen and papilla cell-penetrating pollen tubes were counted every 5 min for 30 min. On *aca13*/*aca13* papilla cells, pollen germination was delayed compared to *ACA13*/*ACA13* papilla cells. At 30 min after pollination, only about 80% of pollen grains had germinated on *aca13*/*aca13* papilla cells, whereas the germination rate was almost 100% on *ACA13*/*ACA13* papilla cells (Figure 2-13A). Pollen tube penetration was correspondingly delayed on *aca13*/*aca13* papilla cells: the penetration rate at 30 min after pollination was only about 50%, whereas it was about 90% on *ACA13*/*ACA13* papilla cells (Figure 2-13B). These results indicate that ACA13 functions in the papilla cell during pollen germination and pollen tube penetration.

Monitoring of $[Ca^{2+}]_{cyt}$ in the papilla cell

Ca^{2+} pump activity of ACA13 may affect $[Ca^{2+}]_{cyt}$ in the papilla cell. To quantify $[Ca^{2+}]_{cyt}$ inside the papilla cell, I performed Ca^{2+} imaging of the W315X mutant line expressing SRK_b and *YC3.60* under the papilla cell-specific BrS_9-*SRK* promoter. Using a confocal leaser microscope, CFP and YFP fluoresence intensities were measured in the upper part of the papilla cell, where pollen grains usually adhere. The YFP/CFP ratio before pollination was significantly ($P < 0.01$) higher in *aca13*/*aca13* papilla cells than in *ACA13*/*ACA13* papilla cells, indicating high $[Ca^{2+}]_{cyt}$ in the *aca13*/*aca13* papilla cells (Figure 2-14). This result suggests that ACA13 is already transporting Ca^{2+} from the cytoplasm to intracellular Ca^{2+} stores or to extracellular space before pollination. Next, to determine $[Ca^{2+}]_{cyt}$ dynamics during self-pollination, I measured YFP/CFP ratios in *ACA13*/*ACA13* and *aca13*/*aca13* papilla cells immediately under the applied pollen grain, every 1 min for 15 min

after self-pollination. The pattern that $[Ca^{2+}]_{cyt}$ increases shortly after self-pollination was repeatedly observed in both *ACA13*/*ACA13* and *aca13*/*aca13* papilla cells (Figure 2-15A and B). Furthermore, no perceptible differences were observed in the elevation of $[Ca^{2+}]_{cyt}$ between *ACA13*/*ACA13* and *aca13*/*aca13* papilla cells after application of self-pollen grains, suggesting that ACA13 is unlikely to participate in $[Ca^{2+}]_{cyt}$ elevation in the papilla cell in the SI response (Figure 2-15C).

Monitoring of $[Ca^{2+}]$ at the surface of the papilla cell

Disruption of *ACA13* demonstrated that ACA13 functions during pollen germination and pollen tube penetration. To investigate whether the delayed pollen germination on the *aca13*/*aca13* papilla cell is caused by reduced Ca^{2+} export from the papilla cell to the pollen grain, I performed a Calcium Green assay using the W315X line. The membrane-impermeable Ca^{2+} indicator Calcium Green 5N was prepared as described in Materials and Methods, and applied to the stigma. After air-drying for 30 min, pollen grains were applied, and, using a confocal laser microscope, fluorescence intensity at the surface of the papilla cell immediately under the applied pollen grain was measured every 1 min for 30 min. After cross-pollination, fluorescence intensity on *ACA13*/*ACA13* papilla cells increased within 15 min, shortly before the pollen grains germinated, whereas the increase on *aca13*/*aca13* papilla cells was weaker and slower (Figure 2-16A). These different patterns between *ACA13*/*ACA13* and *aca13*/*aca13* papilla cells after cross-pollination were also observed between papilla cells of Col-0 WT and of the Col-0 T-DNA line containing homozygously disrupted *ACA13* (Iwano et al., 2014). The relative intensity at 15 min after pollination was significantly lower at the surface of *aca13*/*aca13* papilla cells than of *ACA13*/*ACA13* papilla cells (Figure 2-16B). After self-pollination, the fluorescence intensity did not change on either *ACA13*/*ACA13* or *aca13*/*aca13* papilla cells, indicating that Ca^{2+} transport form the papilla cell is inhibited completely (Figure 2-16C). These findings demonstrate that ACA13 exports Ca^{2+} from the papilla cell to the pollen grain only during cross-pollination.

Subcellular localization of ACA13

To understand the behavior of ACA13 during cross- and self-pollination, I monitored the subcellular localization of ACA13 by confocal laser microscopy. ACA13 fused with the yellow fluorescent protein Venus, a variant of green fluorescent protein (GFP), was expressed under the control of the *BrS9-SRK* promoter in C24 with SRK_b (Nagai et al., 2002). First, I

observed papilla cells before pollination that were immersed in water to obtain clear images. ACA13-Venus fluorescence was detected near the papilla cell plasma membrane and also as individual dot-like signals (Figure 2-17A and B) (Yakabe, 2008). Next, I monitored ACA13-Venus in the papilla cell during cross- and self-pollination. After cross-pollination, when the pollen grain germinated, ACA13-Venus signals were observed directly under the pollen tube penetration site, and when the pollen tube was growing in the papilla cell, ACA13-Venus signals accumulated around the pollen tube. In contrast, no such changes were observed when a self-pollen grain was attached (Figure 2-17C and D).

In addition, localization of ACA13 before and during cross-pollination was examined by immune electron microscopy with *A. thaliana* Col-0 expressing ACA13-Venus under the control of the ACA13 promoter. ACA13-Venus signals were detected with rabbit anti-GFP antibody as the primary antibody and 15-nm gold particle-conjugated goat anti-rabbit antibody as the secondary antibody. Before pollination, ACA13-Venus signals were mainly detected at the plasma membrane and on vesicles near the Golgi apparatus (Figure 2-18A to C). However, at 20 min after pollination, when the pollen tube was growing in the papilla cell wall, ACA13-Venus signals were abundant at regions of the plasma membrane associated with the pollen tube (Figure 2-18D and E). The average number of gold particles was 3.4 particles/μm, which was significantly ($P < 0.005$) higher than that before pollination (1.1 particles/μm).

These findings from live-cell imaging and immune electron microscopy experiments indicate that ACA13 is localized at the plasma membrane and on vesicles before pollination, and accumulates only during cross-pollination at the pollen tube penetration site to supply Ca^{2+} to pollen and the pollen tube.

2-4 Discussion

Previously, functions of several ACAs have been reported. From morphological phenotypes of *aca8* and *aca10* mutants, ACA8 and ACA10 are thought to have a role in plant development, and they appear also to act in plant immunity as positive regulators in early microbe-associated molecular pattern responses (George et al., 2008; Frei dit Frey et al., 2012). ACAs also function in plant reproduction. *ACA7* is expressed strongly in anther and pollen, and *aca7* mutants produced sterile pollen grains, suggesting that ACA7 has a role in

pollen development (Lucca and León, 2012). *ACA9* is also expressed specifically in anthers and pollen grains. Disruption of *ACA9* resulted in reduced fertility caused by defective pollen tube growth and failure to release sperm cells (Schiøtt et al., 2004).

In this study, I investigated the function of ACA13 in the papilla cell during cross- and self-pollination, in relation to Ca^{2+} dynamics. FRET-based Ca^{2+} monitoring using YC3.60 showed that $[Ca^{2+}]_{cyt}$ before pollination was significantly higher in papilla cells of *aca13*/*aca13* than of *ACA13*/*ACA13* plants, suggesting that ACA13 begins to transport Ca^{2+} from the cytoplasm before pollination. After self-pollination, the elevation of $[Ca^{2+}]_{cyt}$ in the papilla cell was not different between *ACA13*/*ACA13* and *aca13*/*aca13* plants, implying that ACA13 is not involved in $[Ca^{2+}]_{cyt}$ elevation during self-pollination. ACAs are thought to have a crucial role in the re-establishment of $[Ca^{2+}]_{cyt}$ after its stimulus-induced rise (Bonza and De Michelis, 2010). If ACA13 functions to maintain the $[Ca^{2+}]_{cyt}$ after its increase in self-pollination, $[Ca^{2+}]_{cyt}$ would be expected to decrease faster in *ACA13*/*ACA13* than in *aca13*/*aca13* papilla cells. However, the $[Ca^{2+}]_{cyt}$ dynamics did not differ markedly between *ACA13*/*ACA13* and *aca13*/*aca13*, and, moreover, a Calcium Green assay indicated that Ca^{2+} efflux to the papilla cell surface did not occur during self-pollination, suggesting that ACA13 is inactivated via phosphorylation during self-pollination. Frei dit Frey et al. (2012) used a BiFC assay to demonstrate that ACA8 interacts with the plasma membrane-resident receptor kinase FLS2, whose interaction with bacterial flg22 is known to trigger a Ca^{2+}-mediated signaling cascade in plant immunity. It is possible that ACA13 is inactivated through a direct interaction with SRK during self-pollination. From this study, ACA13 is unlikely to contribute to $[Ca^{2+}]_{cyt}$ elevation in the papilla cell during self-pollination. However, a recent study in my laboratory showed that two Ca^{2+} channels, GLR3.5 and GLR3.7, which are highly expressed in papilla cells, contribute to Ca^{2+} influx into the papilla cell cytoplasm, and are thus at least partly responsible for the increase of $[Ca^{2+}]_{cyt}$ after self-pollination (Ito, 2014).

This study demonstrated that ACA13 in the papilla cell functions to export Ca^{2+}, which is required for pollen germination and pollen tube growth, to the cross-pollen grain, and is therefore crucial for fertility. However, the Calcium Green assay indicated that Ca^{2+} transport from *aca13*/*aca13* papilla cells was only delayed, and not inhibited totally, indicating that other ACA member(s) can complement the loss of ACA13 (Figure 2-16A). Although the phylogenetic analysis revealed that ACA12 has the highest (67%) amino acid identity with ACA13 among the ten *A. thaliana* ACAs (Figure 2-5), double disruption of

ACA12 and *ACA13* using T-DNA lines did not show any additional reduction in seed setting (Iwano et al., 2014). This may be explained by the microarray data, which demonstrate that expression of ACA12 in papilla cells is indeed very low (Figure 2-6). Even though the amino acid identity between ACA13 and either ACA1 or ACA11 is lower (both 46%), ACA1 and ACA11 both showed a similar expression pattern to that of ACA13, and both may thus contribute to Ca^{2+} export from the papilla cell.

Although ACAs are similar to animal PMCAs, which localize to the plasma membrane, localization of ACAs is more variable and includes not only the plasma membrane (ACA8, 9 and 10) but also the ER (ACA2) and the vacuole (ACA4 and 11) (reviewed by Bonza and De Michelis, 2010). ACA13 was observed to be localized to the plasma membrane and to vesicles near the Golgi apparatus before pollination, and ACA13-Venus signals accumulated at the pollen tube penetration site of the papilla cell and then around the pollen tube during cross-pollination (Figure 2-17, 2-18). During self-pollination, no accumulation of ACA13-Venus was observed in the papilla cell, suggesting that vesicular transport of ACA13 does not occur. Different actin structures in the papilla cell were reported during cross- and self-pollination (Iwano et al., 2007), which may have a role in this vesicle transport. Actin polymerization is required for cytoplasmic streaming, and affects vesicle trafficking (Simon and Pon, 1996; Cheung et al., 2010), whereas actin depolymerization is thought to be regulated by Ca^{2+} signaling (Vantard and Blanchoin, 2002; Pei et al., 2012).

From these findings, I propose the following model for the function of ACA13 (Figure 2-19). The microarray data suggests that *ACA13* expression in the papilla cell is accelerated after pollination, presumably by compatibility signaling from pollen coat. The live-cell imaging and the immune electron microscopy of the papilla cell before pollination indicated that ACA13 is localized to the plasma membrane and to vesicles. Furthermore, these vesicles possibly serve as intracellular Ca^{2+} stores, because monitoring of $[Ca^{2+}]_{cyt}$ in the papilla cell indicated that ACA13 already exports Ca^{2+} from the cytoplasm before pollination. Monitoring of ACA13 localization demonstrated that ACA13 accumulates immediately under the pollen grain during cross-pollination, presumably via compatibility signaling to supply the Ca^{2+} that is required for pollen germination. $[Ca^{2+}]$ at the surface of the papilla cell increased rapidly before pollen germination, suggesting that Ca^{2+} is released directly from the vesicular Ca^{2+} stores after fusion with the plasma membrane. ACA13 also accumulates around the growing pollen tube after pollen tube penetration into the papilla cell.

In self-pollination, although the increase of $[Ca^{2+}]_{cyt}$ in the papilla cell probably occurs via GLRs, Ca^{2+} efflux to the surface of the papilla cell did not take place at all, thus suggesting that ACA13 at the plasma membrane is inactivated, possibly via phosphorylation at its N terminus. After self-pollination, ACA13 did not accumulate under the pollen grain, perhaps because vesicle transport is inhibited by actin filament depolymerization in the papilla cell induced by Ca^{2+}-mediated SI signaling.

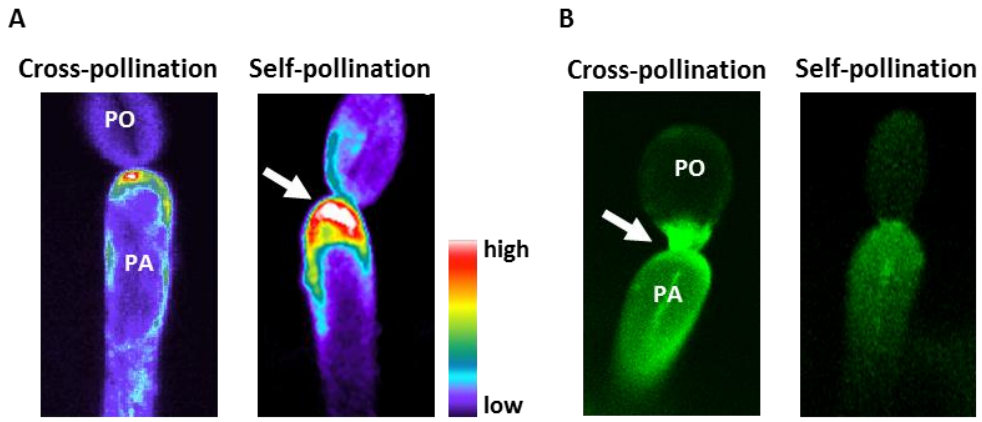

Figure 2-1. Ca^{2+} dynamics during cross- and self-pollination (M. Iwano et al., unpublished data).

(**A**) Fluorescence images in pseudo color using Yellow Cameleon (YC3.60), showing $[Ca^{2+}]_{cyt}$ in the papilla cells at 10 min after cross- or self-pollination.

(**B**) Calcium Green fluorescence images of Ca^{2+} at the surface of the papilla cell at 15 min after cross- or self-pollination.

Arrows show high $[Ca^{2+}]$. PO, pollen grain; PA, papilla cell.

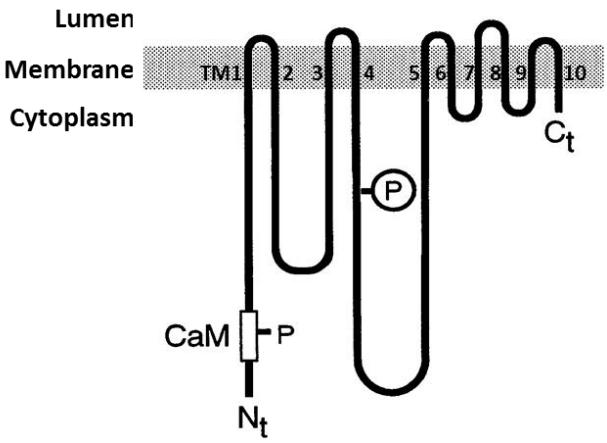

Figure 2-2. Structure of auto-inhibited Ca^{2+}-ATPases.

Schematic structure of type IIB-Ca^{2+}-ATPases of plants (modified from Geisler et al., 2000) with 10 transmembrane domains (TM1-10), a phosphorylated aspartate residue (encircled P) and a regulatory domain (white box) including CAM-binding domain(s) (CaM) and phosphorylation site(s) (P). Protein length: 1014 - 1086 aa. Nt, N terminus; Ct, C terminus.

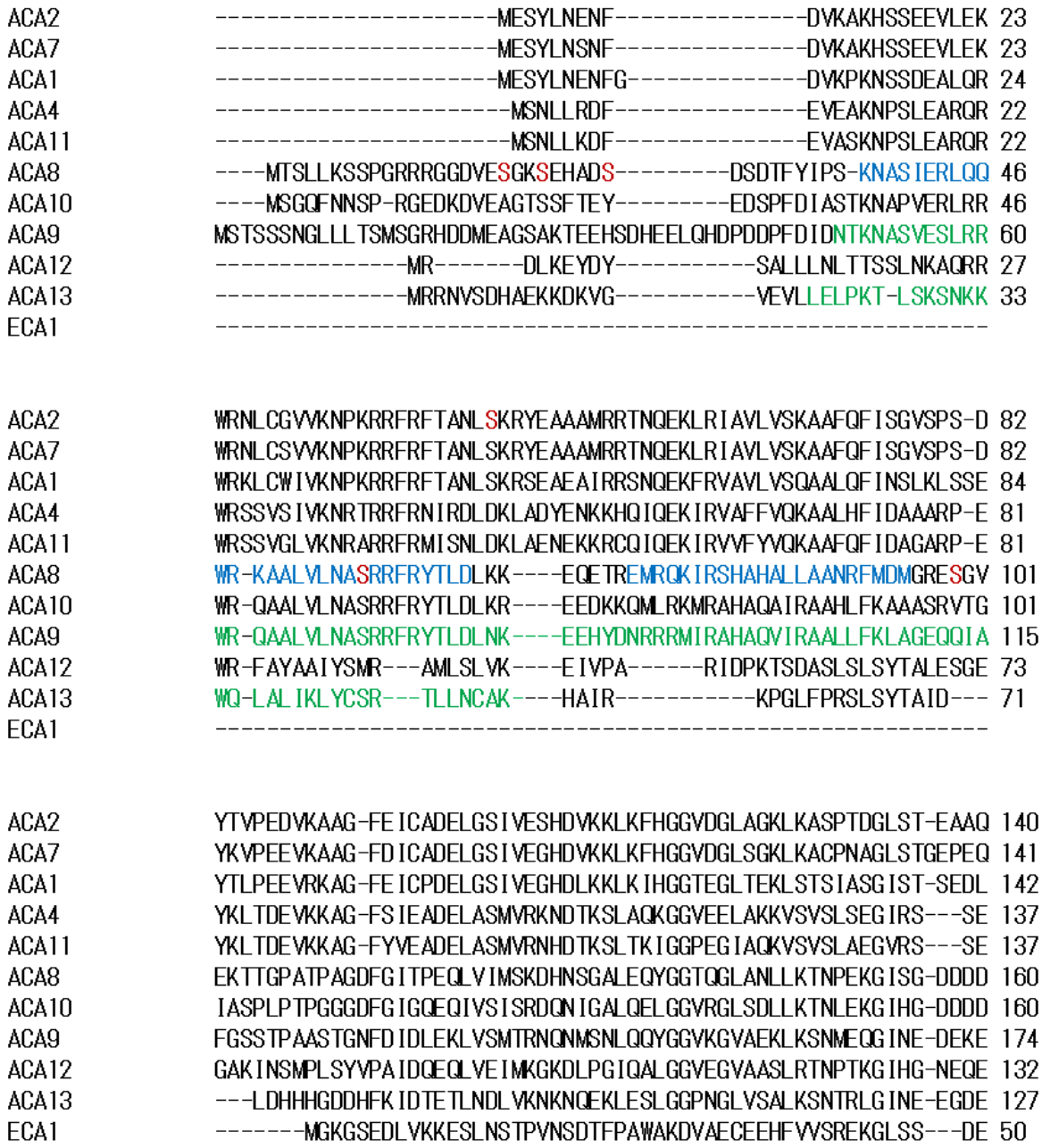

Figure 2-3. Multiple sequence alignment of ACA family proteins in *A. thaliana*.

Amino acid sequence alignments of the N-terminal regions are shown. ECA1 was used as an outgroup. Colored amino acid symbols are as follows: red, phosphorylation sites (Hwang et al., 2000; Giacometti et al., 2012); blue, calmodulin-binding sites (Tidow et al., 2012); green, predicted calmodulin-binding sites from Calmodulin Target Database (http://calcium.uhnres.utoronto.ca/ctdb/ctdb/home.html).

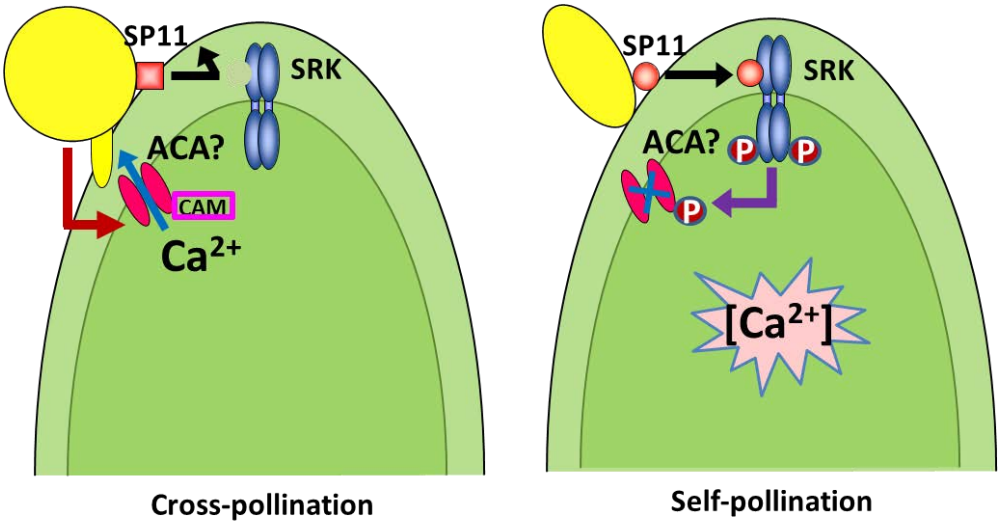

Figure 2-4. A model for ACA functions in cross- and self-pollination.

In cross-pollination, compatibility signaling facilitates ACA activity via calmodulin (CAM)-binding, and ACA transports Ca^{2+} from the papilla call (green) to the pollen grain (yellow). In self-pollination, ACA is inactivated via phosphorylation, leading to $[Ca^{2+}]_{cyt}$ elevation.

P, phosphorylation.

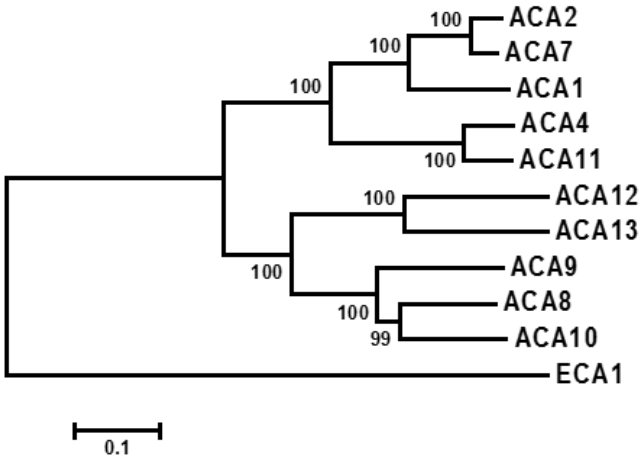

Figure 2-5. Phylogenetic analysis of ACA family in *A. thaliana*.

Bootstrap values from 2000 replicates are shown as percentage values at the nodes. The scale measures evolutionary distance based on the amino acid sequences. ECA1 was used as an outgroup. Bar = 0.1 amino acid substitutions per site.

	Before pollination	Cross-pollination		Self-pollination	
		15 min	30 min	15 min	30 min
ACA1	2.62	3.63	5.11	8.85	6.11	10.93
ACA2	2.62	0.63	0.56	0.39	0.72	0.33
ACA4	0.53	0.29	0.20	0.32	0.25	0.43
ACA7	0.29	0.14	0.31	0.76	0.45	0.19
ACA8	1.25	0.91	1.48	1.38	1.79	2.80
ACA9	0.94	1.31	2.92	3.35	3.11	1.78
ACA10	2.34	2.58	4.69	4.40	4.85	3.91
ACA11	7.66	16.97	22.83	28.30	22.23	26.84
ACA12	0.01	0.02	0.02	0.01	0.02	0.03
ACA13	4.49	51.86	117.93	178.76	143.98	186.46

high

low

Underlying cells

Papilla cells

Figure 2-6. Expression profiling of the ACA family in *A. thaliana*.

Normalized expression values in underlying cells before pollination and in papilla cells before pollination, at 15 min and at 30 min after cross- or self-pollination are shown. The numbers are averages of normalized expression levels for three biological replicates.

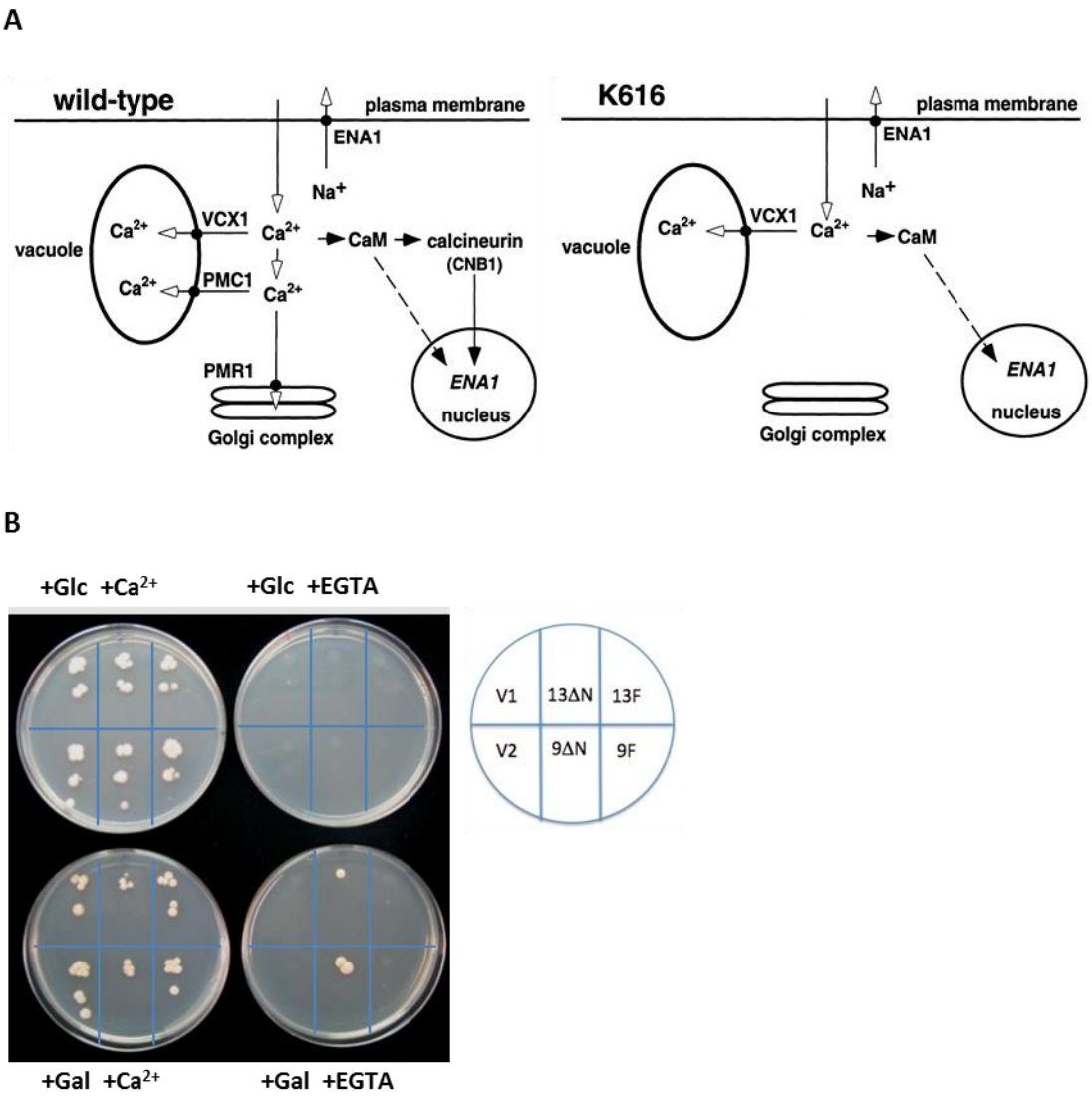

Figure 2-7. Complementation of yeast K616 by ACA13.

(**A**) Schematic structure of *Saccharomyces cerevisiae* wild-type and the mutant strain K616 lacking *PMC1*, *PMR1* and *CNB1* (modified from Geisler et al., 2000). PMC1, Ca^{2+}-transporting P-type ATPase 1; PMR1, Ca^{2+}/Mn^{2+}-transporting P-type ATPase 1; VCX1, vacuolar H^{+}/Ca^{2+} antiporter 1; CNB1, calcineurin subunit B-type 1; ENA1, Na^{+}/Li^{+}-exporting P-type ATPase 1.

(**B**) Growth of K616 on medium containing either galactose (Gal) or glucose (Glc) and either $CaCl_2$ or EGTA was complemented with *GAL1:ΔN-ACA13* and *GAL1:ΔN-ACA9* as positive control in the pYES2 vector (Schiøtt et al., 2004).

V1 and V2, pYES2 empty vector; 13ΔN and 9ΔN, *GAL1*:ΔN-*ACA13* and *GAL1*:ΔN-*ACA9*, respectively, in pYES2; 13F and 9F, *GAL1*:*ACA13* and *GAL1*:*ACA9* (full-length), respectively, in pYES2.

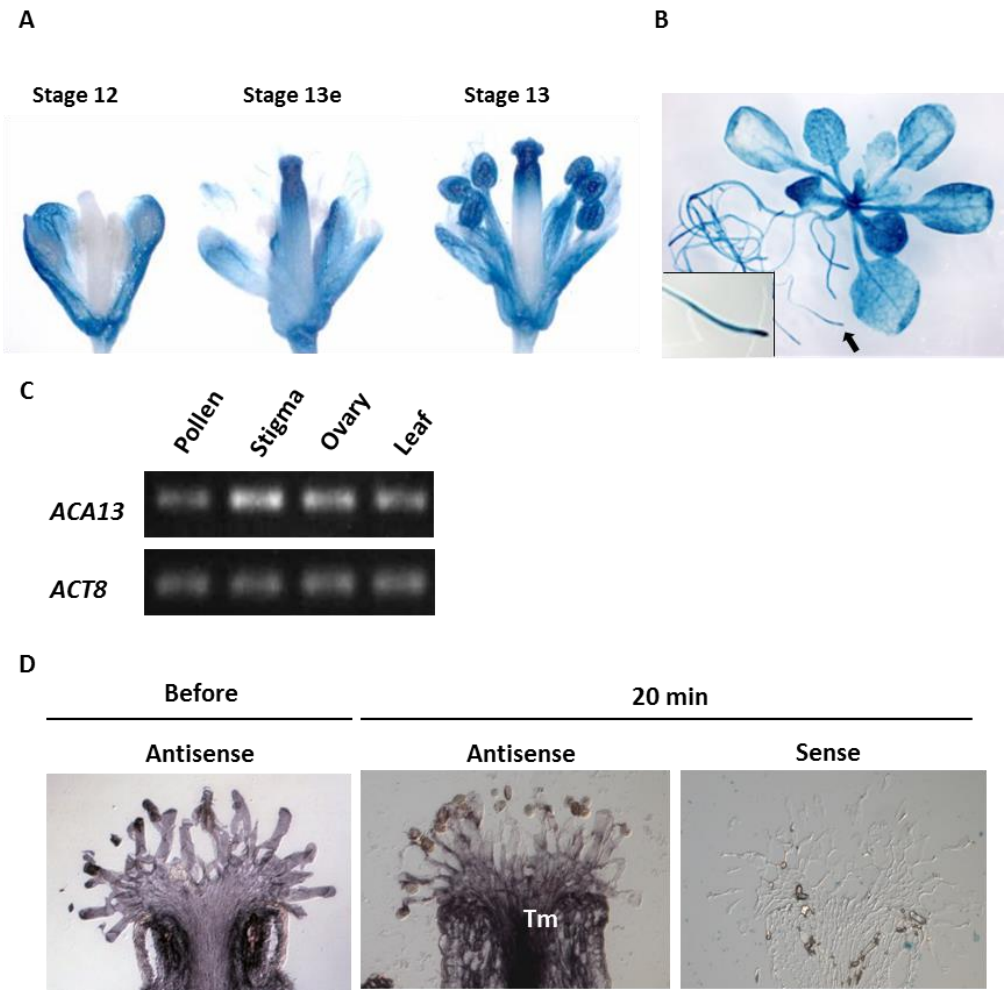

Figure 2-8. Transcription of *ACA13*.

(A) and **(B)** *ACA13:GUS* activity. **(A)** GUS expression in flowers at stage 12, early stage 13 (stage 13e) and stage 13. **(B)** Expression in 3-week-old plants. A root tip (arrow) is enlarged in the inset.

(C) RT-PCR of *ACA13* in pollen, stigma, ovary and leaf. *ACT8* (*AT1G49240*) was amplified as control.

(D) In situ hybridization to localize *ACA13* mRNA in the stigma before and at 20 min after pollination (performed by Moriyama, 2007). Tm, transmitting tract. Antisense, probe sequence is complementary to the sequence of ACA13 mRNA; Sense, probe sequence is the same as that of ACA13 mRNA.

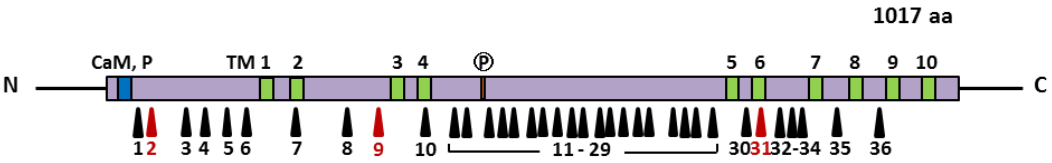

Mutant No.		Change in amino acid	Change in characteristics
1		A54V	- -
2	*	R56X	basic → stop codon
3		L91F	- -
4		T117I	polar → nonpolar
5		R132Q	basic → polar
6		S137F	polar → nonpolar
7		A200T	nonpolar → polar
8		V260M	- -
9	*	W315X	nonpolar → stop codon
10		A396V	- -
11		D427N	acidic → polar
12		A436V	- -
13		T451I	polar → nonpolar
14		G452S	nonpolar → polar
15		T453I	polar → nonpolar
16		V461I	- -
17		A499T	nonpolar → polar
18		P511S	nonpolar → polar
19		E522K	acidic → basic
20		D527N	acidic → polar
21		E529K	acidic → basic
22		E562K	acidic → basic
23		T581M	polar → nonpolar
24		F582L	- -
25		D595N	acidic → polar
26		E631K	acidic → basic
27		D644N	acidic → polar
28		L730F	- -
29		S763F	polar → nonpolar
30		A824V	- -
31	*	Q836X	polar → stop codon
32		P866S	nonpolar → polar
33		P872S	nonpolar → polar
34		P872L	- -
35		R899K	- -
36		E934K	acidic → basic

Asterisks indicate nonsense mutants.

Figure 2-9. Positions of nonsense and missense mutations in ACA13 from TILLING collection.

Nonsense and missense mutations are indicated with red arrowheads (Nos. 2, 9, 31) and black arrowheads (Nos. 1, 3-8, 10-30, 32-36), respectively. ACA13 has an auto-inhibited regulatory domain (blue box) including a CAM-binding domain (CaM) and a phosphorylation site (P), transmembrane domains (TM1-10) (green boxes) and a phosphorylated aspartate residue (encircled P) (orange box).

N, N terminus; C, C terminus.

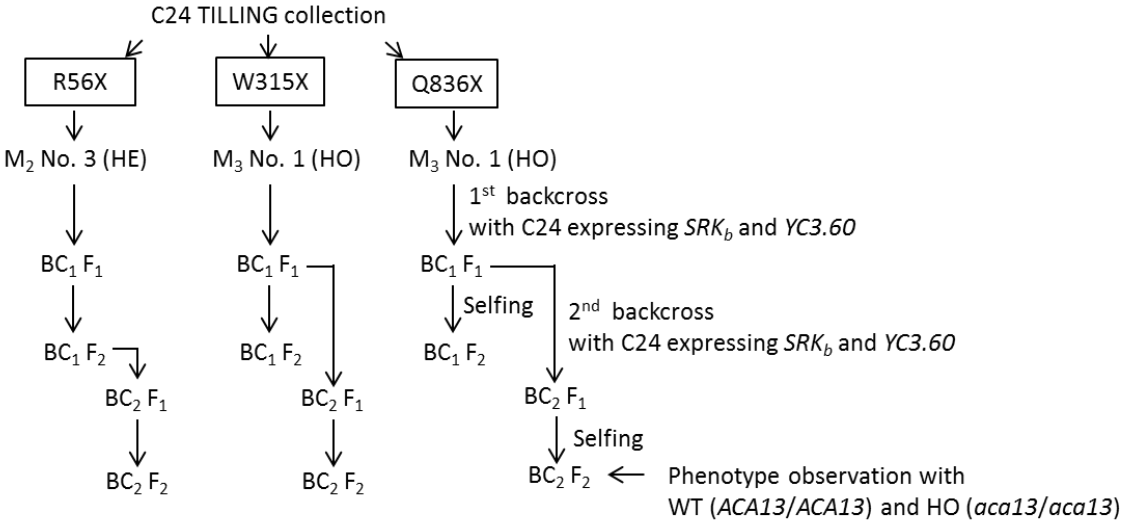

Mutant line	Generation	Genotype	Number of plants		Growth and fertility
R56X	M_2	HO	2	(No.1 - 2)	dwarf, sterile
		HE	4	(No.3 - 6)	normal, fertile
	BC_1F_2	HO	17	(No.7 - 23)	dwarf, sterile
			1	(No.24)	normal, fertile
		HE	25	(No.25 - 49)	normal, fertile
		WT	13	(No.50 - 62)	normal, fertile
			1	(No.63)	dwarf, sterile
	BC_2F_2	HO	3	(No.64 - 66)	normal, fertile
		HE	4	(No.67 - 70)	normal, fertile
		WT	4	(No.71 - 74)	normal, fertile
W315X	M_3	HO	4	(No.1 - 4)	normal, fertile
	BC_1F_2	HO	2	(No.5 - 6)	normal, fertile
		HE	4	(No.7 - 10)	normal, fertile
		WT	4	(No.11 - 14)	normal, fertile
	BC_2F_2	HO	4	(No.15 - 18)	normal, fertile
		HE	4	(No.19 - 22)	normal, fertile
		WT	4	(No.23 - 26)	normal, fertile
Q836X	M_3	HO	4	(No.1 - 4)	normal, fertile
	BC_1F_2	HO	4	(No.5 - 8)	normal, fertile
		HE	3	(No.9 - 11)	normal, fertile
		WT	3	(No.12 - 14)	normal, fertile
	BC_2F_2	HO	4	(No.15 - 18)	normal, fertile
		HE	4	(No.19 - 22)	normal, fertile
		WT	4	(No.23 - 26)	normal, fertile

Figure 2-10. Establishment of ACA13 mutant lines.

Construction and processing of the three nonsense mutant lines (R56X, W315X and Q836X) are represented from screening of the ethyl methanesulfonate-mutagenized C24 TILLING collection to setting BC_2F_2 lines (*ACA13*/*ACA13* and *aca13*/*aca13*) for phenotype observation. C24 expressing SRK_b and *YC3.60* was used for backcrossing to generate self-incompatibility and to enable $[Ca^{2+}]_{cyt}$ monitoring.

$M_{2/3}$, $M_{2/3}$ mutagenized populations; $BC_{1/2}F_{1/2}$, filial generations after backcrossing; WT, wild type; HE, heterozygous; HO, homozygous. The terms WT, HE and HO are restricted to the ACA13 locus.

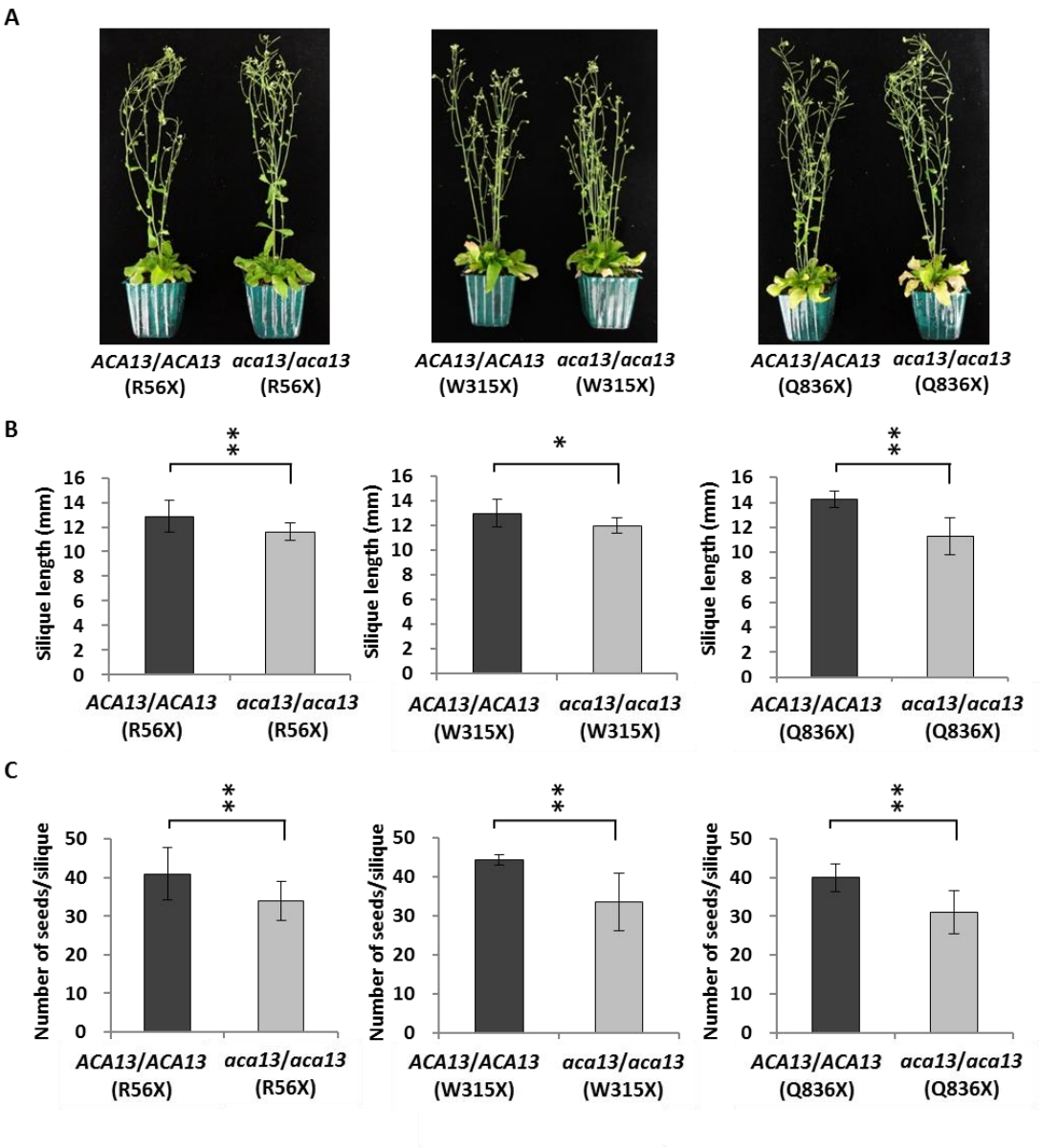

Figure 2-11. Plant growth phenotype, silique length, and number of seeds of the ACA13 mutant lines R56X, W315X and Q836X.

(**A**) Eight-week-old *ACA13*/*ACA13* and *aca13*/*aca13* plants expressing SRK_b and *YC3.60*.

(**B**) Silique length of *ACA13*/*ACA13* and *aca13*/*aca13* plants expressing SRK_b and *YC3.60*. Data shown are means ± s.d. (*ACA13*/*ACA13* (W315X, R56X and Q836X), n = 24; *aca13*/*aca13* (W315X), n = 32; *aca13*/*aca13* (R56X and Q836X) n = 24).

(**C**) Number of seeds per silique from *ACA13*/*ACA13* and *aca13*/*aca13* plants. Data shown are means ± s.d. (*ACA13*/*ACA13* (W315X, R56X and Q836X), n = 24; *aca13*/*aca13* (W315X), n = 32; *aca13*/*aca13* (R56X and Q836X) n = 24).

Asterisks indicate either significantly shorter silique length or significantly lower number of seeds from *aca13*/*aca13* compared to *ACA13*/*ACA13* (*P < 0.05; **P < 0.01).

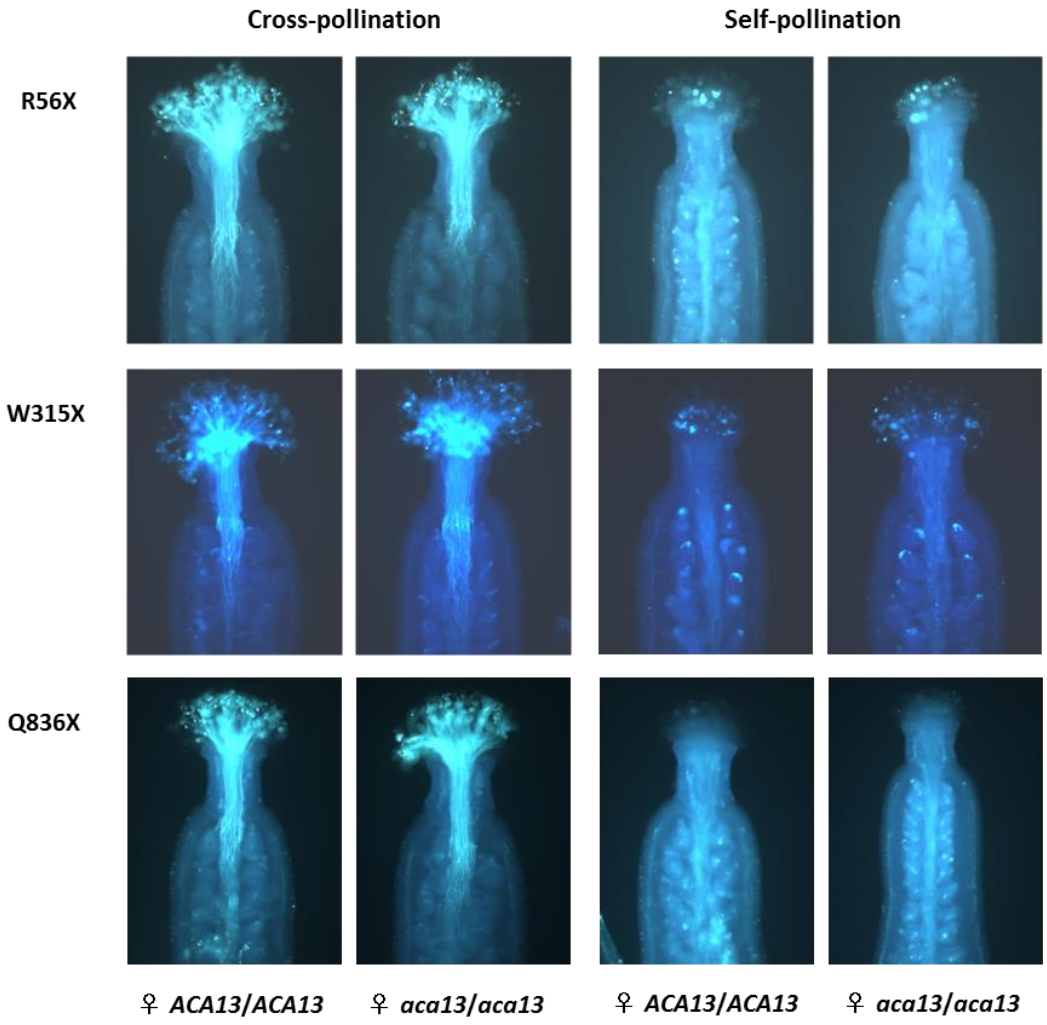

Figure 2-12. Aniline blue staining of pistils from the ACA13 mutant lines R56X, W315X and Q836X after cross- and self-pollination.

Pollen tube growth of *ACA13*/*ACA13* and *aca13*/*aca13* plants was visualized by aniline blue staining at 2 h after pollination.

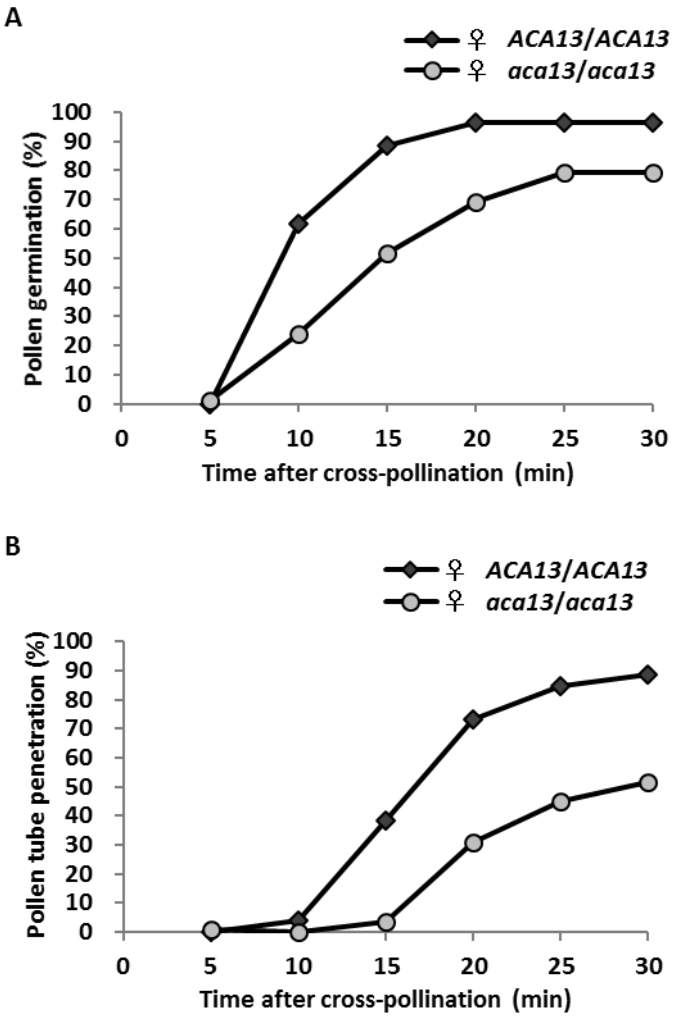

Figure 2-13. Pollination assay of the ACA13 mutant line W315X.

(**A**) and (**B**) Pollen germination rate (**A**) and pollen tube penetration rate (**B**) of C24 WT pollen (cross pollen) on papilla cells of *ACA13*/*ACA13* and *aca13*/*aca13* are shown in time course. Pollen germination and pollen tube penetration were examined every 5 min after pollination (*ACA13*/*ACA13*, $n = 26$; *aca13*/*aca13*, $n = 29$).

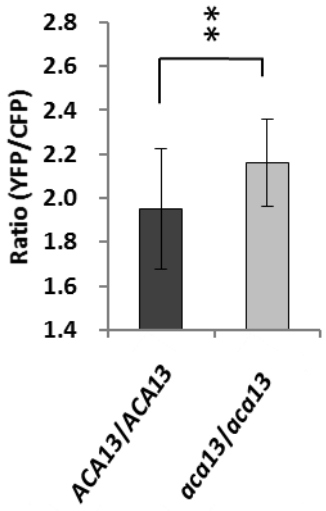

Figure 2-14. $[Ca^{2+}]_{cyt}$ in papilla cells of the ACA13 mutant line W315X before pollination. $[Ca^{2+}]_{cyt}$ is shown as a FRET ratio (YFP/CFP). Asterisks indicate a significant difference between the ratios in *ACA13*/*ACA13* and *aca13*/*aca13* plants ($P < 0.01$). Data shown are means ± s.d. (*ACA13*/*ACA13*, $n = 38$; *aca13*/*aca13*, $n = 37$).

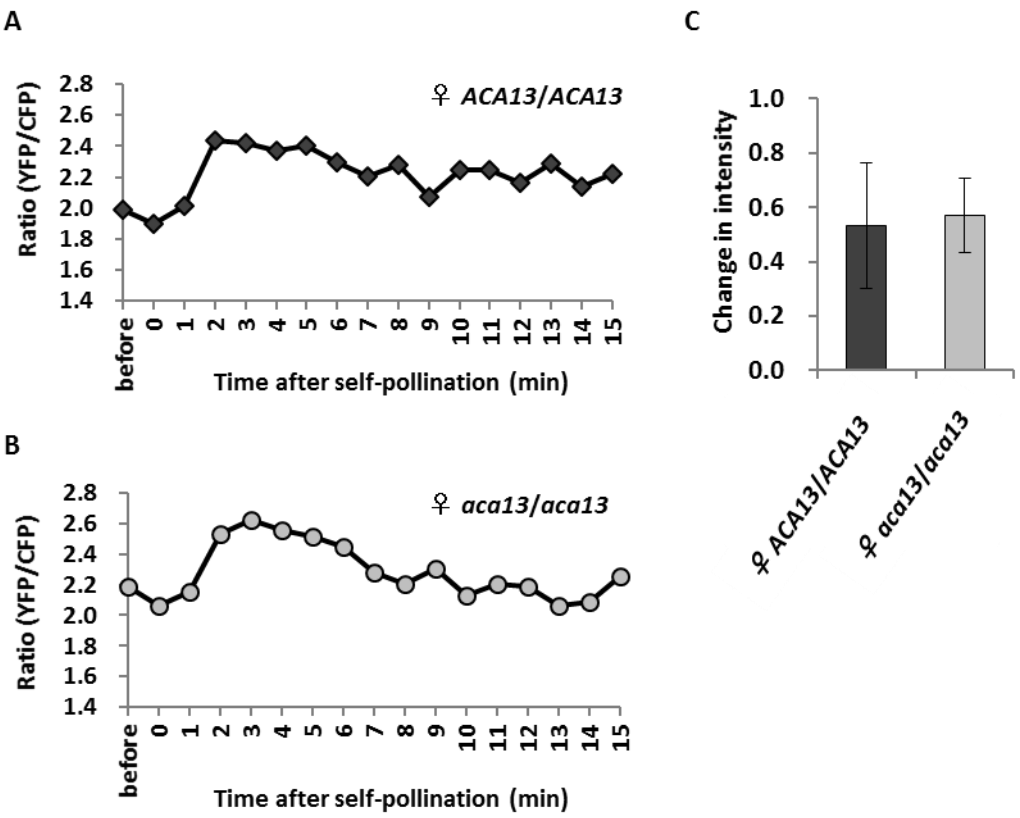

Figure 2-15. $[Ca^{2+}]_{cyt}$ in papilla cells of the ACA13 mutant line W315X after self-pollination.

(**A**) and (**B**) Typical changes of $[Ca^{2+}]_{cyt}$ in papilla cells of *ACA13*/*ACA13* (**A**) and of *aca13*/*aca13* (**B**) are shown as FRET ratios (YFP/CFP) in time courses (*ACA13*/*ACA13*, n = 7; *aca13*/*aca13*, n = 7).

(**C**) Difference in YFP/CFP ratios between the value at 0 min and the highest value after pollination (*ACA13*/*ACA13*, n = 7; *aca13*/*aca13*, n = 7).

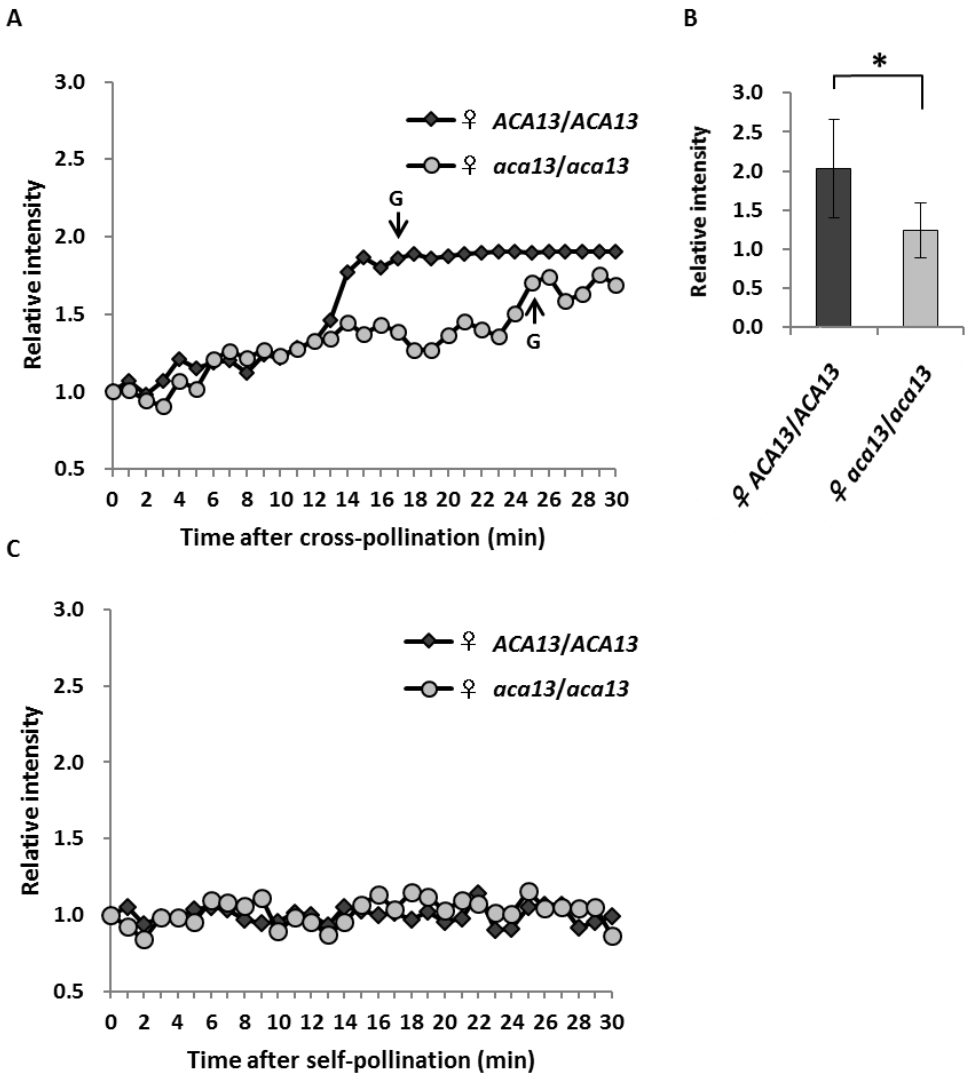

Figure 2-16. Calcium Green assay with papilla cells of the ACA13 mutant line W315X after cross- and self-pollination.

Relative intensity shows the ratio of fluorescence intensity at each time point to that at 0 min after pollination.

(**A**) Typical changes in fluorescence intensity on papilla cells immediately under the applied pollen grain, measured after cross-pollination.

G, time point of pollen germination.

(**B**) Fluorescence intensities at 15 min after cross-pollination. The asterisk indicates a significant difference between *ACA13*/*ACA13* and *aca13*/*aca13* ($P < 0.05$). Data are means ± s.d. (*ACA13*/*ACA13*, $n = 7$; *aca13*/*aca13*, $n = 6$).

(**C**) Typical changes in fluorescence intensity on papilla cells immediately under the applied pollen grain, measured after self-pollination.

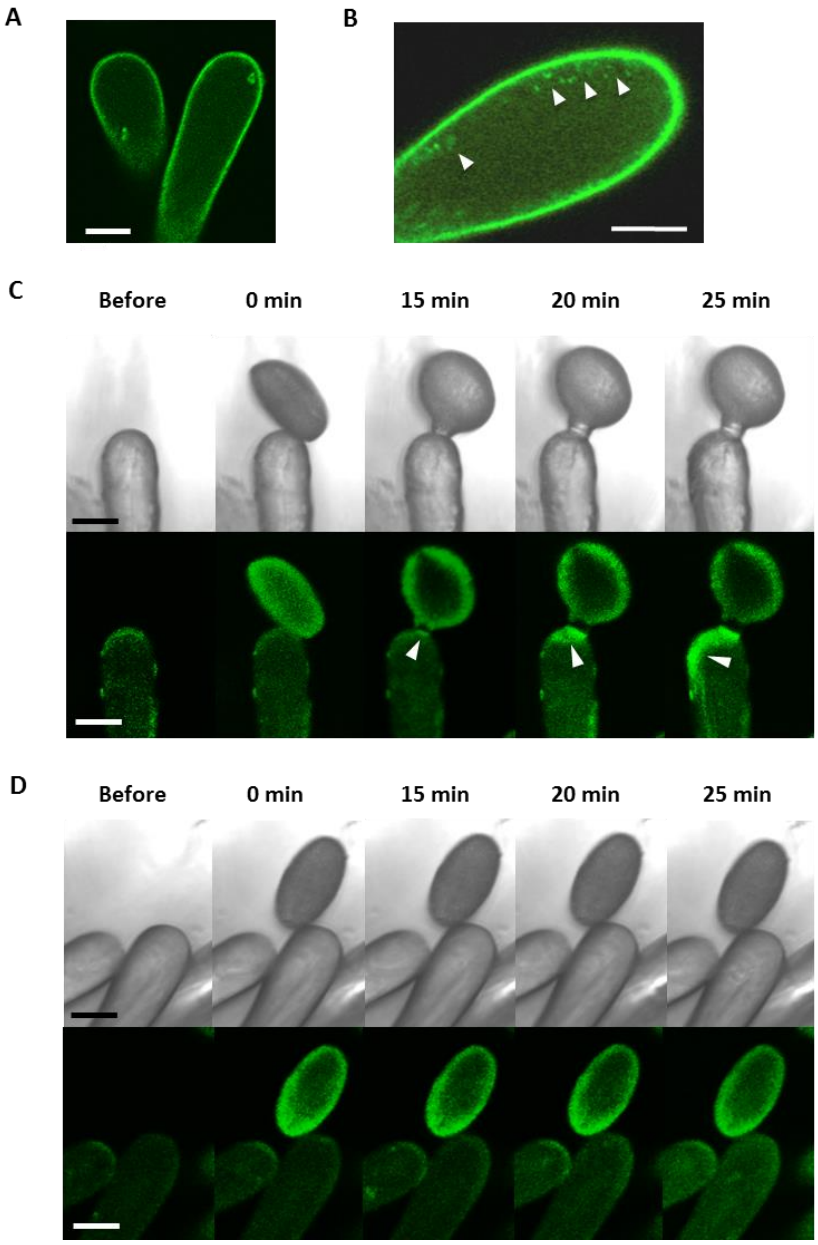

Figure 2-17. Localization of Venus-tagged ACA13 in papilla cells.

(**A**) and (**B**) Fluorescence images of papilla cells before pollination. (**A**) C24 expressing *BrS$_9$-SRK:ACA13-Venus* (*n* = 5). (**B**) Col-0 expressing *BrSLG:ACA13-Venus* (Yakabe, 2008). Arrowheads show dot-like ACA13-Venus signals.

(**C**) and (**D**) Representative bright-field and fluorescence images of C24 papilla cells expressing *BrS$_9$-SRK:ACA13-Venus* before pollination and after cross- (**C**) and self-pollination (**D**). Arrowheads indicate the accumulation of ACA13-Venus at the pollen tube penetration site (cross-pollination, *n* = 6; self-pollination, *n* = 6).

Bar = 10 μm.

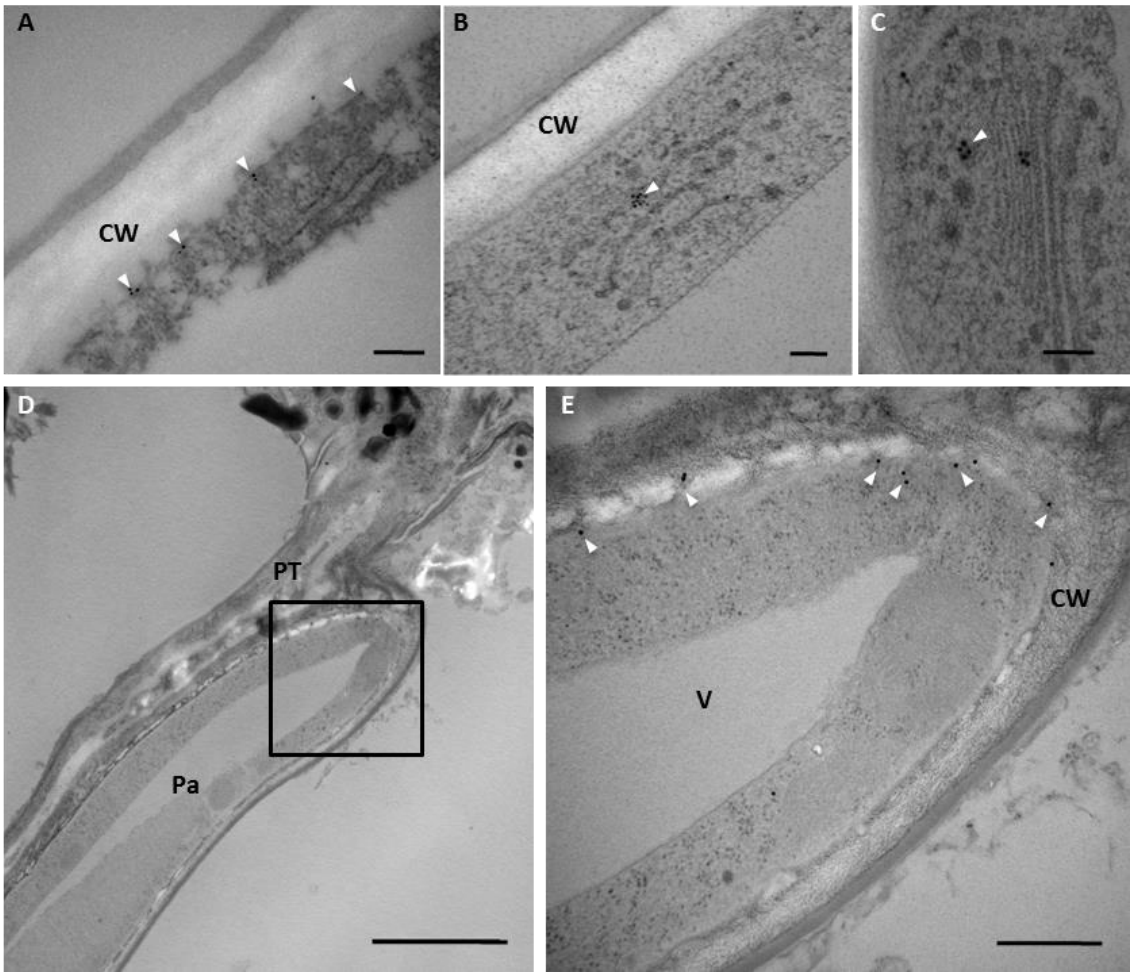

Figure 2-18. Localization of ACA13 in Col-0 expressing *BrSLG:ACA13-Venus* papilla cells before and after pollination.

Venus-tagged ACA13 was detected using rabbit anti-GFP antibody as the primary antibody and 15-nm gold particle-conjugated goat anti-rabbit antibody as the secondary antibody. Gold particles are indicated by arrowheads.

(**A**) to (**C**) Papilla cell before pollination. Gold particles were detected at the plasma membrane (**A**) and on vesicles near the Golgi body (**B** and **C**) (arrowheads) in the papilla cell. Bar = 100 nm.

(D) Papilla cell at 20 min after pollination. Bar = 2.5 μm.

(E) Enlargement of the square in **(D)**. Bar = 500 nm.

CW, cell wall; PT, pollen tube; Pa, papilla cell; V, vacuole.

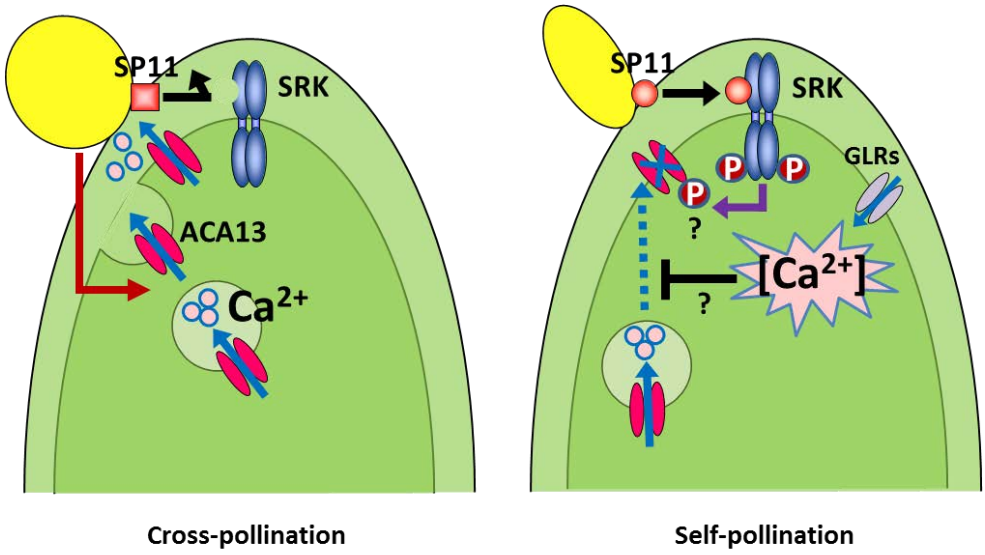

Figure 2-19. A model for the functions of ACA13 in cross- and self-pollination.

ACA13 is localized to the plasma membrane and to vesicles. In cross-pollination, ACA13 accumulates via compatibility signaling immediately under the pollen grain to supply the Ca^{2+} that is required for pollen germination. In self-pollination, Ca^{2+} efflux to the surface of the papilla cell is inhibited, and ACA13 at the plasma membrane is inactivated. The vesicular transport of ACA13 is also inhibited by SI signaling. $[Ca^{2+}]_{cyt}$ increase in the papilla cell occurs via GLRs.

P, phosphorylation.

Conclusions

At early times during cross- and self-pollination in the Brassicaceae, different interactions occur between the papilla cell and the pollen grain. In the papilla cell, compatibility signaling is thought to function during cross-pollination and to lead to successful fertilization, while SI signaling acts after the SRK-SP11 interaction to prevent fertilization during self-pollination. In this study, I investigated candidate factors that control different events in the papilla cell.

In the microarray analysis of the papilla cell, I identified 587 genes that were expressed preferentially in papilla cells before pollination. While these genes belonged to diverse categories, prominently enriched were genes involved in fatty acid synthesis, phenylpropanoid synthesis and stress response, consistent with the feature that the papilla cell faces the external environment to capture pollen grains. The numbers of genes that were expressed preferentially after either cross- or self-pollination were comparatively high at 30 min after pollination, but few were identified at 15 min after pollination. Since various interactions are visible between the papilla cell and the pollen grain at this time point, I conclude that factors operating in the papilla cell at early times after cross- or self-pollination are mostly not controlled via transcription immediately beforehand. Instead, they may be regulated via post-transcriptional modifications; alternatively, genes acting in cross-pollination may be induced after both cross- and self-pollination, and their activity may be inhibited after self-pollination. Indeed, ACA13, which functions in cross-pollination, was expressed highly before pollination, and was further induced after both cross- and self-pollination.

Another interesting finding from the microarray analysis was that several genes which have been reported to be induced after transient $[Ca^{2+}]_{cyt}$ elevation were expressed preferentially after self-pollination, which suggested that $[Ca^{2+}]_{cyt}$ in the papilla cell rises only after self-pollination. A recent study in my laboratory confirmed this speculation, and a Ca^{2+}-mediated signaling pathway in the papilla cell is suggested to control the SI response after the SRK-SP11 interaction. Although the Ca^{2+} pump activity of ACA13 may be inhibited during self-pollination, functional analyses indicated that ACA13 probably does not contribute to the increase of $[Ca^{2+}]_{cyt}$ in the papilla cell.

ACA13 is localized to the plasma membrane and vesicles of the papilla cell, and is

likely to be activated already before pollination to transport Ca^{2+} from the cytoplasm. I discovered that ACA13 accumulates toward the pollen grain and growing pollen tube to supply Ca^{2+} during cross-pollination, and thus to promote successful fertilization.

Although diverse events that occur in the papilla cell during cross- and self-pollination have been documented for decades, little is yet known about the factors functioning in compatibility and SI signaling, or about the mechanisms underlying these processes. In this study, I succeeded in identifying candidate genes and characterizing a Ca^{2+} pump, ACA13, that functions during cross-pollination. Findings from this work will provide a better understanding of reproduction mechanisms in the Brassicaceae.

Acknowledgements

First and foremost, I would like to express my gratitude to my supervisor, Prof. Seiji Takayama, who has supported me with his patience and knowledge throughout my four-and-a-half-years' stay in the Intercellular Communications Laboratory at NAIST.

I would like to thank Asst. Prof. Megumi Iwano for her helpful guidance and encouragement. I am also grateful to Prof. Hiroshi Shiba, Asst. Prof. Yuko Wada, Asst. Prof. Kohji Murase, Asst. Prof. Sota Fujii, Dr. Hiroko Shimosato-Asano, Dr. Eiko Miura, Dr. Mitsuru Kakita, Dr. Tetsuyuki Entani and Dr. Ken-ichi Kubo for their constructive comments and advice. I thank Momoko Okamura, Yoshie Ryokume, Satomi Ikeda and Rina Nagai for their technical assistance, and I am also grateful to Mana Abe for her help in secretarial work.

In addition, I would like to thank my committee members, Prof. Akiho Yokota, Prof. Taku Demura and Prof. Takashi Hashimoto, for their constructive comments and suggestions.

I thank Prof. Nori Kurata and Dr. Masahiro Fujita at the National Institute of Genetics for their assistance in microarray experiments. I am grateful to Prof. Gen Tamiya and Asst. Prof. Masao Ueki at Tohoku University for their assistance in statistical analysis of microarray data. I also thank Assoc. Prof. Hideki Nakayama and Dr. Pulla Kathioen-Nakayama at Nagasaki University for their support in the complementation experiment with K616. I would like to thank Dr. Ian Smith for editing my writing with helpful comments.

Finally, I would like to thank sincerely everyone at and outside NAIST who has supported me in any way over these years.

References

Bernard, A., and Joubès, J. (2013). Arabidopsis cuticular waxes: advances in synthesis, export and regulation. Prog. Lipid Res. 52: 110-129.

Bonza, M.C., and De Michelis, M.I. (2010). The plant Ca^{2+}-ATPase repertoire: biochemical features and physiological functions. Plant Biology 13: 421-430.

Cheung, A.Y., Niroomand, S., Zou, Y., and Wu, H.M. (2010). A transmembrane formin nucleates subapical actin assembly and controls tip-focused growth in pollen tubes. Proc. Natl. Acad. Sci. USA 107: 16390-16395.

Cominelli, E., Sala, T., Calvi, D., Gusmaroli, G., and Tonelli, C. (2008). Over-expression of the Arabidopsis AtMYB41 gene alters cell expansion and leaf surface permeability. Plant J. 53: 53-64.

Copois, V., Bibeau, F., Bascoul-Mollevi, C., Salvetat, N., Chalbos, P., Bareil, C., Candeil, L., Fraslon, C., Conseiller, E., Granci, V., Mazière, P., Kramar, A., Ychou, M., Pau, B., Martineau, P., Molina, F., and Del Rio, M. (2007). Impact of RNA degradation on gene expression profiles: assessment of different methods to reliably determine RNA quality. J Biotechnol. 127: 549-559.

Cosgrove, D.J. (2005). Growth of the plant cell wall. Nat Rev Mol Cell Biol. 6: 850-861.

Cunningham, K.W., and Fink, G.R. (1994). Calcineurin-dependent growth control in *Saccharomyces cerevisiae* mutants lacking PMC1, a homolog of plasma membrane Ca^{2+} ATPases. J. Cell Biol. 124: 351-363.

De Graaf, B.H., Vatovec, S., Juárez-Díaz, J.A., Chai, L., Kooblall, K., Wilkins, K.A., Zou, H., Forbes, T., Franklin, F.C., and Franklin-Tong, V.E. (2012). The Papaver self-incompatibility pollen S-determinant, PrpS, functions in *Arabidopsis thaliana*. Curr. Biol. 22: 154-159.

Dickinson, H. (1995). Dry stigmas, water and self-incompatibility in *Brassica*. Sex. Plant Reprod. 8: 1-10.

Dodd, A.N., Kudla, J., and Sanders, D. (2010). The language of calcium signaling. Annu. Rev. Plant Biol. 61: 593-620.

Doughty, J., Dixon, S., Hiscock, S.J., Willis, A.C., Parkin, I.A., and Dickinson, H.G. (1998). PCP-A1, a defensin-like *Brassica* pollen coat protein that binds the S locus glycoprotein, is the product of gametophytic gene expression. Plant Cell 10: 1333-1347.

Du, Z.1., Zhou, X., Ling, Y., Zhang, Z., and Su, Z. (2010). AgriGO: a GO analysis toolkit for the agricultural community. Nucleic Acids Res. 38: 64-70.

Dunkley, T.P.J., Hester, S., Shadforth, I.P., Runions, J., Weimar, T., Hanton, S.L., Griffin, J.L., Bessant, C., Brandizzi, F., Hawes, C., Watson, R.B., Dupree, P., and Lilley, K.S. (2006). Mapping the Arabidopsis organelle proteome. Proc. Natl. Acad. Sci. USA 103: 6518-6523.

Dutta, R., and Robinson, K.R. (2004). Identification and characterization of stretch-activated ion channels in pollen protoplasts. Plant Physiol. 135: 1398-1406.

Elleman, C.J., Franklin-Tong, V., and Dickinson, H.G. (1992). Pollination in species with dry stigmas: the nature of the early stigmatic response and the pathway taken by pollen tubes. New Phytol. 121: 413-424.

Elleman, C.J., and Dickinson, H.G. (1986). Pollen-stigma interactions in Brassica. IV. Structural reorganization in the pollen grains during hydration. J. Cell Set. 80: 141-157.

Elleman, C.J., and Dickinson, H.G. (1990). The role of the exine coating in pollen–stigma interactions in Brassica oleracea L. New Phytol. 114: 511–518.

Felsenstein, J. (1985). Confidence limits on phylogenies: an approach using the bootstrap. Evolution 39: 783-791.

Flick, J.S., and Johnston, M. (1990). Two systems of glucose repression of the *GAL1* promoter in *Saccharomyces cerevisiae*. Mol Cell Biol. 10: 4757–4769.

Franke, R., Höfer, R., Briesen, I., Emsermann, M., Efremova, N., Yephremov, A., and Schreiber, L. (2009). The DAISY gene from Arabidopsis encodes a fatty acid elongase condensing enzyme involved in the biosynthesis of aliphatic suberin in roots and the chalaza-micropyle region of seeds. Plant J. 57: 80-95.

Franklin-Tong, V.E., Holdaway-Clarke, T.L., Straatman, K.R., Kunkel, J.G., and Hepler, P.K. (2002). Involvement of extracellular calcium influx in the self- incompatibility response of *Papaver rhoeas*. Plant J. 29: 333-345.

Franklin-Tong, V.E., Ride, J.P., Read, N.D., Trewavas, A.J., and Franklin, F.C.H. (1993). The self-incompatibility response in *Papaver rhoeas* is mediated by cytosolic free calcium. Plant J. 4: 163-177.

Frei dit Frey, N., Mbengue, M., Kwaaitaal, M., Nitsch, L., Altenbach, D., Häweker, H., Lozano-Duran, R., Njo, M.F., Beeckman, T., Huettel, B., Borst, J.W., Panstruga, R., and Robatzek, S. (2012). Plasma membrane calcium ATPases are important components of receptor-mediated signaling in plant immune responses and development. Plant Physiol. 159: 798-809.

Frietsch, S., Wang, Y.-F., Sladek, C., Poulsen, L.R., Romanowsky, S.M., Schroeder, J.I., and Harper, J.F. (2007). A cyclic nucleotide-gated channel is essential for polarized tip growth of pollen. Proc. Natl. Acad. Sci. USA 104: 14531-14536.

Geisler, M., Axelsen, K.B., Harper, J.F., and Palmgren, M.G. (2000). Molecular aspects of higher plant P-type Ca^{2+}-ATPases. Biochim. Biophys. Acta 1465: 52-78.

George, L., Romanowsky, S.M., Harper, J.F., and Sharrock, R.A. (2008). The ACA10 Ca^{2+}-ATPase regulates adult vegetative development and inflorescence architecture in Arabidopsis. Plant Physiol. 146: 716-728.

Giacometti, S., Marrano, C.A., Bonza, M.C., Luoni, L., Limonta, M., and De Michelis, M.I. (2012). Phosphorylation of serine residues in the N-terminus modulates the activity of ACA8, a plasma membrane Ca^{2+}-ATPase of *Arabidopsis thaliana*. J. Exp. Bot. 63: 1215-1224.

Gonnet, G.H., Cohen, M.A., and Benner, S.A. (1992). Exhaustive matching of the entire protein sequence database. Science 256: 1443-1445.

Gu, T., Mazzurco, M., Sulaman, W., Matias, D.D., and Goring, D.R. (1998). Binding of a novel arm repeat protein to the kinase domain of the S-locus receptor kinase. Proc. Natl. Acad. Sci. USA 95: 382-387.

Hashimoto, K., and Kudla, J. (2011). Calcium decoding mechanisms in plants. Biochimie 93: 2054-2059.

Heslop-Harrison, J., Knox, R.B., and Heslop-Harrison, Y. (1974). Pollen wall proteins: exine held fractions associated with the incompatibility response in Cruciferae. Theor. Appl. Genet. 44: 133-137.

Hiscock, S.J., and Allen, A.M. (2008). Diverse cell signalling pathways regulate pollen-stigma interactions: the search for consensus. New Phytol. 179: 286-317.

Hiscock, S.J., and Dickinson, H.G. (1993). Unilateral incompatibility within the Brassicaceae: further evidence for the involvement of the self-incompatibility (S)-locus. Theor. Appl. Genet. 86: 744-753.

Hoang, M.H., Nguyen, X.C., Lee, K., Kwon, Y.S., Pham, H.T., Park, H.C., Yun, D.J., Lim, C.O., and Chung, W.S. (2012). Phosphorylation by AtMPK6 is required for the biological function of AtMYB41 in Arabidopsis. Biochem. Biophys. Res. Commun. 422: 181-186.

Huang, L., Berkelman, T., Franklin, A.E., and Hoffman, N.E. (1993). Characterization of a gene encoding a Ca^{2+}-ATPase-like protein in the plastid envelope. Proc. Natl. Acad. Sci. USA 90: 10066-10070.

Hwang, I., Harper, J. F., Liang, F., and Sze, H. (2000). Calmodulin activation of an endoplasmic reticulum-located calcium pump involves an interaction with the N-terminal autoinhibitory domain. Plant Physiol. 122: 157-168.

Hülskamp, M., Kopczak, S.D., Horejsi, T.F., Kihl, B.K., and Pruitt, R.E. (1995). Identification of genes required for pollen-stigma recognition in *Arabidopsis thaliana*. Plant J. 8: 703-714.

Ito, K. (2014). アブラナ科植物における Ca^{2+}を介した自家不和合性情報伝達経路の解析. Doctoral Dissertation, Graduate School of Biological Sciences, NAIST (in Japanese).

Iwano, M., Igarashi, M., Tarutani, Y., Kaothien-Nakayama, P., Nakayama, H., Moriyama, H., Yakabe, R., Entani, T., Shimosato-Asano, H., Ueki, M., Tamiya, G., and Takayama, S. (2014). A pollen coat-inducible autoinhibited Ca^{2+}-ATPase expressed in stigmatic papilla cells is required for compatible pollination in the Brassicaceae. Plant Cell 26: 636-649.

Iwano, M., Shiba, H., Matoba, K., Miwa, T., Funato, M., Entani, T., Nakayama, P., Shimosato, H., Takaoka, A., Isogai, A., and Takayama, S. (2007). Actin dynamics in papilla cells of *Brassica rapa* during self- and cross-pollination. Plant Physiol. 144: 72-81.

Iwano, M., Shiba, H., Miwa, T., Che, F.-S., Takayama, S., Nagai, T., Miyawaki, A., and Isogai, A. (2004). Ca^{2+} dynamics in a pollen grain and papilla cell during pollination of Arabidopsis. Plant Physiol. 136: 3562-3571.

Jeworutzki, E., Roelfsema, M.R., Anschütz, U., Krol, E., Elzenga, J.T., Felix, G., Boller, T., Hedrich, R., and Becker, D. (2010). Early signaling through the Arabidopsis pattern recognition receptors FLS2 and EFR involves Ca-associated opening of plasma membrane anion channels. Plant J. 62: 367-378.

Kakita, M. (2007). アブラナ科植物の自家不和合性におけるリン酸化を介した情報伝達系の解析. Doctoral Dissertation, Graduate School of Biological Sciences, NAIST (in Japanese).

Kakita, M., Murase, K., Iwano, M., Matsumoto, T., Watanabe, M., Shiba, H., Isogai, A., and Takayama, S. (2007). Two distinct forms of *M*-locus protein kinase localize to the plasma membrane and interact directly with *S*-locus receptor kinase to transduce self-incompatibility signaling in *Brassica rapa*. Plant Cell 19: 3961-3973.

Kanatani A. (2008). アブラナ科植物の自家不和合性における情報伝達系の解析. Masters Dissertation, Graduate School of Biological Sciences, NAIST (in Japanese).

Kang, Y., and Nasrallah, J.B. (2001). Use of genetically ablated stigmas for the isolation of genes expressed specifically in the stigma epidermis. Sex Plant Reprod. 14: 85–94.

Kaplan, B., Davydov, O., Knight, H., Galon, Y., Knight, M.R., Fluhr, R., and Fromm, H. (2006). Rapid transcriptome changes induced by cytosolic Ca^{2+} transients reveal ABRE-related sequences as Ca^{2+}-responsive cis elements in Arabidopsis. Plant Cell 18: 2733-2748.

Kho, Y.O., and Baër, J. (1968). Observing pollen tubes by means of fluorescence. Euphytica 17: 298-302.

Kitashiba, H., Liu, P., Nishio, T., Nasrallah, J.B., and Nasrallah, M.E. (2011). Functional test of Brassica self-incompatibility modifiers in *Arabidopsis thaliana*. Proc. Natl. Acad. Sci. USA 108: 18173-18178.

Lai, K.S., Kaothien-Nakayama, P., Iwano, M., and Takayama, S. (2012). A TILLING resource for functional genomics in *Arabidopsis thaliana* accession C24. Genes Genet. Syst. 87: 291-297.

Larkin, M.A., Blackshields G., Brown N.P., Chenna, R., McGettigan, P.A., McWilliam, H., Valentin, F., Wallace, I.M., Wilm, A., Lopez, R., Thompson, J.D., Gibson, T.J., and Higgins, D.G. (2007). Clustal W and Clustal X version 2.0. Bioinformatics 23: 2947-2948.

Lee, S.M., Kim, H.S., Han, H.J., Moon, B.C., Kim, C.Y., Harper, J.F., and Chung, W.S. (2007). Identification of a calmodulin-regulated autoinhibited Ca^{2+}-ATPase (ACA11) that is localized to vacuole membranes in Arabidopsis. FEBS Lett. 581: 3943-3949.

Lippold, F., Sanchez, D.H., Musialak, M., Schlereth, A., Scheible, W.R., Hincha, D.K., and Udvardi, M.K. (2009). AtMyb41 regulates transcriptional and metabolic responses to osmotic stress in Arabidopsis. Plant Physiol. 149: 1761-1772.

Lucca, N., and León, G. (2012). Arabidopsis *ACA7*, encoding a putative auto-regulated Ca^{2+}-ATPase, is required for normal pollen development. Plant Cell Rep. 31: 651-659.

Luu, D.T., Heizmann, P., Dumas, C., Trick, M., and Cappadocia, M. (1997). Involvement of *SLR1* genes in pollen adhesion to the stigmatic surface in Brassicaceae. Sex. Plant Reprod. 10: 227–235.

Luu, D.T., Marty-Mazars, D., Trick, M., Dumas, C. and Heizmann, P. (1999). Pollen-stigma adhesion in *Brassica* spp involves SLG and SLR1 glycoproteins. Plant Cell 11: 251-262.

Luu, D.T., Passelegue, E., Dumas, C., and Heizmann, P. (1998). Pollen stigma capture is not species specific discriminant within the Brassicaceae family. Comptes Rendus a l'Acadmie des Sciences 321: 747-755.

Lü, S., Song, T., Kosma, D.K., Parsons, E.P., Rowland, O., and Jenks, M.A. (2009). Arabidopsis CER8 encodes long-chain acyl-coa synthetase 1 (LACS1) that has overlapping functions with LACS2 in plant wax and cutin synthesis. Plant J. 59: 553-564.

Mayfield, J.A., and Preuss, D. (2000). Rapid initiation of Arabidopsis pollination requires the oleosin-domain protein GRP17. Nat. Cell Biol. 2: 128-130.

McCormack, E., Tsai, Y.C., and Braam, J. (2005). Handling calcium signaling: Arabidopsis CaMs and CMLs. Trends Plant Sci. 10: 383-389.

Medford, J.I., Elmer, J.S., and Klee, H.J. (1991). Molecular cloning and characterization of genes expressed in shoot apical meristems. Plant Cell 3: 359-370.

Michard, E., Lima, P.T., Borges, F., Silva, A.C., Portes, M.T., Carvalho, J.E., Gilliham, M., Liu, L., Obermeyer, G., and Feijó, J.A. (2011). Glutamate receptor-like genes form Ca^{2+} channels in pollen tubes and are regulated by pistil D-serine. Science 332: 434-437.

Moriyama, H. (2007). アブラナ科植物における和合受粉－受精機構の解析. Masters Dissertation, Graduate School of Biological Sciences, NAIST (in Japanese).

Murase, K., Shiba, H., Iwano, M., Che, F.S., Watanabe, M., Isogai, A., and Takayama, S. (2004). A membrane-anchored protein kinase involved in *Brassica* self-incompatibility signaling. Science 303: 1516-1519.

Nagai, T., Ibata, K., Park, E.S., Kubota, M., Mikoshiba, K., and Miyawaki, A. (2002). A variant of yellow fluorescent protein with fast and efficient maturation for cell-biological applications. Nat. Biotechnol. 20: 87-90.

Nagai, T., Yamada, S., Tominaga, T., Ichikawa, M., and Miyawaki, A. (2004). Expanded dynamic range of fluorescent indicators for Ca^{2+} by circularly permuted yellow fluorescent proteins. Proc. Natl. Acad. Sci. USA 101: 10554-10559.

Nasrallah, M.E., Liu, P., Sherman-Broyles, S., Boggs, N.A., and Nasrallah, J.B. (2004). Natural variation in expression of self-incompatibility in *Arabidopsis thaliana*: implications for the evolution of selfing. Proc. Natl. Acad. Sci. USA 101: 16070-16074.

Ohara, K. (2010). アブラナ科植物の受粉過程で機能する乳頭細胞内発現遺伝子の探索. Masters Dissertation, Graduate School of Biological Sciences, NAIST (in Japanese).

Pei, W., Du, F., Zhang, Y., He, T., and Ren, H. (2012). Control of the actin cytoskeleton in root hair development. Plant Sci. 187: 10-18.

Poulter, N.S., Wheeler, M.J., Bosch, M., and Franklin-Tong, V.E. (2010). Self-incompatibility in Papaver: identification of the pollen S-determinant PrpS. Biochem. Soc. Trans. 38: 588-592.

Preuss, D., Lemieux, B., Yen, G., and Davis, R.W. (1993). A conditional sterile mutation eliminates surface components from Arabidopsis pollen and disrupts cell signaling during fertilization. Genes Dev. 7: 974-985.

Provart, N., and Zhu, T. (2003). A browser-based functional classification superviewer for Arabidopsis genomics. Currents Comput. Mol. Biol. 271-272.

Qin, Y., Leydon, A.R., Manziello, A., Pandey, R., Mount, D., Denic, S., Vasic, B., Johnson, M.A., and Palanivelu, R. (2009). Penetration of the stigma and style elicits a novel transcriptome in pollen tubes, pointing to genes critical for growth in a pistil. PLoS Genet. 5(8): 1-19.

Robert, L.S., Allard, S., Gerster, J.L., Cass, L., and Simmonds, J. (1994). Molecular analysis of two Brassica napus genes expressed in the stigma. Plant Mol Biol. 26:1217-1222.

Rose, J.K., Braam, J., Fry, S.C., and Nishitani, K. (2002). The XTH family of enzymes involved in xyloglucan endotransglucosylation and endohydrolysis: current perspectives and a new unifying nomenclature. Plant Cell Physiol. 43: 1421-1435.

Saitou, N., and Nei, M. (1987). The neighbor-joining method: a new method for reconstructing phylogenetic trees. Mol. Biol. Evol. 4: 406-425.

Samuel, M.A., Chong, Y.T., Haasen, K.E., Aldea-Brydges, M.G., Stone, S.L., and Goring, D.R. (2009). Cellular pathways regulating responses to compatible and self-incompatible pollen in Brassica and Arabidopsis stigmas intersect at Exo70A1, a putative component of the exocyst complex. Plant Cell 21: 2655-2671.

Sarmah, B.K., and Sarla, N. (1995). Overcoming prefertilization barriers in the cross *Diplotaxis siettiana* x *Brassica juncea* using irradiated mentor pollen. Biol. Plantarum 37: 329-334.

Schiøtt, M., Romanowsky, S.M., Baekgaard, L., Jakobsen, M.K., Palmgren, M.G., and Harper, J.F. (2004). A plant plasma membrane Ca^{2+} pump is required for normal pollen tube growth and fertilization. Proc. Natl. Acad. Sci. USA 101: 9502-9507.

Schnurr, J., Shockey, J., and Browse, J. (2004). The acyl-CoA synthetase encoded by LACS2 is essential for normal cuticle development in Arabidopsis. Plant Cell 16: 629-642.

Seo, P.J., Lee, S.B., Suh, M.C., Park, M.J., Go, Y.S., and Park, C.M. (2011). The MYB96 transcription factor regulates cuticular wax biosynthesis under drought conditions in Arabidopsis. Plant Cell 23: 1138-1152.

Sessions, R.A., and Zambryski, P.C. (1995). Arabidopsis gynoecium structure in the wild type and in *ettin* mutants. Development 121: 1519-1532.

Sherman-Broyles, S., Boggs, N., Farkas, A., Liu, P., Vrebalov, J., Nasrallah, M.E., and Nasrallah, J.B. (2007). S locus genes and the evolution of self-fertility in *Arabidopsis thaliana*. Plant Cell 19: 94-106.

Simon, V.R., and Pon, L.A. (1996). Actin-based organelle movement. Experientia 52: 1117-1122.

Smyth, D.R., Bowman, J.L., and Meyerowitz, E.M. (1990). Early flower development in Arabidopsis. Plant Cell 2: 755-776.

Steinhorst, L., and Kudla, J. (2013). Calcium - a central regulator of pollen germination and tube growth. Biochim. Biophys. Acta 1833: 1573-1581.

Swanson, R., Clark, T., and Preuss, D. (2005). Expression profiling of Arabidopsis stigma tissue identifies stigma-specific genes. Sex. Plant Reprod. 18: 163-171.

Takahashi, H., Kamakura, H., Sato, Y., Shiono, K., Abiko, T., Tsutsumi, N., Nagamura, Y., Nishizawa, N.K., and Nakazono, M. (2010). A method for obtaining high quality RNA from paraffin sections of plant tissues by laser microdissection. J. Plant Res. 123: 807-813.

Takayama, S., Shiba, H., Iwano, M., Shimosato, H., Che, F.S., Kai, N., Watanabe, M., Suzuki, G., Hinata, K., and Isogai, A. (2000). The pollen determinant of self-incompatibility in *Brassica campestris*. Proc. Natl. Acad. Sci. USA 97: 1920-1925.

Takayama, S., Shimosato, H., Shiba, H., Funato, M., Che, F.S., Watanabe, M., Iwano, M., and Isogai, A. (2001). Direct ligand-receptor complex interaction controls *Brassica* self-incompatibility. Nature 413: 534-538.

Takayama, S., and Isogai, A. (2005). Self-incompatibility in plants. Annu. Rev. Plant Biol. 56: 467-489.

Takehisa, M. (2009). シロイヌナズナを用いたアブラナ科植物自家不和合情報伝達機構の解析. Masters Dissertation, Graduate School of Biological Sciences, NAIST (in Japanese).

Tamura, K., Stecher, G., Peterson, D., Filipski, A., and Kumar, S. (2013). MEGA6: Molecular Evolutionary Genetics Analysis version 6.0. Mol. Biol. Evol. 30: 2725-2729.

Tena, G., Boudsocq, M., and Sheen, J. (2011). Protein kinase signaling networks in plant innate immunity. Curr. Opin. Plant Biol. 14: 519-529.

Thimm, O., Bläsing, O., Gibon, Y., Nagel, A., Meyer, S., Krüger, P., Selbig, J., Müller, L.A., Rhee, S.Y., and Stitt, M. (2004). MAPMAN: a user-driven tool to display genomics data sets onto diagrams of metabolic pathways and other biological processes. Plant J. 37: 914-939.

Tidow, H., Poulsen, L.R., Andreeva, A., Knudsen, M., Hein, K.L., Wiuf, C., Palmgren, M.G., and Nissen, P. (2012). A bimodular mechanism of calcium control in eukaryotes. Nature 491: 468-72.

Todd, J., Post-Beittenmiller, D., and Jaworski, J.G. (1999). KCS1 encodes a fatty acid elongase 3-ketoacyl-CoA synthase affecting wax biosynthesis in *Arabidopsis thaliana*. Plant J. 17: 119-130.

Tsuchimatsu, T., Suwabe, K., Shimizu-Inatsugi, R., Isokawa, S., Pavlidis, P., Städler, T., Suzuki, G., Takayama, S., Watanabe, M., and Shimizu, K.K. (2010). Evolution of self-compatibility in Arabidopsis by a mutation in the male specificity gene. Nature 464: 1342-1346.

Tung, C.W., Dwyer, K.G., Nasrallah, M.E., and Nasrallah, J.B. (2005). Genome-wide identification of genes expressed in Arabidopsis pistils specifically along the path of pollen tube growth. Plant Physiol. 138: 977-989.

Vantard, M., and Blanchoin, L. (2002). Actin polymerization processes in plant cells. Curr. Opin. Plant Biol. 5: 502-506.

Wang, W., Wang, L., Chen, C., Xiong, G., Tan, X.Y., Yang, K.Z., Wang, Z.C., Zhou, Y., Ye D., and Chen, L.Q. (2011). Arabidopsis CSLD1 and CSLD4 are required for cellulose deposition and normal growth of pollen tubes. J. Exp. Bot. 62: 5161-5177.

Yakabe, R. (2009). アブラナ科植物の和合・不和合受粉過程の解明. Masters Dissertation, Graduate School of Biological Sciences, NAIST (in Japanese).

Zheng, H., Rowland, O., and Kunst, L. (2005). Disruptions of the Arabidopsis Enoyl-CoA reductase gene reveal an essential role for very-long-chain fatty acid synthesis in cell expansion during plant morphogenesis. Plant Cell 17: 1467-1481.

Zinkl, G.M., Zwiebel, B.I., Grier, D.G., and Preuss, D. (1999). Pollen-stigma adhesion in Arabidopsis: a species-specific interaction mediated by lipophilic molecules in the pollen exine. Development 126: 5431-5440.

Zuckerkandl, E., and Pauling, L. (1965). Molecules as documents of evolutionary history. J. Theor. Biol. 8: 357-366.

Supplemental Table 1. Primer sequences used in this study.

	Primer name	Sequence 5'-3'
for checking insert		
(*SRK$_b$* in C24 expressing *SRK$_b$*)		
	SRK$_b$ 8-1-3_F	GCTAAGGATGGTAGATCACAAG
	SRK$_b$ 8-1-3_R	GTACTTGGATATGTCGAGGG
	121TR3	CCCAGTACATTAAAAACGTCCGCA
(*SCR$_b$* in C24 SI)		
	lyrata SCR$_b$_F	ATGAGGAATGCTACTTTCTTC
	lyrata SCR$_b$_R	TAGCAAAATCTACAGTCGCAT
(*YC3.60* in C24 expressing *SRK$_b$* and *YC3.60*)		
	YC3.60_interF	GCATGCATGACCAACTGACA
	YC3.60_interR	CGAGGTTTGTCATGACGTGA
for RT-PCR		
	RT-ACA13_F	CAATCGGCCACGATGCAGCTG
	RT-ACA13_R	GCTTTGTCAGGTGTTCAACG
	ACT8_F	AGCACTTTCCAGCAGATGTG
	ACT8_R	GAAAGAAATGTGATCCCGTCATG
for TILLING screening of ACA13 mutants		
(i)	ACA13-1F TILLING	6-FAM-TACCCATCGCTTTCACAAAACAACAAATT
	ACA13-1R TILLING	VIC-CTATCTCATCGCTCTTCGTAGTCTTTCCGT
(ii)	ACA13-2F TILLING	6-FAM-AGCTTGGGGACAAATGATGAGTCATATCT
	ACA13-2R TILLING	VIC-CCATCACTTTGATTCTTTCGACTTTCTCTA
(iii)	ACA13-3F TILLING	6-FAM-AGTGAAGAAAGCTGTTGAGGATTGTCAATT
	ACA13-3R TILLING	VIC-CGCTGTTCAATGAAAATGATCAATCTTTAT
*	6-FAM	TCGAGGTCGACGGTATCGAT
**	VIC	TGACGAGTAGACGCTGGTAG
	* and ** sequences were added to the forward or reverse primers, respectively.	
for genotyping of ACA13 mutants		
(i)	ACA13-1F	TACCCATCGCTTTCACAAAACAACAAATT
	ACA13-1R	CTATCTCATCGCTCTTCGTAGTCTTTCCGT
(ii)	ACA13-2F	AGCTTGGGGACAAATGATGAGTCATATCT
	ACA13-2R	CCATCACTTTGATTCTTTCGACTTTCTCTA
(iii)	ACA13-3F	AGTGAAGAAAGCTGTTGAGGATTGTCAATT
	ACA13-3R	CGCTGTTCAATGAAAATGATCAATCTTTAT

Supplemental Table 2. Genes expressed preferentially in papilla cells before pollination compared to underlying cells.

TAIR locus	Description
Protein fate	
AT5G63750	E3 ubiquitin-protein ligase ARI13
AT3G05200	E3 ubiquitin-protein ligase ATL6
AT1G55250	E3 ubiquitin-protein ligase BRE1-like 2
AT2G24540	F-box protein
AT2G27310	F-box protein
AT2G41170	F-box protein
AT3G17510	CBL-interacting serine/threonine-protein kinase (CIPK1)
AT4G00330	calmodulin-binding receptor-like cytoplasmic kinase 2
AT4G13000	AGC (cAMP-dependent, cGMP-dependent and protein kinase C) kinase family protein
AT5G35370	G-type lectin S-receptor-like serine/threonine-protein kinase
AT5G11400	inactive serine/threonine-protein kinase
AT2G28930	protein kinase APK1b
AT3G57640	protein kinase family protein
AT5G25440	protein kinase family protein
AT5G37790	protein kinase family protein
AT5G40540	protein kinase family protein
AT2G34650	protein kinase pinoid
AT1G74490	protein kinase superfamily protein
AT2G45590	receptor-like serine/threonine-protein kinase
AT4G25390	receptor-like serine/threonine-protein kinase
AT3G16800	protein phosphatase 2C
AT4G31750	protein phosphatase 2C 59
AT4G31860	protein phosphatase 2C 60
AT4G32950	protein phosphatase 2C 61
AT5G66080	protein phosphatase 2C 79
AT5G57480	AAA-type ATPase family protein
AT5G02240	ABA modulated tyrosine-phosphorylated protein
AT5G67340	ARM repeat superfamily protein
AT3G52500	aspartyl protease family protein
AT3G54780	C3HC4-type RING finger protein
AT3G19100	CDPK-related kinase 2
AT4G12100	cullin-like protein 5
AT3G05720	importin alpha isoform 7

AT2G30500	Kinase interacting (KIP1-like) family protein
AT1G24140	metalloproteinase
AT2G21430	papain family cysteine protease
AT5G58140	phototropin 2
AT4G02075	protein pitchoun 1
AT1G01630	protein sec fourteen-like protein-20
AT1G33850	ribosomal protein S19 family protein
AT4G30400	RING-H2 finger protein ATL13
AT2G46160	RING-H2 finger protein ATL67
AT1G20823	RING-H2 finger protein ATL80
AT2G21540	SEC14-like 3 protein
AT1G14820	SEC14p-like phosphatidylinositol transfer family protein
AT1G22180	SEC14p-like phosphatidylinositol transfer family protein
AT2G22970	serine carboxypeptidase-like 11
AT3G02110	serine carboxypeptidase-like 25
AT2G35780	serine carboxypeptidase-like 26
AT5G22980	serine carboxypeptidase-like 47
AT2G31010	serine/threonine kinase
AT4G21323	subtilase family protein
AT5G56150	ubiquitin-conjugating enzyme E2 30
AT5G10480	very-long-chain (3R)-3-hydroxyacyl-[acyl-carrier protein] dehydratase pasticcino 2
AT1G79110	zinc ion binding protein

RNA fate

AT3G11580	AP2/B3-like transcriptional factor family protein
AT1G16060	AP2-like ethylene-responsive transcription factor
AT1G79700	AP2-like ethylene-responsive transcription factor
AT3G61970	B3 domain-containing transcription factor (NGA2)
AT2G23340	ethylene-responsive transcription factor ERF008
AT1G22190	ethylene-responsive transcription factor ERF058
AT5G61890	ethylene-responsive transcription factor ERF114
AT2G47460	transcription factor (MYB12)
AT4G34990	transcription factor (MYB32)
AT2G36890	transcription factor (RAX2)
AT2G22760	transcription factor bHLH19
AT5G56270	WRKY transcription factor 2
AT1G62300	WRKY transcription factor 6
AT4G01720	WRKY transcription factor 47
AT2G25000	WRKY transcription factor 60

AT5G49330	myb domain protein 111
AT3G28910	myb domain protein 30
AT2G02820	myb domain protein 88
AT2G40260	myb family transcription factor
AT2G37060	nuclear transcription factor Y subunit B-8
AT5G62260	AT hook motif DNA-binding protein
AT3G13640	ABC transporter E family member 1
AT4G30080	auxin response factor 16
AT4G14560	auxin-responsive protein (IAA1)
AT3G15540	auxin-responsive protein (IAA19)
AT1G02030	C2H2-like zinc finger protein
AT1G03790	CCCH-type zinc finger protein SOMNUS
AT2G38340	dehydration-responsive element-binding protein 2E
AT5G59730	exocyst subunit exo70 family protein H7
AT3G50890	homeobox protein 28
AT5G47370	homeobox-leucine zipper protein HAT2
AT3G60390	homeobox-leucine zipper protein HAT3
AT4G21750	homeobox-leucine zipper protein meristem L1
AT5G05090	homeodomain-like superfamily protein
AT5G45580	homeodomain-like superfamily protein
AT1G31140	MADS-box protein gordita
AT5G50450	MYND-type zinc finger protein
AT1G47760	protein agamous-like 102
AT5G66610	protein DA1-related 7
AT3G25882	protein NIM1-interacting 2
AT5G60100	pseudo-response regulator 3
AT5G43170	zinc-finger protein 3
AT1G03457	RNA recognition motif-containing protein
AT4G03110	RNA-binding protein-defense related 1
AT5G10800	RNA recognition motif (RRM)-containing protein
AT5G50250	chloroplast RNA-binding protein 31B
Lipid metabolism	
AT1G01120	3-ketoacyl-CoA synthase 1 (KCS1)
AT1G04220	3-ketoacyl-CoA synthase 2 (KCS2)
AT2G15090	3-ketoacyl-CoA synthase 8 (KCS8)
AT4G34250	3-ketoacyl-CoA synthase 16 (KCS16)
AT5G43760	3-ketoacyl-CoA synthase 20 (KCS20)
AT3G44540	fatty acid reductase 4 (FAR4)

AT2G47240	long chain acyl-CoA synthetase 1 (LACS1)
AT1G49430	long-chain acyl-CoA synthetase 2 (LACS2)
AT1G64400	long-chain acyl-CoA synthetase 3 (LACS3)
AT2G38540	non-specific lipid-transfer protein 1 (LTP1)
AT5G01870	pathogenesis-related lipid transfer protein (LTP10)
AT3G55360	very-long-chain enoyl-CoA reductase (CER10)
AT1G24360	3-oxoacyl-[acyl-carrier-protein] reductase
AT1G74960	3-oxoacyl-[acyl-carrier-protein] synthase II
AT3G07690	6-phosphogluconate dehydrogenase-like protein
AT5G27200	acyl carrier protein 5
AT5G16240	acyl-[acyl-carrier-protein] desaturase
AT1G21540	acyl-activating enzyme
AT2G17650	AMP-binding protein
AT5G15530	biotin carboxyl carrier protein 2
AT1G47480	carboxylesterase 2
AT5G16390	chloroplastic acetylcoenzyme A carboxylase 1
AT4G14440	delta3, delta2-enoyl CoA isomerase
AT1G06080	delta-9 acyl-lipid desaturase 1
AT1G06090	delta-9 desaturase-like 1 protein
AT1G06350	delta-9 desaturase-like 4 protein
AT1G06360	delta-9 desaturase-like 5 protein
AT1G01610	glycerol-3-phosphate sn-2-acyltransferase
AT5G42930	lipase class 3-like protein
AT3G23410	long-chain-alcohol oxidase FAO3
AT3G16170	malonate--CoA ligase
AT1G07420	methylsterol monooxygenase
AT3G48610	non-specific phospholipase C6
AT2G29980	omega-3 fatty acid desaturase
AT1G06800	phospholipase A1-Igamma1
AT1G06520	sn-glycerol-3-phosphate 2-O-acyltransferase
AT4G22753	sterol 4-alpha methyl oxidase 1-3
AT2G15230	triacylglycerol lipase 1

Signaling

AT3G12000	**S-locus related protein (SLR1)**
AT1G61550	G-type lectin S-receptor-like serine/threonine-protein kinas
AT2G02780	LRR receptor-like serine/threonine-protein kinase
AT1G18390	serine/threonine-protein kinase
AT1G28390	serine/threonine-protein kinase-like protein

AT5G20050	receptor-like protein kinase
AT3G14840	leucine-rich repeat transmembrane protein kinase
AT4G16350	calcineurin B-like protein 6 (CBL6)
AT3G59440	calmodulin like (CML4)
AT2G43290	calmodulin like (CML5)
AT3G03000	calmodulin like (CML18)
AT1G66400	calmodulin like (CML23)
AT5G37770	calmodulin like (CML24)
AT1G21550	calmodulin like (CML44)
AT3G10660	calcium-dependent protein kinase (CPK2)
AT4G09570	calcium-dependent protein kinase (CPK4)
AT1G74740	calcium-dependent protein kinase (CPK30)
AT2G24300	calmodulin-binding protein
AT4G31000	calmodulin-binding protein
AT3G22910	calcium-transporting ATPase 13 (ACA13)
AT5G43310	COP1-interacting protein-like protein
AT3G55950	CRINKLY4 related 3
AT1G31930	extra-large GTP-binding protein 3
AT5G58670	phosphoinositide phospholipase C 1
AT3G55940	phosphoinositide phospholipase C 7
AT3G26490	phototropic-responsive NPH3 family protein
AT5G43980	plasmodesmata-located protein 1
AT1G08860	protein bonzai 3
AT1G35140	protein exordium like 1
AT4G15800	protein ralf-like 33
AT2G21880	RAB GTPase-like protein 7A
AT3G07410	RAB GTPase-like protein A5B
AT1G02900	rapid alkalinization factor 1
AT4G39890	Ras-related protein RABH1c

Transport

AT3G47750	ABC transporter A family member 4 (ABCA4)
AT5G61740	ABC transporter A family member 10 (ABCA10)
AT2G39350	ABC transporter G family member 1 (ABCG1)
AT1G51500	ABC transporter G family member 12 (ABCG12)
AT3G21090	ABC transporter G family member 15 (ABCG15)
AT3G55110	ABC transporter G family member 18 (ABCG18)
AT3G55130	ABC transporter G family member 19 (ABCG19)
AT1G66950	ABC transporter G family member 39 (ABCG39)

AT1G64170	cation/H(+) antiporter 16 (CHX16)
AT5G41610	cation/H(+) antiporter 18 (CHX18)
AT3G51860	vacuolar cation/proton exchanger (CAX3)
AT4G32500	potassium channel (AKT5)
AT4G32650	potassium channel (KAT3)
AT2G30070	potassium transporter 1 (KUP1)
AT2G35060	potassium transporter 11 (KUP11)
AT1G62280	S-type anion channel (SLAH1)
AT1G33080	MATE efflux family protein
AT1G61890	MATE efflux family protein
AT3G26590	MATE efflux family protein
AT4G18910	NOD26-like intrinsic protein 1;2
AT5G50200	high-affinity nitrate transporter 3.1
AT1G22550	peptide/nitrate transporter
AT1G72140	peptide/nitrate transporter
AT2G38060	phosphate transporter 4;2
AT1G26130	phospholipid-transporting ATPase 12
AT5G41160	purine permease 12
AT1G22710	sucrose transport protein (SUC2)
AT5G15240	transmembrane amino acid transporter family protein
AT5G41800	transmembrane amino acid transporter family protein
AT1G64200	V-type proton ATPase subunit E3

Secondary metabolism

AT5G05260	cytochrome P450 CYP79A2
AT2G26250	3-ketoacyl-CoA synthase 10
AT3G21240	4-coumarate--CoA ligase 2
AT1G65060	4-coumarate--CoA ligase 3
AT3G21230	4-coumarate--CoA ligase 5
AT5G52570	beta-carotene hydroxylase 2
AT2G45400	brassinosteroid metabolic pathway protein (BEN1)
AT3G57010	calcium-dependent phosphotriesterase superfamily protein
AT1G78955	camelliol C synthase 1
AT5G13930	chalcone synthase
AT5G05270	chalcone-flavanone isomerase family protein
AT3G55120	chalcone--flavonone isomerase 1
AT1G80820	cinnamoyl-CoA reductase
AT4G30470	cinnamoyl-CoA reductase like protein
AT4G39330	cinnamyl alcohol dehydrogenase 9

AT3G54250	diphosphomevalonate decarboxylase
AT1G53520	fatty-acid-binding protein 3
AT4G36220	ferulic acid 5-hydroxylase 1
AT3G51240	flavanone 3-hydroxylase
AT5G07990	flavonoid 3'-monooxygenase
AT5G08640	flavonol synthase
AT4G11820	hydroxymethylglutaryl-CoA synthase
AT1G78960	lupeol synthase 2
AT3G44300	nitrilase 2
AT1G77520	O-methyltransferase family protein
AT5G57800	protein eceriferum 3
AT5G14700	Rossmann-fold NAD(P)-binding domain-containing protein
AT3G57020	strictosidine synthase family protein
AT1G74010	strictosidine synthase-like protein
AT4G28680	tyrosine decarboxylase
Stress response	
AT5G42050	DCD (Development and Cell Death) domain protein
AT4G22235	defensin-like protein 95
AT4G22230	defensin-like protein 96
AT4G22214	defensin-like protein 99
AT2G43510	defensin-like protein 195
AT1G33560	disease resistance protein ADR1
AT2G17880	DNAJ heat shock N-terminal domain-containing protein
AT2G21510	DNAJ heat shock N-terminal domain-containing protein
AT3G05890	hydrophobic protein RCI2B
AT1G17860	kunitz type trypsin and protease inhibitor domain-containing protein
AT1G61560	MLO-like protein 6
AT2G17480	MLO-like protein 8
AT5G53760	MLO-like protein 11
AT1G70830	MLP-like protein 28
AT5G06320	NDR1/HIN1-Like protein 3
AT1G75040	pathogenesis-related protein 5
AT1G55010	plant defensin 1.5
AT3G26460	polyketide cyclase/dehydrase and lipid transport superfamily protein
AT4G23680	polyketide cyclase/dehydrase and lipid transport superfamily protein
AT5G64900	precursor of peptide 1
AT4G04220	receptor like protein 46
AT5G47910	respiratory burst oxidase-D

AT3G26450	SRPBCC ligand-binding domain-containing protein
AT1G75030	thaumatin-like protein 3
AT1G63750	TIR-NBS-LRR class disease resistance protein

Hormone metabolism

AT1G76690	12-oxophytodienoate reductase 2
AT2G19590	1-aminocyclopropane-1-carboxylate oxidase 1
AT1G77330	1-aminocyclopropane-1-carboxylate oxidase 5
AT5G44210	ethylene-responsive transcription factor 9
AT5G25190	ethylene-responsive transcription factor ERF003
AT5G14920	gibberellin-regulated protein
AT2G22475	GLABRA2 expression modulator
AT5G10720	histidine kinase 5
AT1G55020	lipoxygenase 1
AT3G10870	methyl esterase 17
AT3G13380	receptor-like protein kinase BRI1-like 3
AT1G29500	SAUR-like auxin-responsive protein
AT2G16580	SAUR-like auxin-responsive protein
AT4G34760	SAUR-like auxin-responsive protein
AT4G36110	SAUR-like auxin-responsive protein
AT4G38850	SAUR-like auxin-responsive protein
AT4G37760	squalene epoxidase 3
AT5G24150	squalene monooxygenase 1,1
AT5G24160	squalene monooxygenase 6
AT1G22400	UDP-glycosyl transferase 85A1

Cell wall

AT3G29030	expansin A5 (EXP5)
AT2G40610	expansin A8 (EXP8)
AT1G26770	expansin A10 (EXP10)
AT3G45970	expansin-like A1 (EXLA1)
AT1G02810	pectin methylesterase 7 (PME7)
AT4G33220	pectin methylesterase 44 (PME44)
AT4G30280	xyloglucan endotransglucosylase/hydrolase 18 (XTH18)
AT4G30290	xyloglucan endotransglucosylase/hydrolase 19 (XTH19)
AT1G32170	xyloglucan endotransglucosylase/hydrolase 30 (XTH30)
AT1G10550	xyloglucan endotransglucosylase/hydrolase 33 (XTH33)
AT1G64670	alpha/beta-hydrolase
AT2G01850	endoxyloglucan transferase A3
AT3G11700	fasciclin-like arabinogalactan protein 18

AT4G13340	leucine-rich repeat extensin-like protein 3
AT2G21140	proline-rich protein 2
AT4G38770	proline-rich protein 4
AT1G41830	SKU5 similar 6
AT4G30440	UDP-D-glucuronate 4-epimerase 1
AT5G15490	UDP-glucose 6-dehydrogenase
Development	
AT5G14930	acyl hydrolase
AT3G61190	BON association protein 1
AT1G05065	CLAVATA3/ESR-related protein 20
AT1G75890	GDSL esterase/lipase (EXL2)
AT5G44020	HAD superfamily, subfamily IIIB acid phosphatase
AT5G44730	haloacid dehalogenase-like hydrolase domain-containing protein
AT5G60690	homeobox-leucine zipper protein revoluta
AT3G61150	homeodomain glabrous 1
AT2G46140	late embryogenesis abundant protein
AT3G53040	late embryogenesis abundant protein
AT5G61430	NAC domain containing protein 100
AT3G04060	NAC domain containing protein 46
AT5G65870	phytosulfokines 5 precursor
AT5G12130	protein pigment defective 149
AT4G28190	protein ultrapetala 1
AT1G19790	SHI-related sequence 7 protein
AT5G66040	thiosulfate sulfurtransferase 16
AT1G74940	uncharacterized protein
Cell fate	
AT1G01750	actin depolymerizing factor 11
AT2G24600	ankyrin repeat family protein
AT5G65020	annexin 2 (ANN2)
AT5G10220	annexin D6 (ANN6)
AT3G16320	cell division cycle protein 27-A
AT1G70210	cyclin-D1-1
AT1G24150	formin-like protein 4
AT1G74790	HIPL1 protein
AT3G50240	kinesin-related protein
AT4G25850	OSBP(oxysterol binding protein)-related protein
AT5G57240	OSBP(oxysterol binding protein)-related protein 4C
AT5G02100	oxysterol-binding protein-related protein 3A

AT3G52400	syntaxin-122
AT1G75780	tubulin beta-1 chain
AT2G33110	vesicle-associated membrane protein 723
AT5G47180	vesicle-associated protein 2-1
DNA fate	
AT4G35220	cyclase family protein
AT5G65090	deformned root hairs 4
AT1G63210	transcription elongation factor (SPT6)
AT3G18950	WD40 domain-containing protein
AT3G50900	uncharacterized protein
Major CHO metabolism.synthesis	
AT1G12240	acid beta-fructofuranosidase 4
AT3G13790	beta-fructofuranosidase, insoluble isoenzyme CWINV1
AT1G47840	hexokinase 3
AT3G52340	sucrose-phosphatase 2
Amino acid metabolism	
AT5G17990	anthranilate phosphoribosyltransferase
AT2G24580	sarcosine oxidase
AT5G38530	tryptophan synthase beta chain
TCA / organic acid transformation	
AT1G10670	ATP-citrate lyase A-1
AT3G15020	malate dehydrogenase 2
Minor CHO metabolism	
AT2G37760	aldo-keto reductase family 4 member C8
AT1G05630	type I inositol-1,4,5-trisphosphate 5-phosphatase 13
Redox	
AT4G31870	glutathione peroxidase 7
AT1G77510	protein disulfide-isomerase 2
Mitochondrial electron transport / ATP synthesis	
AT5G25450	cytochrome bd ubiquinol oxidase
AT2G43400	electron-transfer flavoprotein--ubiquinone oxidoreductase
Oxidative pentose phosphate pathway	
AT1G12230	transaldolase-like protein
Tetrapyrrole synthesis	
AT1G69720	heme oxygenase 3
Glycolysis	
AT1G74030	enolase 1
Metal handling	

AT3G11050 ferritin 2

Co-factor and vitamine metabolism

AT1G10060 branched-chain-amino-acid aminotransferase 1

Nucleotide metabolism

AT5G50370 adenylate kinase 2

Miscellaneous

AT5G45340 abscisic acid 8'-hydroxylase 3
AT5G42250 alcohol dehydrogenase-like 7
AT5G20960 aldehyde oxidase 1
AT1G54870 aldehyde reductase
AT5G44930 arabinosyltransferase
AT3G60130 beta glucosidase 16
AT2G28470 beta-galactosidase 8
AT5G20230 blue-copper-binding protein
AT2G03505 carbohydrate-binding X8 domain-containing protein
AT1G13130 cellulase (glycosyl hydrolase family 5) protein
AT3G53280 cytochrome p450 71b5
AT1G13100 cytochrome P450 71b29
AT2G45580 cytochrome P450 76C3
AT4G00360 cytochrome P450 86A2
AT3G53290 cytochrome P450, family 71, subfamily B, polypeptide 30 pseudogene
AT2G46660 cytochrome P450, family 78, subfamily A, polypeptide 6
AT1G65450 dual transcription unit and alternative splicing protein GLAUCE
AT1G53140 dynamin related protein 5A
AT5G15350 early nodulin-like protein 17
AT1G72970 embryo sac development arrest 17
AT2G31990 exostosin family protein
AT2G34810 FAD-binding and BBE domain-containing protein
AT5G11320 flavin-binding monooxygenase family protein
AT3G50760 galacturonosyltransferase-like 2
AT1G24170 galacturonosyltransferase-like 8
AT2G27360 GDSL esterase/lipase
AT2G42990 GDSL esterase/lipase
AT3G14220 GDSL esterase/lipase
AT3G16370 GDSL esterase/lipase
AT4G18970 GDSL esterase/lipase
AT4G28780 GDSL esterase/lipase
AT4G16230 GDSL-like Lipase/Acylhydrolase superfamily protein

AT3G56060	glucose-methanol-choline (GMC) oxidoreductase family protein
AT5G17220	glutathione S-transferase phi 12
AT1G10370	glutathione S-transferase U17
AT5G04500	glycosyltransferase family protein 47
AT1G04040	HAD superfamily, subfamily IIIB acid phosphatase
AT5G02540	NAD(P)-binding Rossmann-fold superfamily protein
AT1G64760	O-glycosyl hydrolases family 17 protein
AT3G04010	O-glycosyl hydrolases family 17 protein
AT1G51990	O-methyltransferase family protein
AT3G03670	peroxidase
AT5G19880	peroxidase
AT5G06720	peroxidase 2
AT4G11290	peroxidase 39
AT5G64110	peroxidase 70
AT3G15820	phosphatidylcholine:diacylglycerol cholinephosphotransferase
AT5G15070	phosphoglycerate mutase-like protein
AT4G13700	purple acid phosphatase 23
AT2G37540	Rossmann-fold NAD(P)-binding domain-containing protein
AT2G29350	senescence-associated protein 13
AT3G21560	sinapic acid:UDP-glucose glucosyltransferase
AT2G15480	UDP-glucosyl transferase 73B5
AT2G31750	UDP-glucosyl transferase 74D1
AT5G59590	UDP-glucosyl transferase 76E2
AT4G15500	UDP-glycosyl transferase 84A4
AT1G22360	UDP-glucosyl transferase 85A2
AT1G22380	UDP-glucosyl transferase 85A3
AT1G55260	bifunctional inhibitor/lipid-transfer protein/seed storage 2S albumin superfamily protein
AT3G43720	bifunctional inhibitor/lipid-transfer protein/seed storage 2S albumin superfamily protein
AT1G48750	bifunctional inhibitor/lipid-transfer protein/seed storage 2S albumin-like protein
AT1G05450	protease inhibitor/seed storage/lipid transfer protein (LTP) family protein
AT4G22470	protease inhibitor/seed storage/lipid transfer protein (LTP) family protein

Unknown

AT2G33850	**uncharacterized protein Br Pis63 homolog**
AT1G21770	acyltransferase-like protein
AT5G11650	alpha/beta fold hydrolase family protein
AT3G48410	alpha/beta-hydrolase domain-containing protein

AT1G32190	alpha/beta-hydrolase-like protein
AT1G78210	alpha/beta-Hydrolases superfamily protein
AT5G25770	alpha/beta-Hydrolases superfamily protein
AT3G05830	alpha-helical IF-like protein
AT4G34260	alpha-L-fucosidase 2
AT4G00910	aluminum activated malate transporter family protein
AT1G50820	aminotransferase-like, plant mobile domain family protein
AT4G14730	Bax inhibitor-1 family protein
AT1G63220	calcium-dependent lipid-binding domain-containing protein
AT5G37740	calcium-dependent lipid-binding domain-containing protein
AT5G07820	calmodulin-binding protein-like protein
AT5G61260	calmodulin-binding protein-like protein
AT2G45600	carboxylesterase 8
AT1G03270	CBS domain-containing protein
AT2G04680	cysteine/histidine-rich C1 domain-containing protein
AT5G58770	dehydrodolichyl diphosphate synthase 2
AT4G35560	DUO1-activated WD40 1
AT2G44770	ELMO/CED-12 domain-containing protein
AT1G73390	endosomal targeting BRO1-like domain-containing protein
AT3G46540	ENTH/VHS family protein
AT5G19100	eukaryotic aspartyl protease family protein
AT2G39050	euonymus lectin S3
AT5G22600	FBD and leucine rich repeat domain-containing protein
AT2G43445	F-box and associated interaction domains-containing protein
AT5G24860	flowering promoting factor 1
AT2G24762	glutamine dumper 4
AT4G21620	glycine-rich protein
AT4G33610	glycine-rich protein
AT5G25425	glycine-rich protein
AT5G19250	GPI-anchored glycoprotein membrane precursor
AT5G26690	heavy-metal-associated domain-containing protein
AT5G20270	heptahelical transmembrane protein1
AT3G24420	hydrolase, alpha/beta fold family protein
AT4G36610	hydrolase, alpha/beta fold family protein
AT4G37470	hydrolase, alpha/beta fold family protein
AT1G23040	hydroxyproline-rich glycoprotein family protein
AT2G22510	hydroxyproline-rich glycoprotein family protein
AT2G34870	hydroxyproline-rich glycoprotein family protein

AT5G65660	hydroxyproline-rich glycoprotein family protein
AT1G62190	kua-ubiquitin conjugating enzyme hybrid localisation domain-containing protein
AT1G65690	late embryogenesis abundant (LEA) hydroxyproline-rich glycoprotein
AT2G46150	late embryogenesis abundant hydroxyproline-rich glycoprotein
AT3G52470	late embryogenesis abundant hydroxyproline-rich glycoprotein
AT3G54200	late embryogenesis abundant hydroxyproline-rich glycoprotein
AT2G45450	little zipper 1 protein
AT2G14560	LURP1 protein
AT1G63010	major facilitator superfamily with SPX domain-containing protein
AT2G17000	mechanosensitive ion channel protein 7
AT5G52330	meprin and TRAF homology domain-containing protein
AT2G30460	nucleotide/sugar transporter family protein
AT3G49210	O-acyltransferase (WSD1-like) family protein
AT3G05320	O-fucosyltransferase family protein
AT5G50390	pentatricopeptide repeat-containing protein
AT1G34640	peptidase
AT1G03210	phenazine biosynthesis PhzC/PhzF protein
AT3G49900	phototropic-responsive NPH3 family protein
AT3G58850	phy rapidly regulated 2 protein
AT1G04280	P-loop containing nucleoside triphosphate hydrolases superfamily protein
AT2G16630	pollen Ole e 1 allergen and extensin family protein
AT2G27385	pollen Ole e 1 allergen and extensin family protein
AT3G54580	proline-rich extensin-like family protein
AT3G49300	proline-rich family protein
AT4G19200	proline-rich family protein
AT1G56580	protein smaller with variable branches
AT5G56510	pumilio 12
AT4G26060	ribosomal protein L18ae family protein
AT5G50940	RNA-binding KH domain-containing protein
AT5G60210	ROP interactive partner 5
AT1G26210	SOB five-like 1 protein
AT1G67650	SRP72 RNA-binding domain protein
AT1G47420	succinate dehydrogenase 5
AT5G38900	thioredoxin superfamily protein
AT1G35180	TRAM, LAG1 and CLN8 (TLC) lipid-sensing domain containing protein
AT2G30010	trichome birefringence-like 45 protein
AT3G08990	yippee-like protein
AT1G02770	uncharacterized protein

AT1G02816	uncharacterized protein
AT1G10020	uncharacterized protein
AT1G10220	uncharacterized protein
AT1G12030	uncharacterized protein
AT1G15640	uncharacterized protein
AT1G19397	uncharacterized protein
AT1G20310	uncharacterized protein
AT1G20816	uncharacterized protein
AT1G22250	uncharacterized protein
AT1G22885	uncharacterized protein
AT1G22890	uncharacterized protein
AT1G33840	uncharacterized protein
AT1G49470	uncharacterized protein
AT1G52855	uncharacterized protein
AT1G56660	uncharacterized protein
AT1G63720	uncharacterized protein
AT1G64340	uncharacterized protein
AT1G64680	uncharacterized protein
AT1G67035	uncharacterized protein
AT1G69610	uncharacterized protein
AT1G70100	uncharacterized protein
AT1G71690	uncharacterized protein
AT1G72240	uncharacterized protein
AT1G76240	uncharacterized protein
AT1G79270	uncharacterized protein
AT1G80120	uncharacterized protein
AT2G28870	uncharacterized protein
AT2G30930	uncharacterized protein
AT2G31110	uncharacterized protein
AT2G31985	uncharacterized protein
AT2G32190	uncharacterized protein
AT2G35850	uncharacterized protein
AT2G36420	uncharacterized protein
AT2G37370	uncharacterized protein
AT2G41800	uncharacterized protein
AT2G43390	uncharacterized protein
AT2G43795	uncharacterized protein
AT2G44230	uncharacterized protein

AT2G46535	uncharacterized protein
AT3G03150	uncharacterized protein
AT3G09280	uncharacterized protein
AT3G11600	uncharacterized protein
AT3G14380	uncharacterized protein
AT3G15115	uncharacterized protein
AT3G18560	uncharacterized protein
AT3G20300	uncharacterized protein
AT3G25640	uncharacterized protein
AT3G27210	uncharacterized protein
AT3G44450	uncharacterized protein
AT3G48180	uncharacterized protein
AT3G48980	uncharacterized protein
AT3G49270	uncharacterized protein
AT3G49845	uncharacterized protein
AT3G50120	uncharacterized protein
AT3G51290	uncharacterized protein
AT3G52550	uncharacterized protein
AT3G55420	uncharacterized protein
AT3G57450	uncharacterized protein
AT3G59430	uncharacterized protein
AT3G60380	uncharacterized protein
AT3G60520	uncharacterized protein
AT3G61840	uncharacterized protein
AT4G02830	uncharacterized protein
AT4G04745	uncharacterized protein
AT4G09890	uncharacterized protein
AT4G13266	uncharacterized protein
AT4G15610	uncharacterized protein
AT4G16215	uncharacterized protein
AT4G18540	uncharacterized protein
AT4G25830	uncharacterized protein
AT4G27652	uncharacterized protein
AT4G30180	uncharacterized protein
AT4G32460	uncharacterized protein
AT5G06270	uncharacterized protein
AT5G20670	uncharacterized protein
AT5G24600	uncharacterized protein

AT5G28610	uncharacterized protein
AT5G37550	uncharacterized protein
AT5G41810	uncharacterized protein
AT5G53710	uncharacterized protein
AT5G59050	uncharacterized protein
AT5G61820	uncharacterized protein
AT5G65300	uncharacterized protein
AT5G65610	uncharacterized protein
AT5G65925	uncharacterized protein
AT5G67390	uncharacterized protein
AT5G67640	uncharacterized protein

Genes are listed whose normalized expression level in papilla cells was significantly ($P < 0.05$) and more than 4-fold higher than in underlying cells.

Supplemental Table 3. Genes expressed in papilla cells preferentially at 30 min after cross-pollination.

TAIR locus	Description	FC
Protein fate		
At3g62230	F-box family protein (DAF1)	2.2
At1g80470	F-box/RNI-like/FBD-like domains-containing protein	2.2
At2g07180	Protein kinase superfamily protein	2.0
At3g01085	Protein kinase superfamily protein	2.8
At3g02810	Protein kinase superfamily protein	2.6
At3g22750	Protein kinase superfamily protein	2.0
At5g16500	Protein kinase superfamily protein	2.0
At3g52010	serine carboxypeptidase-like 37 (scpl37)	2.3
At1g47270	tubby like protein 6	2.0
Miscellaneous enzymes		
At5g39400	Calcium/lipid-binding (CaLB) phosphatase (PTEN1)	2.4
At4g33860	Glycosyl hydrolase family 10 protein	2.3
At5g20390	Glycosyl hydrolase superfamily protein	2.8
At1g48020	pectin methylesterase inhibitor 1 (PMEI1)	2.6
At2g31430	Plant invertase/pectin methylesterase inhibitor superfamily protein	2.0
At2g47050	Plant invertase/pectin methylesterase inhibitor superfamily protein	2.1
At3g36659	Plant invertase/pectin methylesterase inhibitor superfamily protein	2.2
At5g50030	Plant invertase/pectin methylesterase inhibitor superfamily protein	2.3
At4g24640	Plant invertase/pectin methylesterase inhibitor superfamily protein (APPB1)	2.0
Signaling		
At1g61563	ralf-like 8 (RALFL8)	2.2
At1g61566	ralf-like 9 (RALFL9)	2.6
At2g22055	ralf-like 15 (RALFL15)	2.9
At3g25165	ralf-like 25 (RALFL25)	2.2
At2g41860	calcium-dependent protein kinase 14 (CPK14)	2.7
At4g18640	Leucine-rich repeat protein kinase family protein (MRH1)	2.2
At2g40116	Phosphoinositide-specific phospholipase C family protein	2.2
At5g15430	Plant calmodulin-binding protein-related	2.4
At3g54800	Pleckstrin homology (PH) and lipid-binding START domains-containing protein	2.7
Cell wall		
At3g57690	arabinogalactan protein 23 (AGP23)	2.4
At2g33100	cellulose synthase-like D1 (CSLD1)	2.4
At1g14420	Pectate lyase family protein	2.1

At3g01270	Pectate lyase family protein	2.2
At5g07430	Pectin lyase-like superfamily protein	2.5
Transport		
At1g08150	cation/H+ exchanger 5 (CHX5)	2.0
At1g08140	cation/H+ exchanger 6A (CHX6A)	2.2
At1g05580	cation/H+ exchanger 23 (CHX23)	2.7
At3g42640	H+-ATPase 8 (AHA8)	2.2
Stress response		
At1g01310	CAP (Cysteine-rich secretory proteins, Antigen 5, and Pathogenesis-related 1 protein) superfamily protein	2.1
At1g04540	Calcium-dependent lipid-binding (CaLB domain) family protein	2.6
At2g13350	Calcium-dependent lipid-binding (CaLB domain) family protein	2.2
At3g48450	RPM1-interacting protein 4 (RIN4) family protein	2.1
Redox regulation		
At2g33270	atypical CYS HIS rich thioredoxin 3 (ACHT3)	2.0
At1g60740	Thioredoxin superfamily protein	2.4
At1g65970	thioredoxin-dependent peroxidase 2 (TPX2)	2.2
Hormone metabolism		
At2g36020	HVA22-like protein J (HVA22J)	2.0
At3g43120	SAUR-like auxin-responsive protein family	2.6
Amino acid metabolism		
At1g72330	alanine aminotransferase 2 (ALAAT2)	2.1
Cell fate		
At3g09530	exocyst subunit exo70 family protein H3 (EXO70H3)	2.5
Development		
At3g04630	WVD2-like 1 (WDL1)	2.3
Lipid metabolism		
At4g04930	fatty acid desaturase family protein	2.2
TCA / organic acid transformation		
At5g04180	alpha carbonic anhydrase 3	2.2
Unknown		
At2g38500	2-oxoglutarate (2OG) and Fe(II)-dependent oxygenase superfamily protein	2.1
At3g26110	Anther-specific protein agp1-like	2.7
At5g24105	arabinogalactan protein 41 (AGP41)	2.1
At1g68110	ENTH/ANTH/VHS superfamily protein	2.3
At4g02650	ENTH/ANTH/VHS superfamily protein	3.0
At5g43185	Expressed protein	2.6
At5g14890	NHL domain-containing protein	2.3

At1g11765	Plant self-incompatibility protein S1 family	2.1
At1g51250	Plant self-incompatibility protein S1 family	3.1
At5g26060	Plant self-incompatibility protein S1 family	2.3
At3g22510	Pre-rRNA-processing protein TSR2	2.2
At3g56180	Protein of unknown function (DUF567)	2.4
At3g54740	Protein of unknown function (DUF593)	2.2
At1g18990	Protein of unknown function (DUF593)	2.4
At5g54240	Protein of unknown function (DUF1223)	2.1
At1g13970	Protein of unknown function (DUF1336)	2.3
At5g28690	Protein of unknown function (DUF1685)	2.7
At3g05725	Protein of unknown function (DUF3511)	2.5
At1g78460	SOUL heme-binding family protein	2.5
At5g15600	SPIRAL1-like4 (SP1L4)	2.2
At1g23150	unknown protein	2.1
At1g58120	unknown protein	2.5
At2g21980	unknown protein	2.2
At2g27180	unknown protein	2.7
At2g46360	unknown protein	2.4
At3g49540	unknown protein	2.2
At4g04980	unknown protein	2.3
At5g39880	unknown protein	2.3
At5g46770	unknown protein	2.7
At5g50830	unknown protein	2.3

Genes are listed whose normalized expression level in papilla cells after cross-pollination was significantly ($P < 0.05$) and more than 2-fold higher than after self-pollination. FC, fold change.

Supplemental Table 4. Genes expressed in papilla cells preferentially at 30 min after self-pollination.

TAIR locus	Description	FC
RNA fate		
AT4G34400	AP2/B3-like transcriptional factor family protein	2.6
AT5G22250	CCR4-associated factor 1B	3.1
AT1G12890	ethylene-responsive transcription factor (ERF088)	3.5
AT5G23420	high-mobility group B6 protein	2.3
AT4G04890	homeobox-leucine zipper protein protodermal factor 2	2.1
AT2G29570	proliferating cell nuclear antigen 2	2.3
AT1G07370	proliferating cellular nuclear antigen 1	3.5
AT3G55980	salt-inducible zinc finger 1 (SZF1)	3.6
AT5G09750	transcription factor (HEC3)	5.8
AT4G01250	WRKY transcription factor 22	7.6
AT2G38470	WRKY transcription factor 33	5.2
AT1G80840	WRKY transcription factor 40	4.8
AT4G23810	WRKY transcription factor 53	10.3
AT3G46080	zinc finger protein (ZAT8)	2.5
AT1G27730	zinc finger protein (STZ/ZAT10)	8.5
Miscellaneous enzymes		
AT4G39510	cytochrome P450, family 96, subfamily A, polypeptide 12	6.5
AT4G27520	early nodulin-like protein 2	3.2
AT2G32030	GCN5-related N-acetyltransferase-like protein	2.5
AT1G28600	GDSL esterase/lipase	2.6
AT1G29670	GDSL esterase/lipase	2.2
AT4G18970	GDSL esterase/lipase	3.3
AT5G45670	GDSL esterase/lipase	2.4
AT5G15720	GDSL esterase/lipase 7	5.6
AT5G58400	peroxidase	2.8
AT5G20740	plant invertase/pectin methylesterase inhibitor domain-containing protein	2.1
Stress response		
AT3G28940	AIG2-like protein	2.5
AT1G19670	chlorophyllase 1	2.1
AT5G25610	dehydration-responsive protein (RD22)	2.7
AT3G50950	disease resistance RPP13-like protein 4	3.8
AT1G24020	MLP-like protein 423 (MLP423)	4.0
AT4G08685	protein (SAH7)	2.0
AT5G22690	TIR-NBS-LRR class disease resistance protein	3.6

Signaling		
AT5G42380	calcium-binding protein (CML37)	5.9
AT1G76650	calcium-binding protein (CML38)	3.2
AT2G41010	calmodulin binding protein 25 (CAMBP25)	2.2
AT3G45640	mitogen-activated protein kinase 3 (MPK3)	2.1
AT2G36570	leucine-rich repeat protein kinase-like protein (PXC1)	3.4
AT1G69270	receptor-like protein kinase 1 (RPK1)	2.7
Protein fate		
AT5G66210	calcium-dependent protein kinase (CPK28)	2.4
AT1G78760	F-box/FBD/LRR-repeat protein	2.3
AT2G31865	poly(ADP-ribose) glycohydrolase 2 (PARG2)	2.9
AT4G35480	RING-H2 finger protein (RHA3b)	2.1
AT4G28560	ROP-interactive CRIB motif-containing protein 7 (RIC7)	2.7
DNA fate		
AT5G46280	DNA replication licensing factor MCM3-like protein	2.1
AT5G59870	histone H2A 6	2.9
AT1G09200	histone H3	2.2
AT5G10400	histone H3	2.4
AT2G07690	minichromosome maintenance protein 5	2.6
Hormone metabolism		
AT1G23080	auxin efflux carrier component 7	2.3
AT1G74670	gibberellin-regulated protein 6	3.4
AT1G56150	SAUR-like auxin-responsive protein	2.3
Secondary metabolism		
AT5G13930	chalcone synthase	3.5
AT5G08640	flavonol synthase 1	2.0
AT1G02205	protein eceriferum 1	4.5
Transport		
AT3G21090	ABC transporter G family member 15	2.1
AT3G17700	cyclic nucleotide-binding transporter (CNGC20)	3.8
AT2G03240	EXS (ERD1/XPR1/SYG1) family protein	2.0
Lipid metabolism		
AT4G24510	fatty acid elongation machinery component eceriferum2	3.4
AT5G51210	oleosin3	4.3
Cell fate		
AT2G24600	ankyrin repeat family protein	2.6
Cell wall		
AT3G10720	pectinesterase 25	2.5

Development		
AT1G75890	GDSL esterase/lipase (EXL2)	2.2
Redox regulation		
AT4G39830	L-ascorbate oxidase	5.3
Unknown		
AT5G23940	acyl-transferase (PEL3)	3.7
AT4G01360	BYPASS1-related protein	3.0
AT2G35760	CASP-like protein	2.1
AT3G51890	clathrin light chain protein	2.4
AT4G36830	GNS1/SUR4 membrane protein	3.0
AT5G19230	GPI-anchored glycoprotein membrane precursor	2.9
AT5G21950	hydrolase, alpha/beta fold family protein	2.7
AT4G38550	phospholipase like protein family	3.0
AT2G20960	phospholipase-like protein (PEARLI 4) domain-containing protein	2.9
AT2G27385	pollen Ole e 1 allergen and extensin family protein	2.1
AT1G15010	unknown protein	2.3
AT1G23830	unknown protein	2.7
AT1G25400	unknown protein	3.3
AT3G47295	unknown protein	2.7
AT3G52550	unknown protein	3.4
AT3G61840	unknown protein	3.9
AT5G36920	unknown protein	2.4
AT5G54970	unknown protein	2.4
AT5G56980	unknown protein	2.9
AT2G01300	unknown protein	2.5
AT2G20835	unknown protein	3.3
AT2G24970	unknown protein	3.0
AT2G32200	unknown protein	2.7
AT1G61255	unknown protein	2.0

Genes are listed whose normalized expression level in papilla cells after self-pollination was significantly ($P < 0.05$) and more than 2-fold higher than after cross-pollination. FC, fold change.